Prague Medical REPORT

(Sborník lékařský)

Multidisciplinary Biomedical Journal
of the First Faculty of Medicine,
Charles University

Vol. 125 (2024) No. 2

Reviews

Case Reports


D
E
C
Fig. 7.
B
C
A
Fig. 6.
B
A
Fig. 8.
C
B
A
B
Fig. 2.
D
A
D
E
Fig. 9.
A
E

Prague Medical Report (Prague Med Rep) is indexed and abstracted by Index-medicus, MEDLINE, PubMed, EuroPub, CNKI, DOAJ, EBSCO, and Scopus.

Abstracts and full-texts of published papers can be retrieved from the World Wide Web (https://pmr.lf1.cuni.cz).

Engraving overleaf: Laurentius Heister, Institutiones chirurgicae, Amsterdam 1750.
Illustration provided by the Institute for History of Medicine and Foreign Languages.

Evidence for Therapeutic Drug Monitoring of Atypical Antipsychotics

Veronika Krejčí[1,2], Irena Murínová[1,3], Ondřej Slanař[2], Martin Šíma[2]

[1] Department of Clinical Pharmacy, Military University Hospital Prague, Prague, Czech Republic;
[2] Institute of Pharmacology, First Faculty of Medicine, Charles University and General University Hospital in Prague, Prague, Czech Republic;
[3] Department of Applied Pharmacy, Faculty of Pharmacy, Masaryk University, Brno, Czech Republic

Received January 30, 2024; Accepted May 7, 2024.

Key words: Personalised medicine – Pharmacokinetics – Risperidone – Olanzapine – Quetiapine – Aripiprazole

Abstract: Second-generation antipsychotics (SGAs), also known as atypical antipsychotics, are a newer class of antipsychotic drugs used to treat schizophrenia, bipolar disorder, and related psychiatric conditions. The plasma concentration of antipsychotic drugs is a valid measure of the drug at its primary target structure in the brain, and therefore determines the efficacy and safety of these drugs. However, despite the well-known high variability in pharmacokinetics of these substances, psychiatric medication is usually administered in uniform dosage schedules. Therapeutic drug monitoring (TDM), as the specific method that can help personalised medicine in dose adjustment according to the characteristics of the individual patient, minimizing the risk of toxicity, monitoring adherence, and increasing cost-effectiveness in the treatment, thus seems to be an elegant tool to solve this problem. Non-response to therapeutic doses, uncertain adherence to medication, suboptimal tolerability, or pharmacokinetic drug-drug interactions are typical indications for TDM of SGAs. This review aims to summarize an overview of the current knowledge and evidence of the possibilities to tailor the dosage of selected SGAs using TDM, including the necessary pharmacokinetic parameters for personalised pharmacotherapy.

This study was supported by the Charles University Project Cooperatio (research area PHAR).

Mailing Address: PharmDr. Veronika Krejčí, Department of Clinical Pharmacy, Military University Hospital Prague, U Vojenské nemocnice 1200, 169 02 Prague 6, Czech Republic; Phone: +420 973 208 309; e-mail: veronika.krejci@uvn.cz

https://doi.org/10.14712/23362936.2024.10

Introduction

Schizophrenia is a neurodevelopmental disorder associated with deficits in cognition, affect, and social functioning, with estimated prevalence in the general population of 0.5–1% (McGrath et al., 2008). The course of schizophrenia is chronic, with relapses in psychotic episodes, disturbed cognitive functioning, poor quality of life, and social decline. Antipsychotic medications have unique efficacy in the treatment of acute psychosis from any cause and in the management of chronic psychotic disorders such as schizophrenia. As a class, antipsychotics are also effective in the treatment of acute agitation, the manic phase of bipolar disorder, and other psychiatric conditions (Taylor et al., 2021). Psychotropic drugs have been used in practice since around 1950s, and today a wide range of effective molecules is available, with recommendations for optimal dosing from the results of randomised controlled trials.

Second-generation antipsychotics (SGAs), also known as atypical antipsychotics, are a group of medications that include among others clozapine, olanzapine, quetiapine, risperidone, paliperidone, lurasidone, aripiprazole, brexpiprazole, cariprazine. The basic pharmacodynamic characteristics of SGAs is summarised in Table 1.

SGAs have a lower risk of extrapyramidal symptoms and tardive dyskinesia compared with first-generation antipsychotics (FGAs). First- and second-generation antipsychotic drugs are more comparable in their clinical efficacy. Factors that influence the selection of an antipsychotic for individual patients include dosing, administration route, pharmacokinetics, side effect profile, and cost (Taylor et al., 2021). Antipsychotic pharmacokinetics and pharmacodynamics exhibit high interindividual variability due to genetic differences – polymorphism (Zhang et al.,

Table 1 – Basic pharmacodynamic characteristics of SGAs

Pharmacodynamic effect	Drug	Blockade of receptors				
		D_2	5-HT_2	α_1	H_1	M
Serotonin-dopamine antagonists (SDAs)	Lurasidone	+	+			
	Paliperidone	+	+	+	±	
	Risperidone	+	+	+	±	
Multi-acting receptor targeted antipsychotics (MARTA)	Clozapine	+	+	+	+	+
	Olanzapine	+	+	+	+	+
	Quetiapine	+	+	+	+	
Serotonin-dopamine activity modulators (SDAMs)	Aripiprazole	+	±			
	Brexpiprazole	+	+	+		
	Cariprazine	+	+			

Source: SmPCs – www.ema.europa.eu
SGAs – second-generation antipsychotics; D_2 – dopamine D_2 receptors; 5-HT_2 – serotonin receptors; α_1 – alpha-1 receptors; H_1 – histamine receptors; M – muscarinic receptors

2018), but also intraindividual variability can arise due to various factors such as comorbidities, lifestyle, and drug interactions. Genetic polymorphism determines a different phenotypic manifestation during drug metabolism and affects its bioavailability, elimination and subsequently dynamics both in terms of the expected effect and in terms of toxicity (Nofziger et al., 2020). Comorbidities have a significant impact on various pharmacokinetic and pharmacodynamic processes. Therefore, population parameters are often inadequate for setting the optimal pharmacotherapy for each patient (Mauri et al., 2017; Hiemke et al., 2018; Baldelli et al., 2021).

The concentration of a drug at its target site determines its efficacy and toxicity. For antipsychotic drugs, the brain, as the target organ, is not directly accessible to drug monitoring. As a result of interindividual variabilities in drug metabolism by hepatic and extrahepatic enzymes or drug transporters involved in absorption, distribution, and elimination, blood concentrations following administration of uniform dose of antipsychotics are highly variable among individuals. Thus, the dose cannot accurately predict the resulting plasma concentration (Mauri et al., 2017). Antipsychotic drugs demonstrated most therapeutic actions by blockade of dopamine D_2-like receptors, with plasma drug concentrations correlating with receptor occupancy (Yokoi et al., 2002). By the high variability of drug concentrations in plasma under the same doses it was found that receptor occupancy correlates better with steady-state plasma concentrations than with daily doses (Agid et al., 2007). The optimal response was observed when the receptors were occupied by 70–80%, and a receptor occupancy of 80% was considered the limit for extrapyramidal side effects (Grundmann et al., 2014; Urban and Cubała, 2017).

It is common for SGAs to use a fixed dose. Due to the above mentioned significant variability in drug pharmacokinetics, therapeutic drug monitoring (TDM) appears to be a useful tool to improve the dosage regimen of psychotropic drugs for the patient by identifying the most appropriate dose (Horvitz-Lennon et al., 2017). Optimised therapy also minimizes the occurrence of adverse effects, which in turn reduces mortality and morbidity rates, resulting in overall cost savings for the treatment. After excluding cases of noncompliance, the most likely causes of pharmacological resistance are genetic and exogenous factors affecting plasma drug concentrations, which are known as “pseudo-pharmacoresistance” (Mauri et al., 2017; Hiemke et al., 2018).

Therefore, the aim of this review was to summarize available up to date evidence about TDM of SGAs.

Literature search

The PubMed database was searched for articles using the paradigm “second-generation antipsychotics” OR “atypical antipsychotics” OR individual international

non-proprietary names (INNs) of these agents AND "pharmacokinetics" OR "pharmacodynamic" OR "TDM" OR "therapeutic drug monitoring".

Results were limited to studies in adult humans and English full-text articles published from January 2000 to January 2024. A total of 834 reports were identified from the initial literature search, out of which 111 relevant publications were found. The list of references for each reviewed paper was analysed and supplementary searches were performed, if they were found within the aim of this paper.

Also, all summaries of product characteristics (SmPCs) for the agents of interest were reviewed (European Medicines Agency, EMA-authorized) to find information about the pharmacologic variables, and one TDM guideline (Hiemke et al., 2018) was also included in the analysis. Sources not containing clear reference to one of the SGAs were excluded, as were the papers without data regarding the pharmacokinetic and pharmacodynamic properties of the previously mentioned antipsychotics.

Pharmacokinetics of SGAs

Since knowledge of pharmacokinetics is essential for the right implementation of TDM, a brief pharmacokinetic characteristics of the individual selected SGAs was also reviewed. The basic pharmacokinetic parameters are summarised in Table 2.

As the basic, lipophilic molecules, most psychoactive drugs have similar chemical properties. A consequence of this similarity is also mirrored in pharmacokinetics. SGAs are well absorbed from the gastrointestinal tract (i.e. with good bioavailability), with easy passage through the blood-brain barrier, with a large volume of distribution (V_d), with linear pharmacokinetics, and a large part of them is metabolised by hepatic enzymes, which results in their susceptibility to drug interactions and relatively slow elimination. However, there are also exceptions (e.g. longer/shorter biological half-life, the existence of an active metabolite, significant renal elimination, etc.) that need to be known to correctly interpret TDM results (Stahl, 2014; Mauri et al., 2018; Taylor et al., 2021).

These agents are subject to drug-drug interactions with other psychotropic agents or with medications used in the treatment of concomitant physical illnesses. Most pharmacokinetic interactions with newer antipsychotics occur at the metabolic level and usually involve changes in the activity of the major drug-metabolising enzymes involved in their biotransformation, i.e. the cytochrome P450 (CYP) monooxygenases and/or uridine diphosphate-glucuronosyltransferases (UGT) (Urichuk et al., 2008). Cytochrome P450 forms involved in the metabolism of SGAs are presented in Table 3.

Tobacco smoking is associated with the induction of drug-metabolizing enzymes, namely CYP1A2 and probably also UGTs (Kroon, 2007; Moschny et al., 2021). Therefore, smoking may influence the elimination of clozapine and olanzapine,

Table 2 – Basic pharmacokinetics parameters of SGAs

Drug	F (%)	Protein binding (%)	T_{max} (hours)	Half-life (hours)	Time to reach steady-state (days)	Usual oral dose range (mg/day)	Usual maximum oral dose (mg/day)
Aripiprazole	87	>99	3–5	75	14	10–30	30
Brexpiprazole	95	>99	4	91	10–12	2–4	4
Cariprazine	100	91–97	3–4	48–96	10–20	1.5–6	6
Clozapine	27–50	97	1–4	9–17	5–7	150–600	900
Lurasidone	9–19	>99	1–3	18–37	7	40–160	160
Olanzapine	60	93	5–8	21–54	5–10	10–20	30
Paliperidone	28	74	24	23	4–5	6–12	12
Quetiapine IR Quetiapine ER	70	83	1–1.5 6	5 8	1–2 2–3	150–750 400–800	800 800
Risperidone	70–85	90	1	EM: 3 PM: 20	4–6	2–6	8

SGAs are listed alphabetically; source: Hiemke et al. (2018); SmPCs – www.ema.europa.eu

SGAs – second-generation antipsychotics; F – bioavailability; T_{max} – time to reach maximum plasma concentrations; IR – immediate release; ER – extended release; EM – extensive metaboliser; PM – poor metaboliser

Table 3 – Forms of cytochrome P450 involved in the metabolism of SGAs and their active metabolites (major metabolic routes are in bold)

Drug	Enzymes responsible for metabolisation	Active metabolite
Aripiprazole	**CYP3A4, CYP2D6**	dehydroaripiprazole
Brexpiprazole	**CYP3A4, CYP2D6**	–
Cariprazine	**CYP3A4**, CYP2D6	desmethyl cariprazine and didesmethyl cariprazine
Clozapine	**CYP1A2, CYP3A4**, CYP2C19, CYP2C9, CYP2D6	norclozapine
Lurasidone	**CYP3A4**, BCRP	two active metabolites (ID-14283 and ID-14326)
Olanzapine	**CYP1A2**, CYP2D6, UGT1A4	N-desmethylolanzapin
Paliperidone	CYP3A4, P-glycoprotein	–
Quetiapine	**CYP3A4**, CYP2D6	norquetiapine
Risperidone	**CYP2D6, CYP3A4, P-glycoprotein**	9-hydroxyrisperidone (= paliperidone)

SGAs are listed alphabetically; source: Hiemke et al. (2018); Carrascal-Laso et al. (2021)
SGAs – second-generation antipsychotics; CYP – cytochrome P450; UGT – uridine diphosphate-glucuronosyltransferase; BCRP – breast cancer resistance protein

whose metabolism is mainly dependent on CYP1A2 and UGTs. Different studies have shown that plasma concentrations of clozapine (and its metabolite norclozapine) and olanzapine are lower, at the same dose, in smokers as compared to non-smokers (Tsuda et al., 2014; Moschny et al., 2021). Smoking cessation, if not accompanied by a dosage decrease, may be associated with increased plasma concentrations of these antipsychotics, possibly resulting in dose-related toxic effects (Gee et al., 2017).

Aripiprazole

Aripiprazole is well absorbed, with peak plasma concentrations occurring within 3 to 5 hours after dosing. Aripiprazole undergoes minimal pre-systemic metabolism. The absolute oral bioavailability of the tablet formulation is 87% (Harrison and Perry, 2004; Mauri et al., 2017). At therapeutic concentrations, aripiprazole and dehydro-aripiprazole are more than 99% bound to serum proteins, primarily to albumin (Aripiprazole, 2009; Gettu and Saadabadi, 2023). Aripiprazole is extensively metabolised by the liver by three major biotransformation pathways: dehydrogenation, hydroxylation, and N-dealkylation. Based on *in vitro* studies, CYP3A4 and CYP2D6 enzymes are responsible for the dehydrogenation and hydroxylation of aripiprazole, while N-dealkylation is catalysed by CYP3A4

(Mauri et al., 2017; Gettu and Saadabadi, 2023). Aripiprazole is the predominant medicinal product moiety in systemic circulation. At steady state, dehydro-aripiprazole, the active metabolite, represents about 40% of aripiprazole area under the concentration-time curve (AUC) in plasma (Aripiprazole, 2009). The mean elimination half-lives for aripiprazole are 75 and 146 hours in extensive and poor metabolisers of CYP2D6, respectively (Aripiprazole, 2009; Hart et al., 2022).

Brexpiprazole

Following its oral administration, brexpiprazole is extensively absorbed, with peak plasma concentrations occurring within 4 hours and the absolute oral bioavailability of the tablet formulation of 95% (Ishigooka et al., 2018). Brexpiprazole steady-state concentrations are attained within 10 to 12 days of dosing (Markovic et al., 2017; Mauri et al., 2017; Brexpiprazole, 2018). Brexpiprazole is highly protein-bound in plasma (more than 99%) (Brexpiprazole, 2018). The metabolism of brexpiprazole was shown to be mainly mediated by CYP3A4 and CYP2D6 leading to the formation of oxidative metabolites, with only one metabolite, DM-3411, present in plasma with more than 10% of plasma exposure. At steady-state, DM-3411 represents 23.1 to 47.7% of brexpiprazole exposure (AUC) in plasma (Brexpiprazole, 2018; Ishigooka et al., 2018). It should be noted that *in vivo* preclinical studies have shown that at clinically relevant plasma exposures of brexpiprazole, DM-3411 brain exposures were below the detection limit. Thus, DM-3411 is considered not to contribute to the therapeutic effects of brexpiprazole (Markovic et al., 2017; Brexpiprazole, 2018). After multiple once-daily administration of brexpiprazole, the terminal elimination half-life of brexpiprazole and DM-3411 is 91 and 85 hours, respectively (Markovic et al., 2017; Brexpiprazole, 2018). Population pharmacokinetic evaluation shows that CYP2D6 poor metabolisers have 47% higher exposure to brexpiprazole compared to extensive metabolisers (Ishigooka et al., 2018).

Cariprazine

The pharmacokinetics of cariprazine was tested in small short-term studies in both healthy volunteers and subjects with schizophrenia, with similar results (Nakamura et al., 2016; Cariprazine, 2017). Cariprazine is rapidly absorbed, reaching peak concentrations between 3 and 4 hours after oral dosing in healthy subjects. Its pharmacokinetics was linear in terms of AUC, but maximum concentration was more than proportional within the dose range from 3 to 5 mg in healthy subjects. Mean half-life was 2–5 days (1.5–12.5 mg/day) in the subjects with schizophrenia (Nakamura et al., 2016). Cariprazine is then primarily cleared by hepatic metabolism, mostly by CYP3A4 and, to a lesser extent, by CYP2D6. There are two active metabolites of note: desmethyl-cariprazine (DCAR) and didesmethyl-cariprazine (DDCAR): cariprazine activity is thought to be mediated by cariprazine itself and its two major active metabolites, which are pharmacologically equipotent to the maternal drug (Nakamura et al., 2016; Mauri et al., 2017). Cariprazine and its major

active metabolites are highly bound to plasma proteins (Cariprazine, 2017). Total cariprazine (sum of cariprazine + DCAR and DDCAR) exposure approaches 50% of steady state exposure in ~1 week of daily dosing while 90% of steady state is achieved in 3 weeks. At a steady state, exposure to DDCAR is approximately two to three-fold higher than to cariprazine, and exposure to DCAR is approximately 30% of cariprazine exposure (Nakamura et al., 2016; Cariprazine, 2017).

Clozapine

After oral administration, the drug is rapidly absorbed. The bound fraction is 97%. In steady-state conditions, peak blood levels occur 2.1 hours after administration (range 0.4 to 4.2 hours), and the Vd is 1.6 l/kg. Its elimination is biphasic, with a mean terminal half-life of 9–17 hours (Clozapine, 2002), resulting in achieving of steady-state plasma concentrations after 5–7 days of dosing. Clozapine is metabolized primarily by CYP1A2, with additional contributions by CYP2C19, CYP2C9, CYP2D6 and CYP3A4. Glucuronidation by UGT1A1, 1A3 and 1A4 is an important pathway in its metabolism (Erickson-Ridout et al., 2012). The main active metabolites are norclozapine (CYP1A2) and clozapine-N-oxide (CYP3A4), that are found in plasma at concentrations that are usually 50–90% and 10–35% of the concentrations of clozapine, respectively (Clozapine, 2002; Mauri et al., 2017; Correll et al., 2022).

Lurasidone

Lurasidone is rapidly absorbed and reaches peak serum concentration in approximately 1–3 hours after oral administration (Mauri et al., 2014). In a food effect study, lurasidone mean C_{max} and AUC were increased approximately by 2–3-times and 1.5–2-times, respectively, when administered with food compared to the levels observed under fasting conditions (Citrome, 2012a; Lurasidone, 2018). Its pharmacokinetics was linear in the range of 20–60 mg in healthy subjects and subjects with schizophrenia, but inter-individual variability was high (30–60%) in terms of C_{max} and AUC. Lurasidone shows a high rate of binding to human plasma albumin and α-1-glycoprotein (99%) (Citrome, 2013). The mean terminal half-life at steady state ranges from 18 to 37 hours in patients with schizophrenia (Lurasidone, 2018). Thus, after repeated oral doses in patients with schizophrenia, steady-state concentrations of lurasidone are reached within 7 days of starting lurasidone (Caccia et al., 2012; Citrome, 2013). Elimination is essentially by metabolism, primarily involving CYP3A4. The two main metabolites, the acidic derivative ID-20219 and its hydroxylated derivative ID-20220, have negligible affinities for D2 receptors and 5-HT1A, 5-HT2A and 5-HT7 receptors (Caccia et al., 2012; Citrome, 2013; Lurasidone, 2018).

Olanzapine

Approximately 85% of an oral olanzapine dose is absorbed, but due to inactivation by first-pass hepatic metabolism, overall oral bioavailability is around 60%. The peak

plasma concentration is reached within 5 to 8 hours (Olanzapine, 2006). The drug is 93% bound to plasma proteins. A mean elimination half-life of 33 hours (range 21–54 hours) leads to achieving the steady-state concentrations within 5–10 days of usage (Darby et al., 2008; Thomas and Saadabadi, 2023). Olanzapine is metabolized primarily by CYP1A2 and UGTs and with lesser extent by CYP2D6, CYP3A4 and flavin monooxygenase. The predominant pharmacologic activity comes from the parent olanzapine (Erickson-Ridout et al., 2011).

Paliperidone

Paliperidone is commercialised as an extended-release (XR) formulation. Following a single dose, paliperidone exhibits a gradual ascending release rate, allowing the plasma concentrations of paliperidone to steadily rise to reach C_{max} approximately 24 hours after dosing (Citrome, 2012b). With once-daily dosing of paliperidone XR, the terminal half-life is about 23 hours with a steady-state concentration attained in 4–5 days of dosing in most subjects (Paliperidone, 2021). The absolute oral bioavailability of paliperidone following paliperidone XR administration is 28% (Paliperidone, 2021). The plasma protein binding of paliperidone is 74% (Citrome, 2012b). Paliperidone XR undergoes very limited hepatic metabolism, with approximately 60% of the unchanged drug excreted via the kidneys and 11% eliminated unchanged in the faeces. Paliperidone XR does not appear to possess enzyme-inducing or enzyme-inhibiting properties as shown by the lack of CYP inhibition in *in vitro* studies with human liver microsomes (Citrome, 2012b; Mauri et al., 2017).

Quetiapine

After oral administration, quetiapine is well absorbed and extensively metabolized. The volume of distribution is 10 ± 4 l/kg. The pharmacokinetics of quetiapine and norquetiapine remains linear across approved dosing ranges (Mauri et al., 2017). Median C_{max} is reached within 1–1.5 hours for immediate-release (IR) formulation, and in 6 hours for extended-release (ER) formulation, respectively (Quetiapine, 2014). The drug is 83% bound to plasma proteins and is eliminated with an elimination half-life of 5–8 hours. Steady-state concentrations are achieved within 1–3 days of administration (Quetiapine, 2014; Maan et al., 2023). Quetiapine is extensively metabolised by the liver (Quetiapine, 2014), predominantly by CYP3A4-mediated sulfoxidation and dealkylation, and by CYP2D6 which is involved in the 7-hydroxylation of quetiapine (together with CYP3A4) (Mauri et al., 2017; Maan et al., 2023).

Risperidone

Risperidone is well and rapidly absorbed after oral administration with peak plasma concentration being reached in about 1 hour and oral bioavailability of about 70–85%. It mainly undergoes 9-hydroxylation in the liver that yields the active

metabolite 9-OH-risperidone, a step that is mainly catalysed by CYP2D6 and, to a lesser extent, by CYP3A4 (Zhou et al., 2006). As the pharmacological properties of 9-OH-risperidone are like those of risperidone, both are regarded as being able to contribute to the drug's overall antipsychotic effects in the treatment of schizophrenia, and thus represent the active moiety (Risperidone, 2008). For this reason, the ratio between risperidone and 9-OH-risperidone may play a crucial role in mediating the clinical effect (Paulzen et al., 2016; Schoretsanitis et al., 2016). Genetic influences, such as CYP2D6 genotype, play an important role in determining the variability of the pharmacokinetic parameters of risperidone (Vandenberghe et al., 2015). The mean half-life of risperidone is 3 hours in extensive metabolisers (most of the population), and 20 hours in poor metabolisers; the mean half-life of the active moiety (risperidone and its main metabolite) is almost constant at about 22 hours in both groups (Risperidone, 2008). Steady-state concentrations are reached within 5 days of treatment. Risperidone and its main metabolite are 89 and 77% bound to plasma proteins, respectively (Risperidone, 2008). Most of the 9-OH-risperidone is removed through renal excretion (Risperidone, 2008).

Therapeutic drug monitoring of SGAs

TDM allows responding to individual differences revealed during treatment by correct interpretation of clinical and laboratory findings. It gives the opportunity to avoid side effects, toxicity or lack of efficacy. Such optimization is intended to reduce the cost of treatment while increasing the patient safety.

In 2018, the TDM group of the Arbeitsgemeinschaft für Neuropsychopharmakologie und Pharmakopsychiatrie (AGNP) has published literature-based guidelines for the optimal use of TDM in psychiatry, and defined 4 levels of recommendation, based on empirical evidence (Table 4) (Hiemke et al., 2018).

Routine TDM is recommended especially for substances with a well-defined therapeutic reference range and a narrow therapeutic index (e.g. clozapine, olanzapine etc.). For other antipsychotics, TDM is recommended in specific situations. Table 5 presents a list of indications for TDM in psychiatry. The validity of these indications has to be examined and evaluated for each case individually (Bhavsar et al., 2024). Like any diagnostic test, TDM should only be requested when there is evidence that the result will provide an answer to a well-defined question (Steen et al., 2016; McCutcheon et al., 2018; Baldelli et al., 2021).

As for the timing of blood collection, it must be considered that TDM-guided psychopharmacotherapy mostly relies on trough drug concentrations (C_{trough}) at steady-state. A steady-state is reached under constant doses after at least 4 to 6 elimination half-lives and C_{trough} at the end of the longest dosing interval. For practicability, most blood samples taken for determination of C_{trough} are withdrawn in the morning before the first dose of the day, which is mostly the time of minimal

Table 4 – Levels of recommendation for TDM in psychiatry

Level	Evidence	Recommendation	Clinical consequences
1 = strongly recommended	Reported drug concentrations are established and evaluated therapeutic reference ranges. Controlled clinical trials have shown beneficial effects of TDM, reports on decreased tolerability or intoxications.	TDM is strongly recommended for dose titration and for special indications.	At therapeutic PC highest probability of response or remission; at "subtherapeutic" PC: response rate like placebo under acute treatment and risk of relapse under chronic treatment; at "supratherapeutic" PC: risk of intolerance or intoxication.
2 = recommended	Reported drug concentrations were obtained from PC at therapeutically effective doses and related to clinical effects; reports on decreased tolerability or intoxications at "supratherapeutic" PC.	TDM is recommended for dose titration and for special indications or problem solving.	TDM will increase the probability of response in non-responders. At "subtherapeutic" PC: risk of poor response; at "supratherapeutic" PC: risk of intolerance or intoxication.
3 = useful	Reported drug concentrations were calculated from PC at effective doses obtained from pharmacokinetic studies. PC related to pharmacodynamic effects are either not yet available or based on retrospective analysis of TDM data, single case reports or non-systematic clinical experience.	TDM is useful for special indications or problem solving.	TDM can be used to control whether PC are plausible for a given dose, or clinical improvement may be attained by dose increase in nonresponders who display too low PC.
4 = potentially useful	PC do not correlate with clinical effects due to unique pharmacology of the drug, e.g., irreversible blockade of an enzyme, or dosing can be easily guided by clinical symptoms, e.g., sleep induction by a hypnotic drug.	TDM is not recommended for dose titration but may be potentially useful for special indications or problem solving.	TDM should be restricted to special indications.

Source: modifying according to Hiemke et al. (2018)
TDM – therapeutic drug monitoring; PC – plasma concentration

Table 5 – Typical indications for measuring drug concentrations in the blood of psychiatric patients

Uncertain adherence to medication
Narrow therapeutic range
Patients with abnormally high or low body weight
Clinical improvement and adverse effects under recommended doses
Combination treatment with a drug known for its interaction potential or suspected drug interaction
Lack of clinical improvement under recommended doses
Patients with pharmacokinetically relevant comorbidity (hepatic or renal insufficiency, cardiovascular disease)
Specific patient groups (pregnant or breastfeeding, children or adolescents, elderly patients > 65 years)
Patients with intellectual disability
Forensic psychiatric patients
Patients with restrictive gastrointestinal resection or bariatric surgery
Problem occurring after switching from an original preparation to a generic form
Presence of a genetic peculiarity concerning drug metabolism (genetic deficiency, gene multiplication)

Source: modifying according to Hiemke et al. (2018)

Table 6 – Recommended therapeutic reference ranges, laboratory alert levels and levels of recommendation for TDM

Drug	Level	Therapeutic reference range (ng/ml)	Laboratory alert level (ng/ml)
Aripiprazole	2	100–350	1000
Brexpiprazole	3	40–140	280
Cariprazine	3	10–20	40
Clozapine	1	100–350	1000
Lurasidone	3	15–40	120
Olanzapine	1	20–80	100
Paliperidone	2	20–60	120
Quetiapine	2	100–500	1000
Risperidone	2	20–60	120

SGAs are listed alphabetically; source: Hiemke et al. (2018); Schoretsanitis et al. (2020)
SGAs – second-generation antipsychotics; TDM – therapeutic drug monitoring

drug concentrations (Urban and Cubała, 2017; Baldelli et al., 2021). A frequent problem, however, is blood sampling at different time points throughout the dosing interval. This leads to concentrations that may be misinterpreted when true trough levels are lower or higher. It is also necessary to consider the pharmaceutical form, which can change the pharmacokinetics of the drug itself (e.g. long-acting injectable antipsychotics or extended-release tablets).

For most used psychotropic drugs, a reference therapeutic range is established, usually given in ng/ml (Table 6) (Hiemke et al., 2018; Schoretsanitis et al., 2020). It is defined by a minimum therapeutic concentration below which there is a risk of ineffectiveness of the drug, and a maximum therapeutic concentration, after exceeding which there is a significantly higher risk of adverse effects and toxicity. Blood concentrations with an increased risk of toxicity are normally much higher than the upper thresholds of therapeutic reference ranges and are defined as "laboratory alert level" (Table 6) (Hiemke et al., 2018). The laboratory alert should lead to a dose reduction when the patient exhibits signs of intolerance or toxicity. When the high drug concentration is well tolerated by the patient and if dose reduction bears the risk of symptom exacerbation, the dose should remain unchanged (Schoretsanitis et al., 2020; Baldelli et al., 2021).

Reference therapeutic ranges of antipsychotics are established for patients aged 18–65 years. These limits are not set for children and seniors. In the case of antipsychotics, they are intended only for patients with psychotic disorders. It is not clear whether they can be applied, for example, to patients with affective disorders,

Table 7 – Ranges of metabolite-to-parent drug concentration ratios

Drug	Active metabolite	Metabolite to compound ratios
Aripiprazole	dehydroaripiprazole	0.3–0.5
Brexpiprazole	–	–
Cariprazine	N, N-didesmethyl-cariprazine	3–6
Clozapine	norclozapine	non-smokers: 0.5–0.6 smokers: 0.4–0.7
Lurasidone	two active metabolites (ID-14283 and ID-14326)	–
Olanzapine	N-desmethyl-olanzapine	non-smokers: 0.1–0.3 smokers: 0.2–0.4
Paliperidone	–	–
Quetiapine	N-desalkyl-quetiapine	0.54–3.10
Risperidone	9-hydroxy-risperidone (= paliperidone)	3.6–22.7

SGAs are listed alphabetically; source: Hiemke et al. (2018); Schoretsanitis et al. (2020)
SGAs – second-generation antipsychotics

which is a group of patients that are relatively often treated with antipsychotics (Hiemke et al., 2018; McCutcheon et al., 2018; Baldelli et al., 2021).

For several SGAs, metabolites actively contribute to the overall clinical effect of the parent compound. For this reason, TDM should contain the quantification of active metabolites. Table 7 shows the ratios of concentrations of metabolites to parent drugs. The calculated ranges contain 68% of the ratios expected at standard doses, i.e. ratios within the range of mean ± 1 SD (standard deviation) assuming a normal distribution (Hiemke et al., 2018; Schoretsanitis et al., 2020). A ratio above or below the "normal ratio" may indicate drug adherence problems or metabolic abnormalities due to genetic variation or drug-drug interactions with comedications exhibiting enzyme-inhibiting or inducing properties.

Aripiprazole

The dose range for aripiprazole is well-defined, and it reliably predicts the plasma level, dopamine receptor occupancy, and clinical response (Sparshatt et al., 2010). Plasma level variation appears to have a minimal impact on clinical response, but it may predict some adverse effects. TDM has a limited value in the clinical use of aripiprazole, but it may be useful in assuring adherence and optimizing the response in individuals.

Kirschbaum et al. (2005, 2008) measured and related to dose, co-medication, and clinical effects of aripiprazole and dehydroaripiprazole serum concentrations in patients with psychiatric disorders, including therapeutic effects and side effects. In several studies, patients were treated with mean doses of 20 mg/day (± 8 SD); range 7.5–60 mg/day of aripiprazole (Kirschbaum et al., 2005, 2008). Serum concentrations correlated significantly with the dose. Mean concentrations of the active metabolite dehydroaripiprazole amounted to 40% of the parent compound. Co-medication with CYP3A4 and CYP2D6 inducers or inhibitors changed serum concentrations up to 51% (Kirschbaum et al., 2008). The authors reported the best improvement with serum concentrations between 150 and 300 ng/ml. None, or only mild side effects were detected in patients, with aripiprazole plasma concentrations between 110 and 249 ng/ml (Kirschbaum et al., 2008). In literature analysing the studies, the safe and effective plasma concentration of aripiprazole is suggested to be in the range of 150–210 ng/ml (Sparshatt et al., 2010; Hart et al., 2022).

In most patients, the relationship between the dose and the achieved concentration is proportional. It should be noted that at a concentration above 100–150 ng/ml, the occupancy of D2 and D3 receptors reaches maximum saturation (Gründer et al., 2008). In other studies, the concentrations achieved by patients of different age, sex, BMI (body mass index), having different smoking habits, and taking other medicines (such as fluoxetine, and paroxetine) were compared. There were no significant effects of these factors on the plasma concentrations of aripiprazole (Molden et al., 2006; Bachmann et al., 2008; Kim et al., 2008). Significant differences

were expressed in patients with different CYP2D6 genotypes who metabolize the drug to a variable extent and reach similar concentrations at doses that differ by up to 40% (Hendset et al., 2007; Zhang et al., 2018).

The EMA recommends (Aripiprazole, 2009) dose adjustment for aripiprazole in patients who are known CYP2D6 poor metabolizers (PMs). Concentration/dose (C/D) ratios recorded in 62 patients treated with oral aripiprazole indicated that PMs typically need 30–40% lower doses to achieve similar serum concentrations as normal metabolizers (NMs) (Hendset et al., 2007). Suzuki et al. (2014b) demonstrated that subjects with any or reduced functional alleles (×5 and ×10) for CYP2D6 had higher C/D ratios of the active moiety of the two compounds than those without the alleles. In a retrospective cohort study including pharmacokinetic data from 890 patients, it was found that aripiprazole active moiety exposure increased 1.6 times and 1.4 times for PMs and intermediate metabolizers (IMs), respectively (Jukic et al., 2019).

Because serum concentrations of aripiprazole and dehydroaripiprazole were highly variable between individuals and distinct ranges were associated with good therapeutic response and minimal side effects (Lopez and Kane, 2013; Bustillo et al., 2018; Jovanović et al., 2020), the authors suggested that TDM could help improve the antipsychotic therapy. According to the AGNP consensus guidelines (Hiemke et al., 2018), aripiprazole TDM is recommended (recommendation level 2) indicating a therapeutic range between 150 and 350 ng/ml (Table 6).

Brexpiprazole

There are limited data available. In any case, following a multiple oral administration, the C_{max} and AUC_{24h} of brexpiprazole and its metabolite DM-3411 increased in a dose-dependent manner (Ishigooka et al., 2018). These results showed dose proportionality for C_{max} and AUC_{24h} of brexpiprazole. Moreover, the C_{max} and AUC_{24h} of brexpiprazole showed an accumulation of about 2.5- to 5.5-fold on day 14, compared with those on day 1 (Ishigooka et al., 2018). Brexpiprazole C_{max} values following multiple once-daily administrations of 1 mg, on days 1 and 14 were 10.2 ± 5.0 ng/ml and 29.3 ± 15.1 ng/ml; of 4 mg, 37.0 ± 13.5 ng/ml and 165 ± 102 ng/ml; of 6 mg, 69.9 ± 29.1 ng/ml and 206 ± 123 ng/ml, respectively. For its metabolite DM-3411, C_{max} values were for the brexpiprazole dosage of 1 mg, 3.04 ± 1.30 ng/ml and 15.3 ± 9.3; for the drug dosage of 4 mg, 11.7 ± 6.7 and 66.9 ± 29.2; for the drug dosage of 6 mg, 25.8 ± 8.4 and 128 ± 52 ng/ml, respectively (Ishigooka et al., 2018). According to the AGNP consensus guidelines (Hiemke et al., 2018), cariprazine TDM is potentially useful (recommendation level 3), indicating a therapeutic range of 40–140 ng/ml (Table 6).

Cariprazine

At present, no data regarding cariprazine TDM is available. Prescribing information of the pharmaceutical company demonstrated that after 12 weeks of treatment

with 6 mg/day of cariprazine, steady-state plasma concentrations range from 32 to 49 ng/ml (Frankel and Schwartz, 2017). However, a therapeutic range of cariprazine has not been established (Cariprazine, 2017). According to the AGNP consensus guidelines (Hiemke et al., 2018), cariprazine TDM is potentially useful (recommendation level 3), indicating a therapeutic range of 10–20 ng/ml (Table 6).

Clozapine

Plasma concentrations of clozapine vary widely among individuals, so oral dose is not a reliable indicator of plasma drug concentrations (Dettling et al., 2000; Spina et al., 2000; Samanaite et al., 2018). This wide variability results from interindividual differences in bioavailability and the fact that clozapine is metabolized by highly variable CYP1A2 activity (Spina et al., 2000; Khan and Preskorn, 2005). However, serum determinations showed an acceptably low mean inter-patient variability of 20%, which means that serum clozapine determinations can be used to assess patient compliance. The high inter-individual and low intra-individual variability of clozapine plasma concentrations confirms the utility of TDM. Both the antipsychotic efficacy and adverse effects of clozapine are positively correlated with plasma drug concentration (Spina et al., 2000; Khan and Preskorn, 2005; Tralongo et al., 2023).

Most investigators have found that a threshold plasma concentration of 350–420 ng/ml is associated with an increased likelihood of a good clinical response to the drug. In addition, most of the data reviewed suggest that increasing the oral dose of clozapine in non-responders to achieve a plasma concentration of at least 350–420 ng/ml may improve response rates to treatment (Fabrazzo et al., 2002; Wong et al., 2006; Kitchen et al., 2021).

Concentrations above 1,000 ng/ml significantly increase the risk of confusion, delirium and generalized seizures (Khan and Preskorn, 2005; Kitchen et al., 2021; Skokou et al., 2022; Tralongo et al., 2023). Clozapine-induced obsessive/compulsive symptoms have been reported by many authors and they were not uncommon side effects. The authors suggest that the emergence of these side effects may be related to higher plasma concentration of clozapine and clinicians should routinely check for and manage these side effects (Lin et al., 2006; Kim et al., 2019).

Plasma concentrations of clozapine (and the probability of reaching a given threshold value) can be influenced by many factors, such as age, sex, and smoking (Krivoy et al., 2021). TDM is useful especially when poor compliance is suspected, in patients with altered pharmacokinetics (e.g. ultrarapid CYP1A2 metabolizers, concomitant treatment with strong CYP1A2 inhibitor), and in non-responders who require the use of very high doses (Eap et al., 2004; Schoretsanitis et al., 2023). Inflammatory reactions may suddenly increase clozapine concentrations and lead to toxic delirium (Clark et al., 2018; Moschny et al., 2021).

Clozapine still represents the gold standard in the treatment of drug-resistant schizophrenia, and the optimal plasma levels for acute and maintenance clozapine

treatment are well known. Experience from the literature shows that TMD in clinically defined subgroups of patients, such as pharmacoresistant schizophrenia, is clinically beneficial.

Lurasidone

At present, no evidence about lurasidone TDM is available. It is reported that following single-dose administration of 40 and 80 mg lurasidone-hydrochloride (corresponds to 37 and 74 mg of the free base), the mean C_{max} values in serum were approximately 54 and 64 ng/ml, respectively. Following steady-state administration of 40 mg and 80 mg, the mean C_{max} values in serum were approximately 48 and 79 ng/ml, respectively (Caccia et al., 2012; Greenberg and Citrome, 2016). According to the AGNP consensus guidelines (Hiemke et al., 2018), lurasidone TDM is potentially useful (recommendation level 3), indicating a therapeutic range of 15–40 ng/ml (Table 6).

Olanzapine

The studies showed that mean plasma olanzapine concentrations vary widely, depending on factors such as the prescribed daily dose and the duration of treatment (Darby et al., 2008). The reviewed studies strongly indicate a relationship between clinical outcomes and plasma olanzapine concentrations (Lane et al., 2002; Bergemann et al., 2004; Mauri et al., 2005). However, a large inter-patient variability in plasma olanzapine concentrations after administration of the same dose is described (Mauri et al., 2007; Citrome et al., 2009). Smokers and men show greater olanzapine clearance than women and non-smokers, which is mirrored in significantly lower mean plasma concentrations that become evident after the fifth week of treatment (Moschny et al., 2021). Stopping smoking may be associated with an increase in side effects, such as extrapyramidal symptoms, within a few days, unless the dose is adjusted (Spina and de Leon, 2007; Urichuk et al., 2008).

The monitoring of blood olanzapine concentrations can be considered very useful in assessing therapeutic efficacy and controlling adverse events. A therapeutic range has been established between 20 and 50 ng/ml. Levels above 50 ng/ml might be associated with a higher risk of extrapyramidal symptoms (Perry et al., 2001; Lane et al., 2002; Fellows et al., 2003; Mauri et al., 2005). A positron emission tomography study analysed the differences in D2 receptor occupancy based on olanzapine dose/plasma olanzapine concentrations. It found a relationship between plasma olanzapine concentrations and D2 occupancy (Gründer et al., 2011). Olanzapine is a potent 5-HT2 blocker and shows greater 5-HT2 than D2 occupancy at all doses. At a plasma concentration of 10.3 ng/ml, olanzapine occupied 50% of the available D2 receptors. Within the usual clinical range of 10–20 mg/day, D2 occupancy varies from 71 to 80% (Moresco et al., 2004; Gründer et al., 2011). Attarbaschi et al. (2007) have explored the relationship between striatal D2 receptor occupancy and extra-pyramidal symptom (EPS) in 17 patients with bipolar disorder receiving

olanzapine 5–45 mg/day for at least 14 days, and found a significant correlation between plasma concentrations and occupancy. The bipolar patients did not show any EPS at D2 occupancy levels of 28–80 ng/ml (Attarbaschi et al., 2007).

Further investigations, including long-term studies, may provide more specific indications and possibly indicate a narrower therapeutic range. According to the AGNP TDM consensus group, olanzapine TDM is strongly recommended (recommendation level 1), as an established therapeutic range (20–80 ng/ml) is proposed to yield an optimal response and minimise side effects (Hiemke et al., 2018) (Table 6).

Paliperidone

In a 6-week study of patients with schizophrenia receiving paliperidone daily doses of 3, 9 and 15 mg, the optimal range of doses was calculated based on position emission tomography measures (receptor occupancy in the striatum and the temporal cortex) and the plasma concentrations of the drug (Arakawa et al., 2008). An optimal D2 receptor occupancy was found at the level of 70–80% at doses of 6–9 mg/day (Arakawa et al., 2008). In the study by Muly et al. (2012), D2 receptor occupancy was evaluated in different areas of the brain in macaques receiving risperidone and paliperidone, and compared with plasma and cerebrospinal fluid concentrations. The optimum plasma concentration range of 40–80 ng/ml for both substances was confirmed (Muly et al., 2012).

The retrospective analysis of data obtained from 217 patients from four medical centres investigated the relationship between serum paliperidone concentrations and clinical outcomes (Nazirizadeh et al., 2010). Intra-individual variability of trough serum concentrations was also analysed in patients treated with either paliperidone XR or risperidone IR (Nazirizadeh et al., 2010). The mean paliperidone concentration was 36 ± 25 ng/ml, and the mean dose-corrected concentration was 4.7 ± 2.9 ng/ml/mg. Among patients receiving paliperidone as antipsychotic monotherapy, who showed at least a much-improved level according to the Clinical Global Impressions Scale (CGI Score), the 25^{th}–75^{th} percentiles of paliperidone concentrations were 20–52 ng/ml; these were very similar to the recommended therapeutic range of 20–60 ng/ml for risperidone plus 9-hydroxy-risperidone (Nazirizadeh et al., 2010).

In other reports, the same therapeutic range of 20–60 ng/ml is proposed, as for risperidone (Liu et al., 2015). In paliperidone therapy, the relation between clinical improvement, risk of extrapyramidal symptoms, increased prolactin levels and plasma concentrations, is not linear (Suzuki et al., 2014a). It has also been noticed that CYP2D6 polymorphism does not significantly affect the plasma concentrations of the drug (Patteet et al., 2015).

The authors concluded that risperidone and paliperidone have a similar therapeutic range and similar intra-individual variability in terms of trough serum concentrations. For treatment optimisation, monitoring of plasma concentrations may be as

useful for paliperidone as for risperidone (Nazirizadeh et al., 2010). According to the AGNP consensus guidelines (Hiemke et al., 2018) paliperidone TDM is recommended (recommendation level 2) (Table 6).

Quetiapine

Only a few short-term studies have investigated the relationship between quetiapine plasma concentrations and clinical responses (DeVane and Nemeroff, 2001; Sparshatt et al., 2008; Handley et al., 2013). Although the data from Takano et al. (2004) argue in favour of the existence of a relationship between plasma quetiapine concentrations and clinical responses, they provide only some preliminary information about the significance of plasma quetiapine concentrations. Other authors have failed to identify an optimal therapeutic range for quetiapine (Melnik et al., 2010; Sparshatt et al., 2011). Only a relationship between the dose and D2 receptor occupancy and preferential D2 receptor binding in the extrastriatal areas was observed (Vernaleken et al., 2010; Gründer et al., 2011; Sparshatt et al., 2011). Similar results were obtained in 80% of patients in mono and polytherapy, significantly lower concentrations were obtained only in patients co-administered with carbamazepine (Hasselstrøm and Linnet, 2004; Castberg et al., 2007).

The influence of age and sex on the increase of quetiapine concentrations was confirmed, with higher concentrations in women having no clinical significance (Aichhorn et al., 2006). An exceptional increase in the concentration of quetiapine has been noticed with valproate co-administration. An additional factor is the polymorphism of CYP3A4 among patients. CYP3A4*22 allele is responsible for an increase in quetiapine concentration (van der Weide and van der Weide, 2015).

The therapeutic range of 100–500 ng/ml was proposed in the AGNP guidelines (Hiemke et al., 2018). TDM is therefore recommended to check that plasma concentrations are acceptable for administered doses and to optimize clinical response in non-responders with low concentrations (Hiemke et al., 2018). However, only a few results are currently available and they do not entirely support the value of plasma concentration for adjusting quetiapine doses in clinical practice; further investigations are therefore necessary.

Risperidone

The overall pharmacological effects of risperidone depend on the sum of the plasma concentrations of risperidone and its metabolite 9-OH-risperidone, and thus monitoring plasma concentrations of the parent compound alone may lead to erroneous interpretations (Yoshimura et al., 2001; Aravagiri et al., 2003). It appears that monitoring plasma concentrations of the active moiety may be useful, but further investigations are needed to clarify the discrepancies in the results obtained so far (Paulzen et al., 2016; Korell et al., 2017). This discrepancy may be due to large variability in plasma drug concentrations and a lack of studies using fixed doses. An important indicator of the efficacy of treatment is the D2 receptor occupancy, which

should reach 65% for a minimal therapeutic effect (Remington et al., 2006; Muly et al., 2012).

Both risperidone and 9-OH-risperidone have large intra- and inter-individual differences in plasma concentrations. Since the pharmacological properties of 9-OH-risperidone are like those of risperidone, both can contribute to the overall antipsychotic effects of the drug in the treatment of schizophrenia and thus constitute the active ingredient (Seto et al., 2011).

In chronic schizophrenic patients with an acute exacerbation of the disorder, plasma levels of risperidone and its active metabolite are correlated with the occurrence of Parkinsonian side effects (Spina et al., 2001; Riedel et al., 2004; Darby et al., 2008). The range of therapeutic plasma concentrations of risperidone has not been established yet: the plasma threshold for Parkinsonian side effects is 74 ng/ml, but the minimum effective plasma concentration of the active ingredient is unclear. Some data suggests that the normal range is between 15 and 60 ng/ml, but this needs to be confirmed (Mauri et al., 2001; Puangpetch et al., 2016; Lu et al., 2021).

The effect of the CYP2D6 genotype on risperidone metabolites clearance, with comparable efficiency of treatment, was proven. Poor metabolizers achieved concentrations of active moiety up to 3.3-fold higher at the same doses (Riedel et al., 2004; Locatelli et al., 2010). Similarly, patients with parkinsonism or dystonia as well as chronic patients, achieved higher concentrations (Spina et al., 2001; Yasui-Furukori et al., 2009). Monitoring levels of prolactin could be an effective indicator of the patient's cooperation. Regarding the unequivocally determined relationship between doses, receptor occupancy levels and therapeutic plasma concentrations, monitoring of the latter would seem appropriate only in individual situations, for example, lack of therapeutic response, unexplained adverse effects, or co-medication.

Studies on the pharmacokinetics of risperidone and its metabolites depending on age, gender, body weight, smoking habits, co-administered drugs, and CYP2D6 genotype have been conducted (Feng et al., 2008; Zhang and Malhotra, 2018; Nofziger et al., 2020). It was shown that there is a linear relationship between age and 9-OH-risperidone clearance (Feng et al., 2008).

The conversion of risperidone to 9-hydroxy-risperidone by CYP2D6 suggests inhibition of CYP2D6 or down-regulation of DNA in the first 2 months. The time course of identified accumulations suggests that both CYP inhibition and DNA regulatory mechanisms may participate in drug metabolism. Therefore, long-term TDM may optimize risperidone therapy (Zhang and Malhotra, 2018; Nofziger et al., 2020).

According to the AGNP consensus guidelines (Hiemke et al., 2018), risperidone TDM is recommended (recommendation level 2) as there are suggested therapeutic ranges obtained from plasma concentrations at therapeutically effective doses: the proposed plasma risperidone concentration range is 20–60 ng/ml (Table 6).

Discussion and Conclusion

TDM of antipsychotics is a specific clinical pharmacology method for monitoring therapy by measuring serum drug concentrations, with subsequent interpretation and good collaboration with the clinician. In personalised medicine, it can help individualise dosing for rational therapy, minimize side effects, reduce mortality and morbidity, and reduce healthcare costs. Studies suggest that the pharmacokinetics of certain drugs is characterized by large inter- and intra-individual differences (age, gender, lifestyle, genetic and metabolic characteristics, drug interactions), a narrow therapeutic range or non-linear dose-concentration ratio. All these features provide the need and desirability for TDM for dose optimization or flexible dosing according to clinical symptoms. Phenotyping and genotyping can enhance TDM at a higher level. Antipsychotic plasma concentrations are a valuable but underutilized tool in several clinical conditions. Improving decision-making through better access to information on the plasma concentration of antipsychotics can have a significant impact on the quality of care and outcomes of patients with schizophrenia. However, it is important to emphasize that TDM is not necessarily required for all new antipsychotics, as there is no clear data supporting a relationship between plasma drug concentrations and clinical outcomes or side effects.

A proven exception is the concentration-dependent proconvulsant effects of clozapine, which make TDM highly recommended for overdose prevention (Dettling et al., 2000; Spina et al., 2000; Samanaite et al., 2018), as outlined in the AGNP-TDM general guidelines (Hiemke et al., 2018). Likewise, TDM is recommended to determine the optimal tolerability of olanzapine and risperidone (Yoshimura et al., 2001). Furthermore, there are no clinical pharmacokinetic data, particularly long-term data, for some other atypical antipsychotics, which will require future research. It should be kept in mind that optimal plasma concentration ranges for clozapine, risperidone and olanzapine are suggested by some authors, but not all. Studies of quetiapine provide limited information, and there is no direct data for aripiprazole; however, there are a few reported investigations that need to be confirmed and expanded.

In addition, TDM is a powerful tool that enables treatment tailored to the specific needs of individual patients, identifying “pseudo-pharmacoresistance” issues such as poor compliance, high individual metabolic levels, excessive patient water consumption, excessive smoking, drug abuse, as well as the occurrence of unpredictable side effects and possible drug interactions. The implementation of TDM is based on several disciplines, following pharmacokinetic, pharmacodynamic, analytical and pharmacoeconomic aspects. Determining the serum concentration of the drug alone cannot be considered sufficient. It is necessary to interpret the result in context of the clinical condition of the patient and other available data, considering the basic diagnosis and the pharmacokinetics of the administered drug.

References

Agid, O., Mamo, D. C., Ginovart, N., Vitcu, I., Wilson, A. A., Zipursky, R. B., Kapur, S. (2007) Striatal vs extrastriatal dopamine D2 receptors in antipsychotic response – A double-blind PET study in schizophrenia. *Neuropsychopharmacology* **32(6)**, 1209–1215.

Aichhorn, W., Marksteiner, J., Walch, T., Zernig, G., Saria, A., Kemmler, G. (2006) Influence of age, gender, body weight and valproate comedication on quetiapine plasma concentrations. *Int. Clin. Psychopharmacol.* **21(2)**, 81–85.

Arakawa, R., Ito, H., Takano, A., Takahashi, H., Morimoto, T., Sassa, T., Ohta, K., Kato, M., Okubo, Y., Suhara, T. (2008) Dose-finding study of paliperidone ER based on striatal and extrastriatal dopamine D2 receptor occupancy in patients with schizophrenia. *Psychopharmacology (Berl.)* **197(2)**, 229–235.

Aravagiri, M., Marder, S. R., Nuechterlein, K. H., Gitlin, M. (2003) Intra- and interindividual variations in steady-state plasma concentrations of risperidone and 9-hydroxyrisperidone in schizophrenic patients treated chronically with various doses of risperidone. *Ther. Drug Monit.* **25(6)**, 657–664.

Aripiprazole (2009) *Summary of Product Characteristics. Committee for Medicinal Products for Human Use. European Medicines Agency. European public assessment report*. Available at: https://www.ema.europa.eu/en/documents/product-information/abilify-epar-product-information_en.pdf (Accessed January 6, 2024)

Attarbaschi, T., Sacher, J., Geiss-Granadia, T., Klein, N., Mossaheb, N., Lanzenberger, R., Asenbaum, S., Dudczak, R., Kasper, S., Tauscher, J. (2007) Striatal D(2) receptor occupancy in bipolar patients treated with olanzapine. *Eur. Neuropsychopharmacol.* **17(2)**, 102–107.

Bachmann, C., Rieger-Gies, A., Heinzel-Gutenbrunner, M., Hiemke, C., Remschmidt, H., Theisen, F. (2008) Large variability of aripiprazole and dehydroaripiprazole serum concentrations in adolescent patients with schizophrenia. *Ther. Drug Monit.* **30(4)**, 462–466.

Baldelli, S., Cheli, S., Montrasio, C., Cattaneo, D., Clementi, E. (2021) Therapeutic drug monitoring and pharmacogenetics of antipsychotics and antidepressants in real life settings: A 5-year single centre experience. *World J. Biol. Psychiatry* **22(1)**, 34–45.

Bergemann, N., Frick, A., Parzer, P., Kopitz, J. (2004) Olanzapine plasma concentration, average daily dose, and interaction with co-medication in schizophrenic patients. *Pharmacopsychiatry* **37(2)**, 63–68.

Bhavsar, N., Dopheide, J. A., Botello, T., Wang, M. (2024) Therapeutic drug level monitoring of antipsychotics at an inpatient psychiatric hospital. *Ther. Drug Monit.* **46(2)**, 210–216.

Brexpiprazole (2018) *Summary of Product Characteristics. Committee for Medicinal Products for Human Use. European Medicines Agency. European public assessment report*. Available at: https://www.ema.europa.eu/en/documents/product-information/rxulti-epar-product-information_en.pdf (Accessed January 6, 2024)

Bustillo, M., Zabala, A., Querejeta, I., Carton, J. I., Mentxaka, O., González-Pinto, A., García, S. M., Meana, J. J., Eguíluz, J. I., Segarra, R. (2018) Therapeutic drug monitoring of second-generation antipsychotics for the estimation of early drug effect in first-episode psychosis: A cross-sectional assessment. *Ther. Drug Monit.* **40(2)**, 257–267.

Caccia, S., Pasina, L., Nobili, A. (2012) Critical appraisal of lurasidone in the management of schizophrenia. *Neuropsychiatr. Dis. Treat.* **8**, 155–168.

Cariprazine (2017) *Summary of Product Characteristics. Committee for Medicinal Products for Human Use. European Medicines Agency. European public assessment report*. Available at: https://www.ema.europa.eu/en/documents/product-information/reagila-epar-product-information_en.pdf (Accessed January 6, 2024)

Carrascal-Laso, L., Isidoro-García, M., Ramos-Gallego, I., Franco-Martín, M. (2021) Review: Influence of the CYP450 genetic variation on the treatment of psychotic disorders. *J. Clin. Med.* **10(18)**, 4275.

Castberg, I., Skogvoll, E., Spigset, O. (2007) Quetiapine and drug interactions. *J. Clin. Psychiatry* **68(10)**, 1540–1545.

Citrome, L. (2012a) Lurasidone in schizophrenia: New information about dosage and place in therapy. *Adv. Ther.* **29(10)**, 815–825.

Citrome, L. (2012b) Oral paliperidone extended-release: Chemistry, pharmacodynamics, pharmacokinetics and metabolism, clinical efficacy, safety and tolerability. *Expert Opin. Drug Metab. Toxicol.* **8(7)**, 873–888.

Citrome, L. (2013) A review of the pharmacology, efficacy and tolerability of recently approved and upcoming oral antipsychotics: An evidence-based medicine approach. *CNS Drugs* **27(11)**, 879–911.

Citrome, L., Stauffer, V. L., Chen, L., Kinon, B. J., Kurtz, D. L., Jacobson, J. G., Bergstrom, R. F. (2009) Olanzapine plasma concentrations after treatment with 10, 20, and 40 mg/d in patients with schizophrenia: An analysis of correlations with efficacy, weight gain, and prolactin concentration. *J. Clin. Psychopharmacol.* **29(3)**, 278–283.

Clark, S., Warren, N., Kim, G., Jankowiak, D., Schubert, K. O., Kisely, S., Forrester, T., Baune, B. T., Siskind, D. (2018) Elevated clozapine levels associated with infection: A systematic review. *Schizophr. Res.* **192**, 50–56.

Clozapine (2002) *Summary of Product Characteristics. Committee for Medicinal Products for Human Use. European Medicines Agency. European public assessment report*. Available at: https://www.ema.europa.eu/en/medicines/human/referrals/leponex (Accessed January 6, 2024)

Correll, C. U., Agid, O., Crespo-Facorro, B., De Bartolomeis, A., Fagiolini, A., Seppälä, N., Howes, O. (2022) A guideline and checklist for initiating and managing clozapine treatment in patients with treatment-resistant schizophrenia. *CNS Drugs* **36(7)**, 659–679.

Darby, J., Pasta, D. J., Wilson, M. G., Herbert, J. S. (2008) Long-term therapeutic drug monitoring of risperidone and olanzapine identifies altered steady-state pharmacokinetics: A clinical, two-group, naturalistic study. *Clin. Drug Investig.* **28(9)**, 553–564.

Dettling, M., Sachse, C., Brockmöller, J., Schley, J., Müller-Oerlinghausen, B., Pickersgill, I., Rolfs, A., Schaub, R. T., Schmider, J. (2000) Long-term therapeutic drug monitoring of clozapine and metabolites in psychiatric in- and outpatients. *Psychopharmacology (Berl.)* **152(1)**, 80–86.

DeVane, C. L., Nemeroff, C. B. (2001) Clinical pharmacokinetics of quetiapine: An atypical antipsychotic. *Clin. Pharmacokinet.* **40(7)**, 509–522.

Eap, C. B., Bender, S., Sirot, E. J., Cucchia, G., Jonzier-Perey, M., Baumann, P., Allorge, D., Broly, F. (2004) Nonresponse to clozapine and ultrarapid CYP1A2 activity. *J. Clin. Psychopharmacol.* **24(2)**, 214–219.

Erickson-Ridout, K. K., Zhu, J., Lazarus, P. (2011) Olanzapine metabolism and the significance of UGT1A448V and UGT2B1067Y variants. *Pharmacogenet. Genomics* **21(9)**, 539–551.

Erickson-Ridout, K. K., Sun, D., Lazarus, P. (2012) Glucuronidation of the second-generation antipsychotic clozapine, and its active metabolite N-desmethylclozapine. Potential importance of the UGT1A1 A(TA)7TAA and UGT1A4 L48V polymorphisms. *Pharmacogenet. Genomics* **22(8)**, 561–576.

Fabrazzo, M., La Pia, S., Monteleone, P., Esposito, G., Pinto, A., De Simone, L., Bencivenga, R., Maj, M. (2002) Is the time course of clozapine response correlated to the time course of clozapine plasma levels? A one-year prospective study in drug-resistant patients with schizophrenia. *Neuropsychopharmacology* **27(6)**, 1050–1055.

Fellows, L. M., Ahmad, F., Castle, D., Dusci, L. J., Bulsara, M., Ilett, K. F. (2003) Investigation of target plasma concentration-effect relationships for olanzapine in schizophrenia. *Ther. Drug Monit.* **25(6)**, 682–689.

Feng, Y., Pollock, B. G., Coley, K. C., Marder, S. R., Miller, D. D., Kirshner, M. A., Aravagiri, M., Schneider, L. S., Bies, R. R. (2008) Population pharmacokinetic analysis for risperidone using highly sparse sampling measurements from the CATIE study. *Br. J. Clin. Pharmacol.* **66(5)**, 629–639.

Frankel, J. S., Schwartz, T. L. (2017) Brexpiprazole and cariprazine: Distinguishing two new atypical antipsychotics from the original dopamine stabilizer aripiprazole. *Ther. Adv. Psychopharmacol.* **7(1)**, 29–41.

Gee, S., Taylor, D., Shergill, S. S., Flanagan, R. J., MacCabe, J. H. (2017) Effects of a smoking ban on clozapine plasma concentrations in a nonsecure psychiatric unit. *Ther. Adv. Psychopharmacol.* **7(2)**, 79–83.

Gettu, N., Saadabadi, A. (2023) *Aripiprazole*. StatPearls [Internet]. Available at: https://www.ncbi.nlm.nih.gov/books/NBK547739/ (Accessed January 6, 2024)

Greenberg, W. M., Citrome, L. (2016) Pharmacokinetics and pharmacodynamics of lurasidone hydrochloride, a second-generation antipsychotic: A systematic review of the published literature. *Clin. Pharmacokinet.* **56(5)**, 493–503.

Gründer, G., Fellows, C., Janouschek, H., Veselinović, T., Boy, C., Bröcheler, A., Kirschbaum, K. M., Hellmann, S., Spreckelmeyer, K. M., Hiemke, C., Rösch, F., Schaefer, W. M., Vernaleken, I. (2008) Brain and plasma pharmacokinetics of aripiprazole in patients with schizophrenia: An [18F]fallypride PET study. *Am. J. Psychiatry* **165(8)**, 988–995.

Gründer, G., Hiemke, C., Paulzen, M., Veselinovic, T., Vernaleken, I. (2011) Therapeutic plasma concentrations of antidepressants and antipsychotics: Lessons from PET imaging. *Pharmacopsychiatry* **44(06)**, 236–248.

Grundmann, M., Kacirova, I., Urinovska, R. (2014) Therapeutic drug monitoring of atypical antipsychotic drugs. *Acta Pharm.* **64(4)**, 387–401.

Handley, S. A., Bowskill, S., Patel, M. X., Flanagan, R. J. (2013) Plasma quetiapine in relation to prescribed dose and other factors: Data from a therapeutic drug monitoring service, 2000–2011. *Ther. Adv. Psychopharmacol.* **3(3)**, 129–137.

Harrison, T. S., Perry, C. M. (2004) Aripiprazole: A review of its use in schizophrenia and schizoaffective disorder. *Drugs* **64(15)**, 1715–1736.

Hart, X. M., Hiemke, C., Eichentopf, L., Lense, X., Clement, H. W., Conca, A., Faltraco, F., De Florio, V., Grüner, J., Havemann-Reinecke, U., Molden, E., Paulzen, M., Schoretsanitis, G., Riemer, T., Gründer, G. (2022) Therapeutic reference range for aripiprazole in schizophrenia revised: A systematic review and metaanalysis. *Psychopharmacology (Berl.)* **239(11)**, 3377–3391.

Hasselstrøm, J. B., Linnet, K. (2004) Quetiapine serum concentrations in psychiatric patients: The influence of comedication. *Ther. Drug Monit.* **26(5)**, 486–491.

Hendset, M., Hermann, M., Lunde, H., Refsum, H., Molden, E. (2007) Impact of the CYP2D6 genotype on steady-state serum concentrations of aripiprazole and dehydroaripiprazole. *Eur. J. Clin. Pharmacol.* **63(12)**, 1147–1151.

Hiemke, C., Bergemann, N., Clement, H.-W., Conca, A., Deckert, J., Domschke, K., Eckermann, G., Egberts, K., Gerlach, M., Greiner, C., Gründer, G., Haen, E., Havemann-Reinecke, U., Hefner, G., Helmer, R., Janssen, G. M. E., Jaquenoud, E., Laux, G., Messer, T., Mößner, R., Müller, M. J., Paulzen, M., Pfuhlmann, B., Riederer, P., Saria, A., Schoppek, B., Schoretsanitis, G., Schwarz, M., Gracia, M. S., Stegmann, B., Steimer, W., Stingl, J. C., Uhr, M., Ulrich, S., Unterecker, S., Waschgler, R., Zernig, G., Zurek, G., Baumann, P. (2018) Consensus guidelines for therapeutic drug monitoring in neuropsychopharmacology: Update 2017. *Pharmacopsychiatry* **51(01/02)**, 9–62.

Horvitz-Lennon, M., Mattke, S., Predmore, Z., Howes, O. (2017) The role of antipsychotic plasma levels in the treatment of schizophrenia. *Am. J. Psychiatry* **174(5)**, 421–426.

Ishigooka, J., Iwashita, S., Higashi, K., Liew, E. L., Tadori, Y. (2018) Pharmacokinetics and safety of brexpiprazole following multiple-dose administration to Japanese patients with schizophrenia. *J. Clin. Pharmacol.* **58(1)**, 74–80.

Jovanović, M., Vučićević, K., Miljković, B. (2020) Understanding variability in the pharmacokinetics of atypical antipsychotics – Focus on clozapine, olanzapine and aripiprazole population models. *Drug Metab. Rev.* **52(1)**, 1–18.

Jukic, M., Smith, R. L., Haslemo, T., Molden, E., Ingelman-Sundberg, M. (2019) Effect of CYP2D6 genotype

on exposure and efficacy of risperidone and aripiprazole: A retrospective, cohort study. *Lancet Psychiatry* **6(5)**, 418–426.

Khan, A. Y., Preskorn, S. (2005) Examining concentration-dependent toxicity of clozapine: Role of therapeutic drug monitoring. *J. Psychiatr. Pract.* **11(5)**, 289–301.

Kim, D. D., Barr, A. M., De Vere White, R., Honer, W. G., Procyshyn, R. M. (2019) Clozapine-induced obsessive-compulsive symptoms: Mechanisms and treatment. *J. Psychiatry Neurosci.* **44(1)**, 71–72.

Kim, J. R., Seo, H. B., Cho, J. Y., Kang, D. H., Kim, Y. K., Bahk, W.-J., Yu, K., Shin, S. G., Kwon, J. S., Jang, I. J. (2008) Population pharmacokinetic modelling of aripiprazole, and its active metabolite, dehydroaripiprazole, in psychiatric patients. *Br. J. Clin. Pharmacol.* **66(6)**, 802–810.

Kirschbaum, K. M., Müller, M. J., Zernig, G., Saria, A., Mobascher, A., Malevani, J., Hiemke, C. (2005) Therapeutic monitoring of aripiprazole by HPLC with column-switching and spectrophotometric detection. *Clin. Chem.* **51(9)**, 1718–1721.

Kirschbaum, K. M., Müller, M. J., Malevani, J., Mobascher, A., Burchardt, C., Piel, M., Hiemke, C. (2008) Serum levels of aripiprazole and dehydroaripiprazole, clinical response and side effects. *World J. Biol. Psychiatry* **9(3)**, 212–218.

Kitchen, D., Till, A., Xavier, P. (2021) Routine clozapine assay monitoring to improve the management of treatment-resistant schizophrenia. *BJPsych Bull.* **46(5)**, 267–270.

Korell, J., Green, B., Remmerie, B., Vermeulen, A. (2017) Determination of plasma concentration reference ranges for risperidone and paliperidone. *CPT Pharmacometrics Syst. Pharmacol.* **6(9)**, 589–595.

Krivoy, A., Whiskey, E., Webb-Wilson, H., Joyce, D. W., Tracy, D. K., Gaughran, F., MacCabe, J. H., Shergill, S. S. (2021) Outcomes in treatment-resistant schizophrenia: Symptoms, function and clozapine plasma concentrations. *Ther. Adv. Psychopharmacol.* **11**, 204512532110371.

Kroon, L. A. (2007) Drug interactions with smoking. *Am. J. Health Syst. Pharm.* **64(18)**, 1917–1921.

Lane, H., Guo, S.-C., Hwang, T., Chen, Y.-S., Cheng, J. J. S., Lee, Y.-C., Hong, C., Hwu, H.-G., Chang, W. (2002) Effects of olanzapine plasma concentrations on depressive symptoms in schizophrenia: A pilot study. *J. Clin. Psychopharmacol.* **22(5)**, 530–532.

Lin, S., Su, S.-F., Pan, C. (2006) Higher plasma drug concentration in clozapine-treated schizophrenic patients with side effects of obsessive/compulsive symptoms. *Ther. Drug Monit.* **28(3)**, 303–307.

Liu, H.-Y., Hwang, T., Tsai, I., Kuo, C. (2015) Use of high-conductivity sample solution with sweeping-micellar electrokinetic capillary chromatography for trace-level quantification of paliperidone in human plasma. *Electrophoresis* **36(4)**, 534–542.

Locatelli, I., Kastelic, M., Koprivšek, J., Kores-Plesničar, B., Mrhar, A., Dolžan, V., Grabnar, I. (2010) A population pharmacokinetic evaluation of the influence of CYP2D6 genotype on risperidone metabolism in patients with acute episode of schizophrenia. *Eur. J. Pharm. Sci.* **41(2)**, 289–298.

Lopez, L. V., Kane, J. M. (2013) Plasma levels of second-generation antipsychotics and clinical response in acute psychosis: A review of the literature. *Schizophr. Res.* **147(2–3)**, 368–374.

Lu, J., Yang, Y., Lü, J., Wang, Z., He, Y., Yan, Y., Fu, K., Jiang, W., Xu, Y., Wu, R., Liu, W., Zhao, J. (2021) Effect of CYP2D6 polymorphisms on plasma concentration and therapeutic effect of risperidone. *BMC Psychiatry* **21(1)**, 70.

Lurasidone (2018) *Summary of Product Characteristics. Committee for Medicinal Products for Human Use. European Medicines Agency. European public assessment report*. Available at: https://www.ema.europa.eu/en/documents/product-information/latuda-epar-product-information_en.pdf (Accessed January 6, 2024)

Maan, J. S., Ershadi, M., Khan, I., Saadabadi, A. (2023) *Quetiapine*. StatPearls [Internet]. Available at: https://www.ncbi.nlm.nih.gov/books/NBK459145/ (Accessed January 6, 2024)

Markovic, M., Gallipani, A., Patel, K. H., Maroney, M. (2017) Brexpiprazole. *Ann. Pharmacother.* **51(4)**, 315–322.

Mauri, M. C., Laini, V., Boscati, L., Rudelli, R., Salvi, V., Orlandi, R., Papa, P. (2001) Long-term treatment of chronic schizophrenia with risperidone: A study with plasma levels. *Eur. Psychiatry* **16(1)**, 57–63.

Mauri, M. C., Steinhilber, C., Marino, R., Invernizzi, E., Fiorentini, A., Cerveri, G., Baldi, M., Barale, F. (2005) Clinical outcome and olanzapine plasma levels in acute schizophrenia. *Eur. Psychiatry* **20(1)**, 55–60.

Mauri, M. C., Volonteri, L. S., Colasanti, A., Fiorentini, A., De Gaspari, I. F., Bareggi, S. R. (2007) Clinical pharmacokinetics of atypical antipsychotics. *Clin. Pharmacokinet.* **46(5)**, 359–388.

Mauri, M. C., Paletta, S., Maffini, M., Colasanti, A., Dragogna, F., Di Pace, C., Altamura, A. C. (2014) Clinical pharmacology of atypical antipsychotics: An update. *EXCLI J.* **13(13)**, 1163–1191.

Mauri, M. C., Paletta, S., Di Pace, C., Reggiori, A., Rovera, C., Fiorentini, A., Altamura, C. (2017) Paliperidone long-acting plasma level monitoring and a new method of evaluation of clinical stability. *Pharmacopsychiatry* **50(4)**, 145–151.

Mauri, M. C., Paletta, S., Di Pace, C., Reggiori, A., Cirnigliaro, G., Valli, I., Altamura, A. C. (2018) Clinical pharmacokinetics of atypical antipsychotics: An update. *Clin. Pharmacokinet.* **57(12)**, 1493–1528.

McCutcheon, R., Beck, K., D'Ambrosio, E., Donocik, J., Gobjila, C., Jauhar, S., Kaar, S., Pillinger, T., Marques, T. R., Rogdaki, M., Howes, O. (2018) Antipsychotic plasma levels in the assessment of poor treatment response in schizophrenia. *Acta Psychiatr. Scand.* **137(1)**, 39–46.

McGrath, J. J., Saha, S., Chant, D., Welham, J. (2008) Schizophrenia: A concise overview of incidence, prevalence, and mortality. *Epidemiol. Rev.* **30(1)**, 67–76.

Melnik, T., Soares, B., Puga, M. E., Atallah, A. N. (2010) Efficacy and safety of atypical antipsychotic drugs (quetiapine, risperidone, aripiprazole and paliperidone) compared with placebo or typical antipsychotic drugs for treating refractory schizophrenia: Overview of systematic reviews. *Sao Paulo Med. J.* **128(3)**, 141–166.

Molden, E., Lunde, H., Lunder, N., Refsum, H. (2006) Pharmacokinetic variability of aripiprazole and the active metabolite dehydroaripiprazole in psychiatric patients. *Ther. Drug Monit.* **28(6)**, 744–749.

Moresco, R. M., Cavallaro, R., Messa, C., Bravi, D., Gobbo, C., Galli, L., Lucignani, G., Colombo, C., Rizzo, G., Velona, I., Smeraldi, E., Fazio, F. (2004) Cerebral D2 and 5-HT2 receptor occupancy in schizophrenic patients treated with olanzapine or clozapine. *J. Psychopharmacol.* **18(3)**, 355–365.

Moschny, N., Hefner, G., Grohmann, R., Eckermann, G., Maier, H., Seifert, J., Heck, J., Francis, F., Bleich, S., Toto, S. (2021) Therapeutic drug monitoring of second- and third-generation antipsychotic drugs – Influence of smoking behavior and inflammation on pharmacokinetics. *Pharmaceuticals (Basel)* **14(6)**, 514.

Muly, E. C., Votaw, J. R., Ritchie, J. C., Howell, L. L. (2012) Relationship between dose, drug levels, and D2 receptor occupancy for the atypical antipsychotics risperidone and paliperidone. *J. Pharmacol. Exp. Ther.* **341(1)**, 81–89.

Nakamura, T., Kubota, T., Iwakaji, A., Imada, M., Kapás, M., Morio, Y. (2016) Clinical pharmacology study of cariprazine (MP-214) in patients with schizophrenia (12-week treatment). *Drug Des. Devel. Ther.* **10**, 327–338.

Nazirizadeh, Y., Vogel, F., Bader, W., Haen, E., Pfuhlmann, B., Gründer, G., Paulzen, M., Schwarz, M. J., Zernig, G., Hiemke, C. (2010) Serum concentrations of paliperidone versus risperidone and clinical effects. *Eur. J. Clin. Pharmacol.* **66(8)**, 797–803.

Nofziger, C., Turner, A., Sangkuhl, K., Whirl-Carrillo, M., Agúndez, J. A. G., Black, J. L., Dunnenberger, H. M., Ruaño, G., Kennedy, M. A., Phillips, M., Hachad, H., Klein, T. E., Gaedigk, A. (2020) PharmVaR GeneFocus: CYP2D6. *Clin. Pharmacol. Ther.* **107(1)**, 154–170.

Olanzapine (2006) *Summary of Product Characteristics. Committee for Medicinal Products for Human Use. European Medicines Agency. European public assessment report*. Available at: https://www.ema.europa.eu/en/documents/product-information/zyprexa-epar-product-information_en.pdf (Accessed January 6, 2024)

Paliperidone (2021) *Summary of Product Characteristics. Committee for Medicinal Products for Human Use. European Medicines Agency. European public assessment report*. Available at: https://www.ema.europa.eu/en/medicines/human/EPAR/invega (Accessed January 6, 2024)

Patteet, L., Haufroid, V., Maudens, K. E., Sabbe, B., Morrens, M., Neels, H. (2015) Genotype and co-medication dependent CYP2D6 metabolic activity: Effects on serum concentrations of aripiprazole, haloperidol, risperidone, paliperidone and zuclopenthixol. *Eur. J. Clin. Pharmacol.* **72(2)**, 175–184.

Paulzen, M., Haen, E., Stegmann, B., Unterecker, S., Hiemke, C., Gründer, G., Schoretsanitis, G. (2016) Clinical response in a risperidone-medicated naturalistic sample: Patients' characteristics and dose-dependent pharmacokinetic patterns. *Eur. Arch. Psychiatry Clin. Neurosci.* **267(4)**, 325–333.

Perry, P. J., Lund, B. C., Sanger, T. M., Beasley, C. M. (2001) Olanzapine plasma concentrations and clinical response: Acute phase results of the North American Olanzapine Trial. *J. Clin. Psychopharmacol.* **21(1)**, 14–20.

Puangpetch, A., Vanwong, N., Nuntamool, N., Hongkaew, Y., Chamnanphon, M., Sukasem, C. (2016) CYP2D6 polymorphisms and their influence on risperidone treatment. *Pharm. Pers. Med.* **9**, 131–147.

Quetiapine (2014) *Summary of Product Characteristics. Committee for Medicinal Products for Human Use. European Medicines Agency. European public assessment report*. Available at: https://www.ema.europa.eu/en/medicines/human/referrals/seroquel-seroquel-xr-and-associated-names (Accessed January 6, 2024)

Remington, G., Mamo, D., Labelle, A., Reiss, J., Shammi, C., Mannaert, E., Mann, S., Kapur, S. (2006) A PET study evaluating dopamine D2 receptor occupancy for long-acting injectable risperidone. *Am. J. Psychiatry* **163(3)**, 396–401.

Riedel, M., Schwarz, M. J., Strassnig, M., Spellmann, I., Müller-Arends, A., Weber, K. S. C., Zach, J., Müller, N., Möller, H. (2004) Risperidone plasma levels, clinical response and side-effects. *Eur. Arch. Psychiatry Clin. Neurosci.* **255(4)**, 261–268.

Risperidone (2008) *Summary of Product Characteristics. Committee for Medicinal Products for Human Use. European Medicines Agency. European public assessment report*. Available at: https://www.ema.europa.eu/en/medicines/human/referrals/risperdal (Accessed January 6, 2024)

Samanaite, R., Gillespie, A., Sendt, K.-V., McQueen, G., MacCabe, J. H., Egerton, A. (2018) Biological predictors of clozapine response: A systematic review. *Front. Psychiatry* **9**, 327.

Schoretsanitis, G., Stegmann, B., Hiemke, C., Gründer, G., Schruers, K., Walther, S., Lammertz, S. E., Haen, E., Paulzen, M. (2016) Pharmacokinetic patterns of risperidone-associated adverse drug reactions. *Eur. J. Clin. Pharmacol.* **72(9)**, 1091–1098.

Schoretsanitis, G., Kane, J. M., Correll, C. U., Marder, S. R., Citrome, L., Newcomer, J. W., Robinson, D. G., Goff, D. C., Kelly, D. L., Freudenreich, O., Piacentino, D., Paulzen, M., Conca, A., Zernig, G., Haen, E., Baumann, P., Hiemke, C., Gründer, G.; American Society of Clinical Psychopharmacology; Pharmakopsychiatrie TTDMTFOTAFNU (2020) Blood levels to optimize antipsychotic treatment in clinical practice: A joint consensus statement of the American Society of Clinical Psychopharmacology and the Therapeutic Drug Monitoring Task Force of the Arbeitsgemeinschaft für Neuropsychopharmakologie und Pharmakopsychiatrie. *J. Clin. Psychiatry* **81(3)**, 19cs13169.

Schoretsanitis, G., Yağcıoğlu, A. E. A., Ruan, C., Eap, C. B., Molden, E., Baptista, T., Clark, S., Fernández-Egea, E., Kim, S. H., Lane, H. Y., Leung, J. G., Amigo, O. M., Motuca, M., Olmos, I., Every-Palmer, S., Procyshyn, R. M., Rohde, C., Suhas, S., Schulte, P. F. J., Spina, E., Takeuchi, H., Verdoux, H., Correll, C. U., de Leon, J. (2023) Clozapine ultrarapid metabolism during weak induction probably exists but requires careful diagnosis. A literature review, five new cases and a proposed definition. *Schizophr. Res.* (Epub ahead of print)

Seto, K., Dumontet, J., Ensom, M. H. H. (2011) Risperidone in schizophrenia: Is there a role for therapeutic drug monitoring? *Ther. Drug Monit.* **33(3)**, 275–283.

Skokou, M., Karavia, E. A., Drakou, Z., Konstantinopoulou, V., Kavakioti, C.-A., Gourzis, P., Kypreos, K. E., Andreopoulou, O. (2022) Adverse drug reactions in relation to clozapine plasma levels: A systematic review. *Pharmaceuticals (Basel)* **15(7)**, 817.

Sparshatt, A., Jones, S., Taylor, D. (2008) Quetiapine: Dose-response relationship in schizophrenia. *CNS Drugs* **22(1)**, 49–68.

Sparshatt, A., Taylor, D., Patel, M. X., Kapur, S. (2010) A systematic review of aripiprazole – Dose, plasma concentration, receptor occupancy, and response: Implications for therapeutic drug monitoring. *J. Clin. Psychiatry* **71(11)**, 1447–1456.

Sparshatt, A., Taylor, D., Patel, M. X., Kapur, S. (2011) Relationship between daily dose, plasma concentrations, dopamine receptor occupancy, and clinical response to quetiapine: A review. *J. Clin. Psychiatry* **72(08)**, 1108–1123.

Spina, E., de Leon, J. (2007) Metabolic drug interactions with newer antipsychotics: A comparative review. *Basic Clin. Pharmacol. Toxicol.* **100(1)**, 4–22.

Spina, E., Avenoso, A., Facciolà, G., Scordo, M. G., Ancione, M., Madia, A. G., Ventimiglia, A., Perucca, E. (2000) Relationship between plasma concentrations of clozapine and norclozapine and therapeutic response in patients with schizophrenia resistant to conventional neuroleptics. *Psychopharmacology (Berl.)* **148(1)**, 83–89.

Spina, E., Avenoso, A., Facciolà, G., Salemi, M., Scordo, M. G., Ancione, M., Madia, A. G., Perucca, E. (2001) Relationship between plasma risperidone and 9-hydroxyrisperidone concentrations and clinical response in patients with schizophrenia. *Psychopharmacology (Berl.)* **153(2)**, 238–243.

Stahl, S. M. (2014) *Prescriber's Guide: Stahl's Essential Psychopharmacology*. Cambridge University Press, Cambridge.

Steen, N. E., Aas, M., Simonsen, C., Dieset, I., Tesli, M., Nerhus, M., Gardsjord, E. S., Mørch, R. H., Agartz, I., Melle, I., Ueland, T., Spigset, O., Andreassen, O. A. (2016) Serum levels of second-generation antipsychotics are associated with cognitive function in psychotic disorders. *World J. Biol. Psychiatry* **18(6)**, 471–482.

Suzuki, H., Gen, K., Otomo, M., Inoue, Y., Hibino, H., Mikami, A., Matsumoto, H., Mikami, K. (2014a) Relationship between the plasma concentration of paliperidone and the clinical and drug-induced extrapyramidal symptoms in elderly patients with schizophrenia. *Hum. Psychopharmacol.* **29(3)**, 244–250.

Suzuki, T., Mihara, K., Nakamura, A., Kagawa, S., Nagai, G., Nemoto, K., Kondo, T. (2014b) Effects of genetic polymorphisms of CYP2D6, CYP3A5, and ABCB1 on the steady-state plasma concentrations of aripiprazole and its active metabolite, dehydroaripiprazole, in Japanese patients with schizophrenia. *Ther. Drug Monit.* **36(5)**, 651–655.

Takano, A., Suhara, T., Ikoma, Y., Yasuno, F., Maeda, J., Ichimiya, T., Sudo, Y., Inoue, M., Okubo, Y. (2004) Estimation of the time-course of dopamine D2 receptor occupancy in living human brain from plasma pharmacokinetics of antipsychotics. *Int. J. Neuropsychopharmacol.* **7(1)**, 19–26.

Taylor, D. M., Barnes, T. R. E., Young, A. H. (2021) *The Maudsley Prescribing Guidelines in Psychiatry*. John Wiley and Sons, Hoboken.

Thomas, K., Saadabadi, A. (2023) *Olanzapine*. StatPearls [Internet]. Available at: https://www.ncbi.nlm.nih.gov/books/NBK532903/ (Accessed January 6, 2024)

Tralongo, F., Konecki, C., Féliu, C., Kaladjian, A., Djerada, Z. (2023) Association between clozapine plasma concentrations and treatment response: A systematic review, meta-analysis and individual participant data meta-analysis. *Clin. Pharmacokinet.* **62(6)**, 807–818.

Tsuda, Y., Saruwatari, J., Yasui-Furukori, N. (2014) Meta-analysis: The effects of smoking on the disposition of two commonly used antipsychotic agents, olanzapine and clozapine. *BMJ Open* **4(3)**, e004216.

Urban, A. E., Cubała, W. J. (2017) Therapeutic drug monitoring of atypical antipsychotics. *Psychiatr. Pol.* **51(6)**, 1059–1077.

Urichuk, L., Prior, T. I., Dursun, S., Baker, G. B. (2008) Metabolism of atypical antipsychotics: Involvement of cytochrome P450 enzymes and relevance for drug-drug interactions. *Curr. Drug Metab.* **9(5)**, 410–418.

van der Weide, K., van der Weide, J. (2015) The influence of the CYP3A4*22 polymorphism on serum concentration of quetiapine in psychiatric patients. *J. Clin. Psychopharmacol.* **34(2)**, 256–260.

Vandenberghe, F., Guidi, M., Choong, E., Von Gunten, A., Conus, P., Csajka, C., Eap, C. B. (2015) Genetics-based population pharmacokinetics and pharmacodynamics of risperidone in a psychiatric cohort. *Clin. Pharmacokinet.* **54(12)**, 1259–1272.

Vernaleken, I., Janouschek, H., Raptis, M., Hellmann, S., Veselinović, T., Bröcheler, A., Boy, C., Cumming, P., Hiemke, C., Rösch, F., Schäfer, W., Gründer, G. (2010) Dopamine D2/3 receptor occupancy by quetiapine in striatal and extrastriatal areas. *Int. J. Neuropsychopharmacol.* **13(07)**, 951–960.

Wong, J., Leung, S.-P., Mak, T., Ng, R. M. K., Chan, K. T., Cheung, H. H.-K., Choi, W., Lai, J. P. S., Tsang, A. W.-K. (2006) Plasma clozapine levels and clinical response in treatment-refractory Chinese schizophrenic patients. *Prog. Neuropsychopharmacol. Biol. Psychiatry* **30(2)**, 251–264.

Yasui-Furukori, N., Saito, M., Nakagami, T., Furukori, H., Suzuki, A., Kondo, T., Kaneko, S. (2009) Clinical response to risperidone in relation to plasma drug concentrations in acutely exacerbated schizophrenic patients. *J. Psychopharmacol.* **24(7)**, 987–994.

Yokoi, F. (2002) Dopamine D2 and D3 receptor occupancy in normal humans treated with the antipsychotic drug aripiprazole (OPC 14597): A study using positron emission tomography and [11C]raclopride. *Neuropsychopharmacology* **27(2)**, 248–259.

Yoshimura, R., Ueda, N., Nakamura, J. (2001) Possible relationship between combined plasma concentrations of risperidone plus 9-hydroxyrisperidone and extrapyramidal symptoms. *Neuropsychobiology* **44(3)**, 129–133.

Zhang, J., Malhotra, A. K. (2018) Recent progress in pharmacogenomics of antipsychotic drug response. *Curr. Psychiatry Rep.* **20(4)**, 24.

Zhang, X., Xiang, Q., Zhao, X., Ma, L., Chen, Y. (2018) Association between aripiprazole pharmacokinetics and CYP2D6 phenotypes: A systematic review and meta-analysis. *J. Clin. Pharm. Ther.* **44(2)**, 163–173.

Zhou, Z., Li, X., Huai-Yan, P., Yu, X., Yang, M., Su, F.-L., Wang, F., Zhu, R., Deng, C., Lin, Q., Wang, C., Li, W.-B., Lin, S., Huan-De, L. (2006) Multiple dose pharmacokinetics of risperidone and 9-hydroxyrisperidone in Chinese female patients with schizophrenia. *Acta Pharmacol. Sin.* **27(3)**, 381–386.

 Prague Medical Report / Vol. 125 (2024) No. 2, p. 130–137

A Severe and Fatal Type A Aortic Dissection in an Adult with a Repaired Tetralogy of Fallot

Manuela Montatore[1], Federica Masino[1], Vincenzo Signorile[2], Marina Balbino[1], RuggieroTupputi[3], Giuseppe Guglielmi[1,3,4]

[1] Department of Clinical and Experimental Medicine, Foggia University School of Medicine, Foggia, Italy;
[2] Cardiology Unit, Anthea Hospital, Bari, Italy;
[3] Radiology Unit, "Dimiccoli" Hospital, Barletta, Italy;
[4] Radiology Unit, "IRCCS Casa Sollievo della Sofferenza" Hospital, San Giovanni Rotondo, Italy

Received January 30, 2024; Accepted May 7, 2024.

Key words: Echocardiography – CT – TOF – Tetralogy of Fallot – Aortic dissection – Emergency

Abstract: We report a case of a 44-year-old woman surgically treated for tetralogy of Fallot who experienced an acute and extensive Stanford A type aortic dissection despite the meticulous follow-up. While aortic dilatation is prevalent in individuals with repaired tetralogy of Fallot, aortic dissection represents a rare consequence, that when it appears, is progressive and usually detected during the check-up visits. In the case reported, the dissection was unexpected and severe, and the patient's clinical state worsened suddenly, leading to death after a few days. Constant awareness for aortic aneurysms is essential in the Fallot tetralogy population, nevertheless, several causes may contribute to the acute worsening of the clinical condition until the patient's death.

Mailing Address: Prof. Giuseppe Guglielmi, MD., Department of Clinical and Experimental Medicine, Foggia University School of Medicine, Viale L. Pinto 1, 71121, Foggia, Italy; e-mail: giuseppe.guglielmi@unifg.it

https://doi.org/10.14712/23362936.2024.11

Introduction

Tetralogy of Fallot (TOF) is one of the most common cyanotic congenital heart diseases, that can be corrected by surgery: in fact, a radical correction is most often performed within one year of life.

In the scientific literature, there is an increase in cases of aortic involvement in many congenital heart diseases, especially in patients later after the repair of TOF such as dilatation and aortic dissection; patients with TOF have more residual findings in adulthood: pulmonary regurgitation and aortic root dilatation which may require surgical management in adulthood. Dilatation of the aorta is also frequent in TOF (up to 69%), however aortic aneurysm (with diameter ≥ 50 mm) was found in 9% only and aortic dissection is very rare in TOF (0–0.06%).

Different post-operative problems can occur and require some extra treatments, or a strict follow-up is always required (Vaikunth et al., 2022). Given the residual findings in the patient of this case, she requires lifelong follow-up by a cardiologist (Grotenhuis et al., 2018).

This case report describes the imaging examination, especially echocardiogram and computed tomography (CT) scans, in a patient who had an acute and severe aortic dissection, with an important hypotensive shock (Kim et al., 2011; Chow et al., 2020).

Case report

A 44-year-old patient came to the Emergency Department transported by ambulance in an unconscious state. The patient's condition immediately appeared severe: the skin was pale, sweaty, and cold; the pulse was extremely weak and there was arterial hypotension.

Given the critical condition, a consultation with the cardiologist was required and a transthoracic echocardiogram was performed. The latter demonstrated an

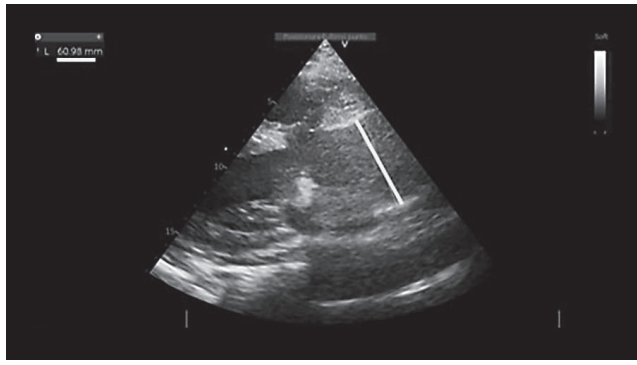

Figure 1 – The transthoracic echocardiography showed the aortic aneurysm with a severe dilatation of the aortic root (about 61 mm).

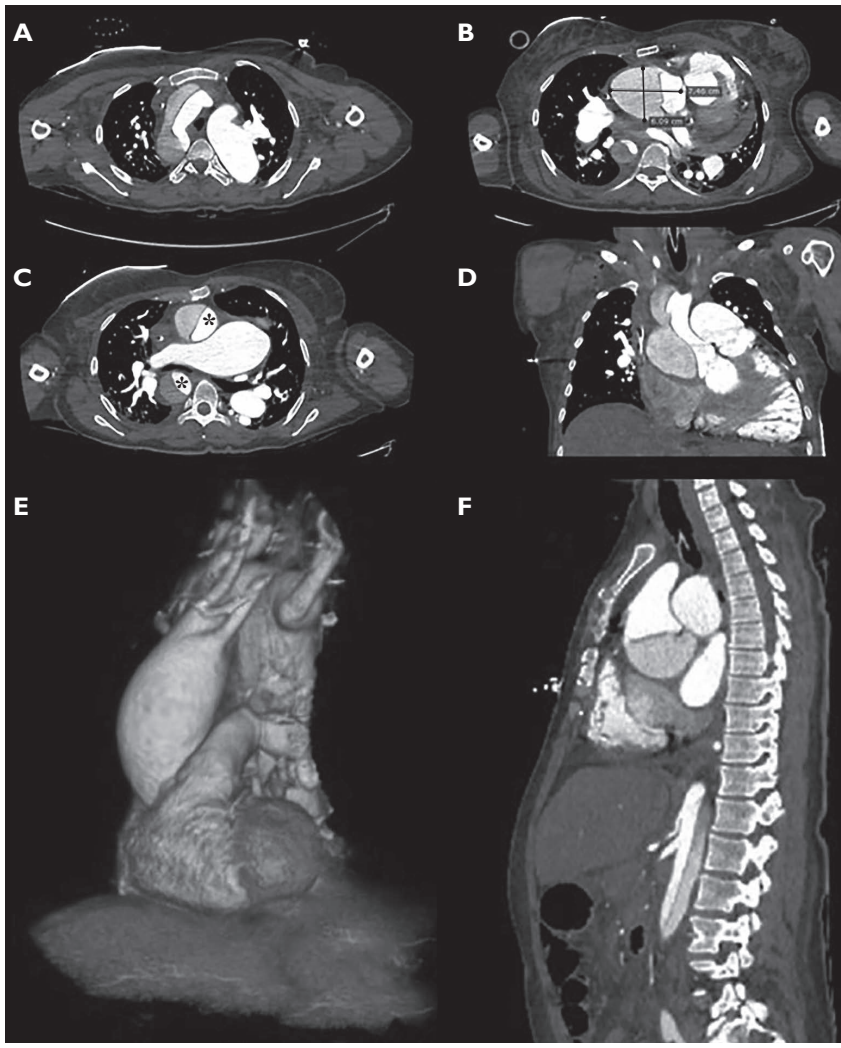

Figure 2 – Computed tomography angiography scan revealed a marked aneurysm of the aorta (A) (maximal dimension of 6×7 cm at the ascending aorta – B), with an intimal flap of dissection involving the aortic root, the aortic arch (C, D, E, F), and the right-sided descending aorta and dividing the true lumen (TL) – the star (C), from the false lumen (FL). There is a severe dilatation also of the ascending aorta (arch and descending are involved too). This dilatation is due to the dissection and the formation of a second lumen (false lumen) from the valvular plane and aortic root.

aneurysmal dilatation with a maximal diameter at the aortic root, resulting in severe aortic insufficiency (Figure 1).

The examination also revealed an intimal flap suspicious of aortic dissection and the presence of a pericardial effusion. After stabilization manoeuvres, the patient was immediately taken to the Radiology Department where a computed tomography

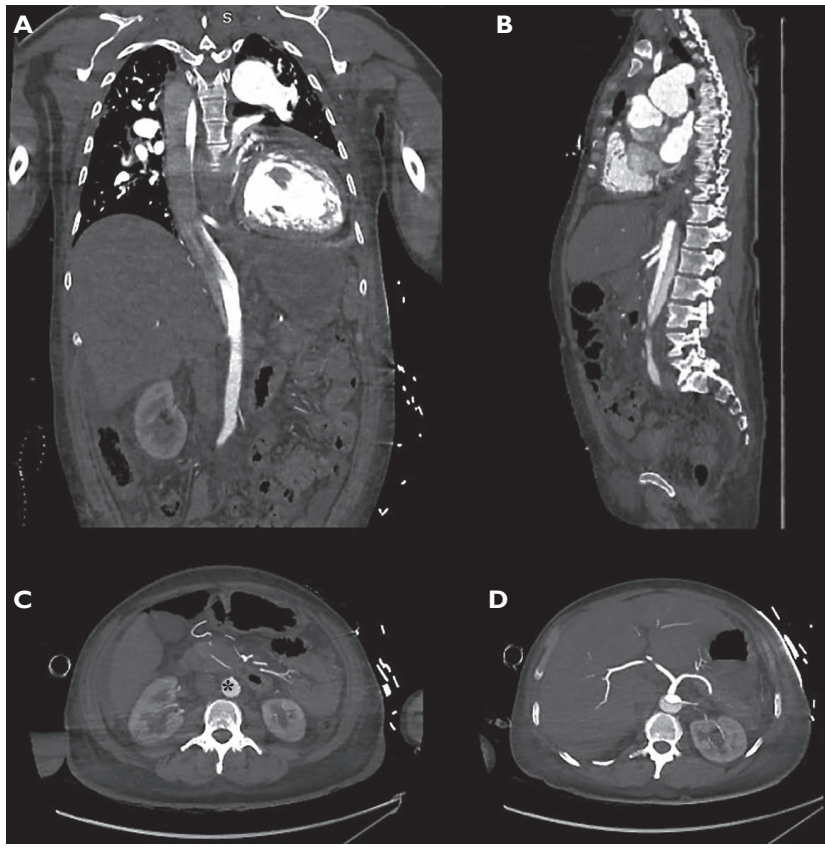

Figure 3 – Computed tomography angiography scan images, showing in coronal (A) and sagittal (B) the extension of the dissection flap extended to the upper limits of the iliac carrefour (shown in axial section, the lower limit of abdominal aortic dissection – C). The coronal section of the artery (B) is not entirely viewable given the scoliotic course of the abdominal aorta. With increased maximum intensity projection, the integrity of the celiac trunk is shown (D).

angiography (CTA) examination was performed. The patient had not been under cardiological control for many years and the aortic size was unknown before the dissection. The CT scan before and after contrast agent administration showed a severe aortic dissection, Standford type A, originating from the aortic root, with a dissection flap detected near the aortic valve, and reaching the abdominal aorta until its bifurcation in the common iliac arteries (Figures 2 and 3).

The Bentall operation was required in case of complicated aortic dissection, severe clinical condition, and CT findings of a type A dissection was not soon performed as the patient was inoperable at that moment and the surgery was delayed due to rather critical clinical conditions: visceral mal-perfusion and deterioration of the neurological state (Zhang et al., 2022; Shehata et al., 2023).

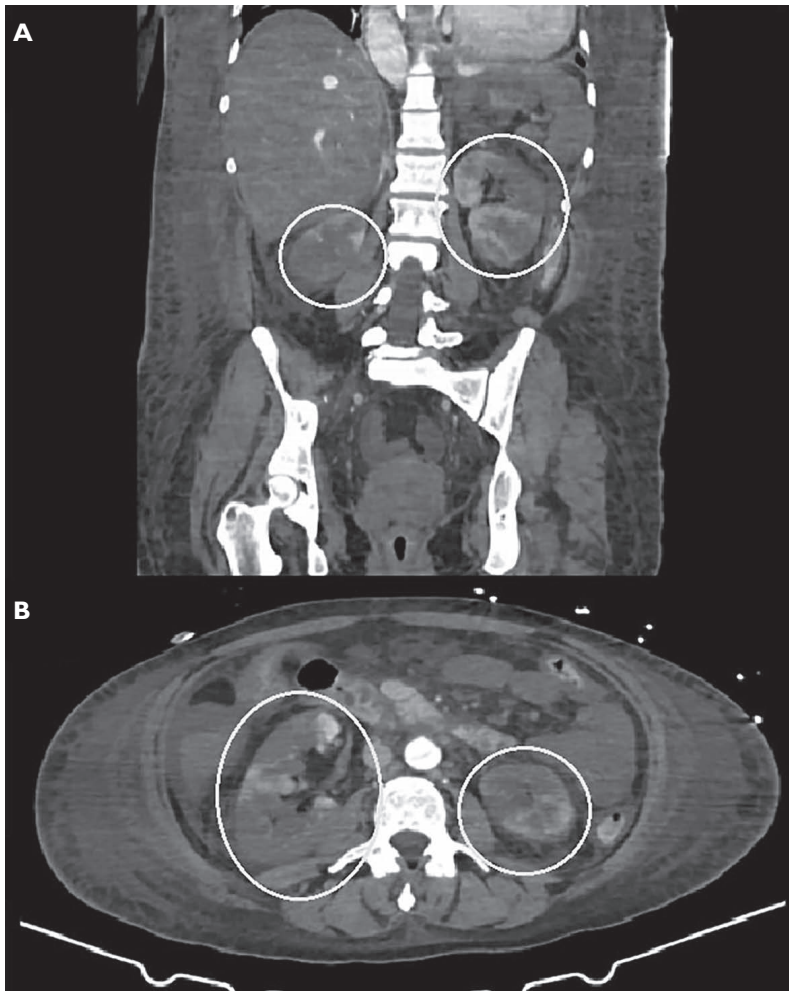

Figure 4 – Computed tomography angiography scans in coronal (A) and axial (B) planes, showed a severe condition of hypotension, with the contrast medium in the aortic vascular lumen even in delayed scans and abdominal visceral mal perfusion, especially liver and kidneys (circled the kidneys, in an end-stage condition due to hypotension), associated with a massive free abdominal fluid and oedema of soft tissues.

Therefore, the patient was hospitalized trying to stabilize volemia and clinical parameters; devices of central venous catheter (CVC), endotracheal tube (ETT), and a nasogastric feeding tube (NG) were implanted; and medical treatment was administered. After two days the CT scans were performed and confirmed the mal perfusion syndrome due to the severe dissection (Figure 4).

Due to the worsening of the clinical conditions of the patient, the surgery was never performed since she died in the days that followed.

Discussion

One of the most frequent congenital cardiac abnormalities is TOF consisting of the coexistence of pulmonary artery stenosis, the subaortic ventricular septal defect, and an anterosuperior deviation of the aortic root and sub-valvular right ventricular hypertrophy (Niwa, 2005; Kim et al., 2011; Vaikunth et al., 2022).

Distension of the aortic root, more commonly, and aortic dissection, more rarely, have been identified as complications following TOF repair, one of the most successful surgical corrections in treating congenital cardiac disorders. According to the literature, the risk factors for aortic dissection in TOF were age over 60 years, men's gender, hypertension, and of course the aortic diameter. In this case, there was a female and young patient, with an anamnesis not totally clear (except for corrective surgery done within the first year of life, as reported by relatives).

Aortic root aneurysm in TOF is a long-term clinical issue since a significantly dilated aorta can produce aortic regurgitation, dissection, or rupture, all of which can be fatal and necessitate surgical intervention (Zhang et al., 2022; Shehata et al., 2023).

The probable cause of dilatation is a congenital anterosuperior deviation of the aortic root with seeding over the ventricular septal defect however, the real mechanism of aortic root dilation remains unknown (Seki et al., 2016; Egbe et al., 2019).

Aortic dissection is a rarer entity in individuals with repaired TOF and when occurs it appears progressive in time, allowing a rapid detection and prompt medical treatment during the follow-up. The role of imaging, and CTA is essential in the evaluation of the aortic condition.

In the case reported the aorta appeared aneurysmatic in the thoracic tract, especially in the root and ascending aorta, as its axial diameter was about 6×7 cm at CT, suggesting an aortic insufficiency.

Moreover, all the aortic extension was characterized by an intimal flap indicating a type A dissection (Stanford classification), the most severe kind of dissection.

Therefore, the type A dissection concerned the ascending aorta, the aortic arch, and the descending aorta until the bifurcation in the common iliac arteries with the exclusion of the mesenteric artery and celiac trunk. Once the presence and the extension of dissection have been recognized, the radiologist must identify the double lumen representing the true and false lumens in CT scans. It must be considered that the true lumen, which was smaller because of the compression by the higher pressure of the false lumen, gave rise to the origin of the celiac trunk, superior mesenteric artery, and right renal artery. On the other hand, the false lumen, which was larger, presented delated enhancement, surrounded the outer curve of the arch, and gave rise to the left renal artery. Moreover, the false lumen had wedges around the true lumen (beak sign) and had a circular configuration because of the persistent systolic pressure, surrounding the true lumen. The radiologist excluded the presence of a thrombus in the first CTA performed. After

a few days, a new CT scan was requested confirming a critical clinical condition of mal-perfusion syndrome, a severe complication of aortic dissection (Crawford et al., 2016).

Therefore, the CT revealed a diffuse hypodensity of ischemic significance of the renal parenchyma bilaterally, with a few thin sectors remaining opaque; the lower mesenteric artery was not visible. Hepatomegaly with diffuse hepatic hypodensity was present: the over-hepatic veins were narrow but opacified and the portal vein was thin. The spleen and pancreatic tail were similarly hypodense, and there was a lot of fluid in the belly.

Unfortunately, the patient's systemic condition fell rapidly, and the patient died a few days later.

Since effective TOF repair allows many patients to live to adulthood, the population of patients with repaired TOF is rapidly growing. Nevertheless, because of the possibility of late complications, such as aortic root dilatation, these patients will require lifelong monitoring (Seki et al., 2016; Egbe et al., 2019). While aortic root dilatation is a well-known issue following TOF surgery, dissection is uncommon and maybe sometimes underreported; in fact, late aortic dissection is a rare but serious complication associated with cardiac surgery that could lead to mal-perfusion and death. The reported case suggests the importance of meticulously monitoring the patient's condition after corrective surgery for TOF.

Conclusion

In the Fallot tetralogy-treated population is required a lifetime follow-up after the radical correction and early indication for surgery for residual findings such as resolution of pulmonary regurgitation or dilatation of the aortic root is essential. Preventive surgery of the dilated aortic root will prevent aortic dissection which can be fatal for the patient.

References

Chow, P. C., Rocha, B. A., Au, T. W. K., Yung, T. C. (2020) Aortic dissection in a Chinese patient 31 years after surgical repair of tetralogy of Fallot. *J. Cardiol. Cases* **22(4)**, 174–176.

Crawford, T. C., Beaulieu, R. J., Ehlert, B. A., Ratchford, E. V., Black, J. H. 3rd (2016) Malperfusion syndromes in aortic dissections. *Vasc. Med*. **21(3)**, 264–273.

Egbe, A. C., Crestanello, J., Miranda, W. R., Connolly, H. M. (2019) Thoracic aortic dissection in tetralogy of Fallot: A review of the National Inpatient Sample database. *J. Am. Heart Assoc*. **8(6)**, e011943.

Grotenhuis, H. B., Dallaire, F., Verpalen, I. M., Van den Akker, M. J. E., Mertens, L., Friedberg, M. K. (2018) Aortic root dilatation and aortic-related complications in children after tetralogy of Fallot repair. *Circ. Cardiovasc. Imaging* **11(12)**, e007611.

Kim, T. S., Na, C. Y., Baek, J. H., Yang, J. S. (2011) Aortic root and ascending aortic aneurysm in an adult with a repaired tetralogy of Fallot. *Korean J. Thorac. Cardiovasc. Surg*. **44(4)**, 292–293.

Niwa, K. (2005) Aortic root dilatation in tetralogy of Fallot long-term after repair – Histology of the aorta in tetralogy of Fallot: Evidence of intrinsic aortopathy. *Int. J. Cardiol*. **103(2)**, 117–119.

Seki, M., Kuwata, S., Kurishima, C., Nakagawa, R., Inuzuka, R., Sugimoto, M., Saiki, H., Iwamoto, Y., Ishido, H., Masutani, S., Senzaki, H. (2016) Mechanism of aortic root dilation and cardiovascular function in tetralogy of Fallot. *Pediatr. Int*. **58(5)**, 323–330.

Shehata, M., Bashir, R., Al-Alao, B., Salmasi, M. Y., Asimakopoulos, G., Hoschtitzky, A. (2023) Type A aortic dissection following a tetralogy of Fallot repair. *JTCVS Tech*. **22**, 145–146.

Vaikunth, S. S., Chan, J. L., Woo, J. P., Bykhovsky, M. R., Lui, G. K., Ma, M., Romfh, A. W., Lamberti, J., Mastrodicasa, D., Fleischmann, D., Fischbein, M. P. (2022) Tetralogy of Fallot and aortic dissection: Implications in management. *JACC Case Rep*. **4(10)**, 581–586.

Zhang, S., Liu, H., Wang, X., Huang, S., Zhang, C. (2022) The surgical strategy for progressive dilatation of aortic root and aortic regurgitation after repaired tetralogy of Fallot: A case report. *Front. Cardiovasc. Med*. **9**, 840946.

 Prague Medical Report / Vol. 125 (2024) No. 2, p. 138–145

A Curious Case of Clear Cell Morphology in a Patient with Lung Cancer: Diagnostic Challenges

Alyssa Bonnier[1], Mufaddal Najmuddin[2], Michael D. Curry[3], Anum Nida[4], Biplab K. Saha[5]

[1] Department of Nursing, Goldfarb College of Nursing, Saint Louis, USA;
[2] Department of Pathology, Ozarks Medical Center, West Plains, USA;
[3] Department of Pathology, University of Missouri Health Systems, Columbia, USA;
[4] Department of Medicine, Ozarks Medical Center, West Plains, USA;
[5] Department of Pulmonary, Critical Care and Sleep Medicine, University of Florida, Gainesville, USA

Received August 30, 2022; Accepted May 7, 2024.

Key words: Lung cancer – Clear cell – Phenotype – Squamous cell – Glycogen

Abstract: An 82-year-old woman with COPD presented to the emergency department with cough, increasing sputum production, wheezing, and worsening shortness of breath for two weeks. On imaging studies, the patient was found to have a right upper lobe spiculated nodule and an endobronchial lesion with near total occlusion of the right lower lobe bronchus with sub-segmental atelectasis. Bronchoscopy with EBUS-TBNA of subcarinal and right hilar lymph nodes revealed lung cancer with clear cell phenotype. Given the predominance of clear cell morphology, the diagnosis of metastatic renal or ovarian cancer was entertained. However, there was no evidence of renal or ovarian lesions on the PET-CT scan, ruling out the possibility. Salivary gland type lung cancer (STLC), which is responsible for less than 1% of all lung cancer cases in adults, was also considered. The two distinct STLCs that may have similar morphologic appearances are hyalinizing clear cell carcinoma (HCCC) and mucoepidermoid carcinoma (MEC). The other type of tumour in the lung that demonstrates a clear cell phenotype is perivascular epithelioid cell neoplasms or PEComa, which are mesenchymal in origin. Immunohistochemical staining was strongly positive for p63, CK5/6, CK7, CK-LMW, and negative for TTF-1, Napsin A, p16, and CK20. Additional staining, including HMB-45, S-100, and mucicarmine, were also negative. Next-generation sequencing for the salivary gland fusion panel, including *EWSR1-ATF1* fusion and *EWSR1* gene rearrangement for HCCC and *MAML2* gene rearrangements for MEC, was negative. She was diagnosed with non-small cell lung cancer favouring squamous cell carcinoma with clear cell phenotype, a rare entity.

Mailing Address: Biplab K. Saha, MD., FCCP, Department of Pulmonary, Critical Care and Sleep Medicine, Medical Sciences Building, Room #M-452, University of Florida, 1600 SW Archer Road, Gainesville, FL 32608, USA; e-mails: spanophiliac@yahoo.com, biplabsaha@ufl.edu

https://doi.org/10.14712/23362936.2024.12

Introduction

Lung cancer is the number one cause of cancer mortality in the world (Centers for Disease Control and Prevention, 2022). Extensive research into the molecular biology of lung cancer has contributed to the discovery of driver mutations, leading to the development of many targeted therapies. Moreover, improved patient care, such as improved surgical techniques and high-intensity focused radiation therapy, have improved overall survival in patients with lung cancer (Howlader et al., 2020).

Lung cancers are primarily classified as small cell lung cancer (SCLC) and non-small cell lung cancer (NSCLC), with the latter representing the majority of newly diagnosed cases (Duma et al., 2019). The NSCLC is subdivided into adenocarcinoma, squamous cell carcinoma (SCC), and large cell carcinoma. Other types of cancers, including salivary gland tumours, sarcomas, and sarcomatoid carcinomas, can also occur in the lungs.

Despite a remarkable improvement in molecular techniques, phenotypic histopathologic characterization of lung cancer is crucial before a battery of immunohistochemical (IHC) stains can be obtained. Appropriate phenotyping can reduce the number of IHC used and save tissue for additional future studies. A "clear cell phenotype" of lung cancer on microscopy has been a source of

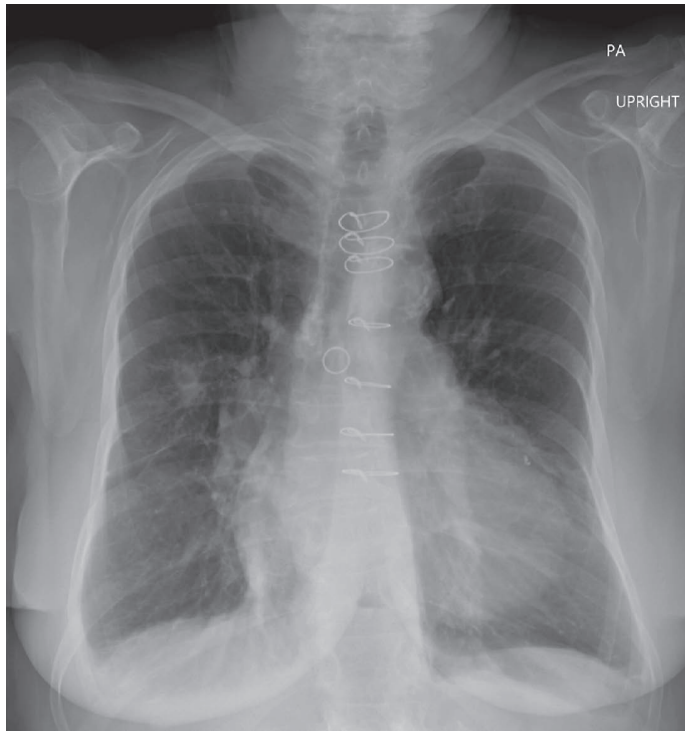

Figure 1 – Posteroanterior chest X-ray showing bilateral hyperinflation with a spiculated right perihilar lung nodule.

confusion for a long time, and a definitive diagnosis of lung cancer type could be challenging. Although initially described as a distinct entity, it is now widely accepted that all lung cancer subtypes can have a clear cell phenotype. Therefore, the 2021 World Health Organization (WHO) classification of thoracic malignancy did not classify "clear cell lung cancer" as a distinct entity. We present the case of an elderly woman with lung cancer for whom a definitive diagnosis of cancer subtype proved challenging due to the presence of "clear cell phenotype".

Case report

An 82-year-old woman presented to the emergency department (ED) with cough, increasing sputum production, wheezing, and worsening shortness of breath for two weeks. The patient was an active smoker with more than a 120-pack-year history. She denied any fever, night sweats, weight loss or loss of appetite. She had no recent history of travel outside the United States and denied any sick contact or any personal history of tuberculosis. Her medical history was significant for chronic obstructive pulmonary disease (COPD), hypertension, and coronary artery disease, for which she had undergone coronary artery bypass graft surgery 20 years ago.

In the ED, she was afebrile with stable blood pressure. However, she was tachycardic, tachypneic, and hypoxemic, requiring 2 l per minute of oxygen to maintain adequate SpO_2. Auscultation of the chest revealed diffuse bilateral wheezing and rhonchi. A chest radiograph revealed bilateral hyperinflated lungs with a spiculated lesion in the right middle lung zone in the peri-hilar area (Figure 1). A computed tomographic angiogram (CTA) of the chest revealed no pulmonary embolism but demonstrated a spiculated nodular lesion in the right upper lobe (RUL) (Figure 2A). An endobronchial lesion with near total occlusion of the right lower lobe (RLL) bronchus with sub-segmental atelectasis was also noted (Figure 2B and C). She was treated with broad spectrum antibiotics

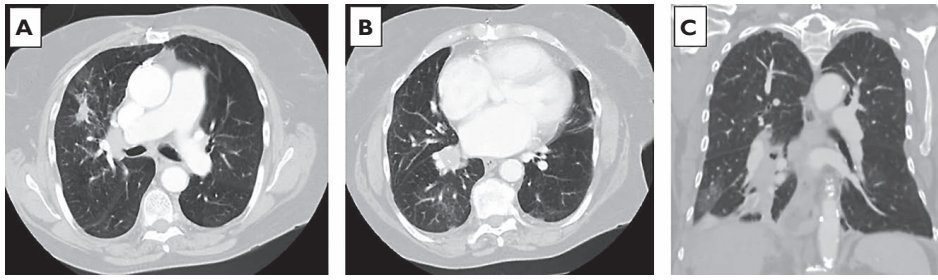

Figure 2 – Axial computed tomography (CT) of the chest showing a spiculated lesion in the right upper lobe (A). Endobronchial lesion nearly occluding the right bronchus intermedius was seen (B). Coronal CT scan showed partial atelectasis of right lower lobe (C).

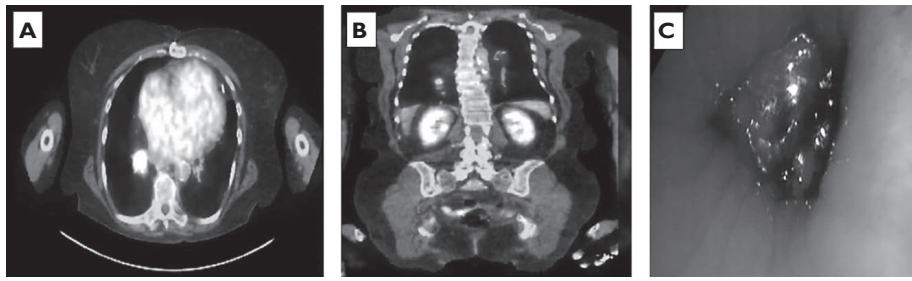

Figure 3 – PET-CT scan showing hypermetabolic endobronchial lesion (A) and right upper lobe lung nodule (B). Bronchoscopy showed fungating endobronchial lesion with near total occlusion of the right lower lobe bronchus and the entrance of the right middle lobe bronchus (C).

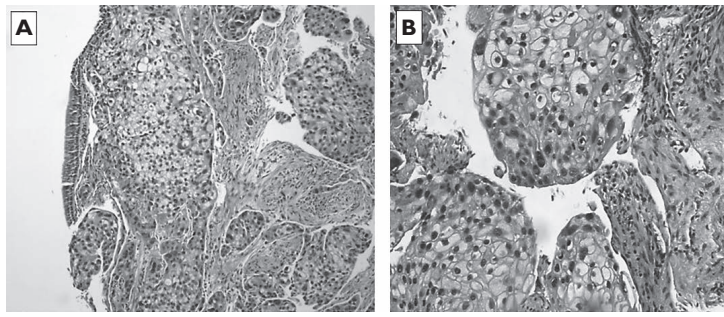

Figure 4 – Hematoxylin and eosin stain of the endobronchial biopsy samples revealed small to moderate sized epithelioid cells arranged in irregular nests and sheets with eosinophilic to clear cytoplasm at 100× (A) and 400× (B) magnification.

and intravenous corticosteroids with clinical improvement and was discharged from the hospital. A subsequent positron emission tomography (PET)-CT scan demonstrated hypermetabolic RLL endobronchial lesion, right hilar lymph node, and equivocal uptake in the subcarinal lymph node. There was no focal extrathoracic fluorodeoxyglucose (FDG) uptake or FDG avidity in the RUL nodule (Figure 3A and B). Bronchoscopic examination revealed an intraluminal polypoid growth in the RLL with near total occlusion of the RLL bronchus and the entrance of the right middle lobe bronchus (Figure 3C). Endobronchial biopsies were obtained from the RLL endobronchial lesion, and endobronchial ultrasound-guided transbronchial needle aspiration (EBUS-TBNA) was performed from stations 7 (subcarinal) and 10R (right hilar). The histopathologic analysis of the endobronchial biopsies showed clear cells arranged in irregular nests and sheets without gland formation or keratinization (Figure 4A and B). TBNA from station 7 demonstrated cells with similar morphology.

Given the predominance of clear cell morphology, the diagnosis of metastatic renal or ovarian cancer was entertained. However, there was no evidence of renal or ovarian lesions on the PET-CT scan, ruling out the possibility. Salivary gland type

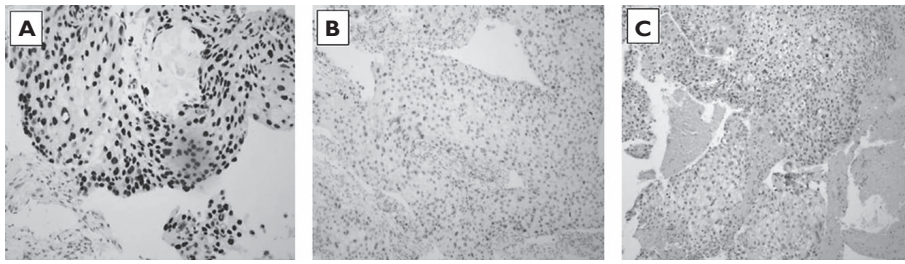

Figure 5 – Immunohistochemical staining showed strong p63 positivity (A), negative TTF-1 (B) and mucin (C) staining.

lung cancer (STLC), which is responsible for less than 1% of all lung cancer cases in adults, was also considered (Macarenco et al., 2008). The two distinct STLCs that may have similar morphologic appearances are hyalinizing clear cell carcinoma (HCCC) and mucoepidermoid carcinoma (MEC). The other type of tumour in the lung that demonstrates a clear cell phenotype is perivascular epithelioid cell neoplasms or PEComa, which are mesenchymal in origin. Immunohistochemical staining was strongly positive for p63, CK5/6, CK7, CK-LMW, and negative for TTF-1, Napsin A, p16, and CK20 (Figure 5). Additional staining, including HMB-45, S-100, and mucicarmine, were negative. The clear cytoplasm of these cells was the result of glycogen deposition, which was periodic acid Schiff (PAS) positive (Figure 6). Immunohistochemistry was performed by MAWD Pathology Group, Columbia, MO, USA (specific details of methods utilized can be obtained by e-mail request to the corresponding author).

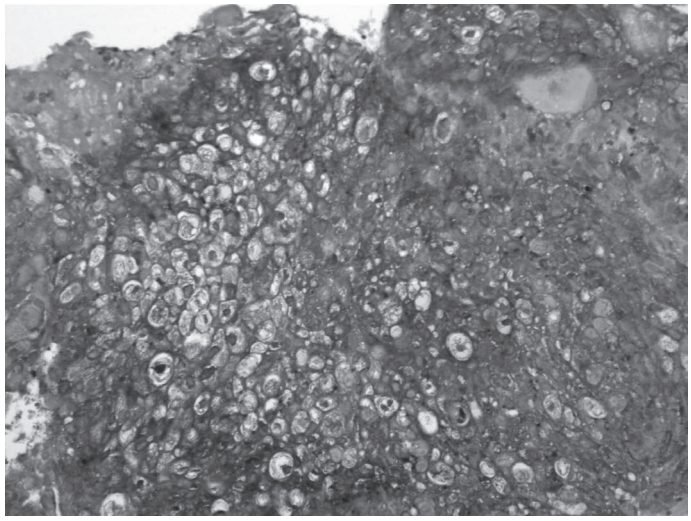

Figure 6 – Periodic acid Schiff (PAS) staining demonstrated strong positivity from the endobronchial biopsy sample (400× magnification).

The RNA-based Next Generation Sequencing (NGS) for salivary gland fusion panel (Neo Genomics), which detects translocations and fusion of a number of specific genes, including *EWSR1-ATF1* fusion and *EWSR1* gene rearrangement for HCCC and *MAML2* gene rearrangements for MEC, was negative. Further review of the slides showed moderate nuclear pleomorphism, with a minority of cancer cells showing giant, highly pleomorphic nuclei, inconsistent with low-grade malignancy, such as HCCC. Given the strong positivity of p63, CK5/6, the patient was diagnosed with NSCLC, favouring SCC, with clear cell type.

Discussion

We have presented a case of NSCLC favouring SCC with clear cell phenotype. SCC with clear cell type is a rare entity that can pose a significant diagnostic challenge. Although a definitive diagnosis of a lung cancer type solely based on morphologic examination could, in some cases, be possible from resected specimens, such confidence is generally lower from small sample biopsies. As approximately 70% of lung cancers are diagnosed at an advanced stage, it is crucial to consider the IHC data for a more definitive diagnosis from small sample biopsies (Travis et al., 2011). Clear cell morphology of lung cancers has been a rare entity and can be a source of confusion among clinicians and pathologists.

Morphologic clear cell pattern can be present in both adenocarcinoma and SCC, and the latest 2021 WHO classification recommends the mention of "clear cell features" in the pathology report while describing this entity (Nicholson et al., 2022). However, SCC with clear cell features typically involves only a part of the tumour histology.

It is crucial to differentiate between adenocarcinoma and SCC of the lung with clear cells, HCCC of lung origin, and metastatic salivary gland tumour to the lung. Additionally, renal cell cancer, ovarian cancer, PEComa, and MEC can have similar histopathology. A PET-CT scan, commonly performed in these patients, can easily identify salivary gland, ovarian and renal neoplasms. IHC plays a crucial role in the exclusion of other competing diagnoses. TTF-1 and Napsin A are markers for adenocarcinoma of lung origin. Markers for epithelial cell lineage, such as CK 5/6 and 7, exclude PEComa and sarcomas, such as clear cell sarcoma. Additionally, PEComas stain positive for HMB-45 and sometimes for S-100 (Zarbis et al., 2007). MEC can have clear cell morphology due to the presence of mucin-impregnated clear cells but can be differentiated by morphologic appearance and mucicarmine stain (Shen and Che, 2014).

Differentiation between SCC and HCCC could prove challenging as the IHC markers are similar. Both SCC and HCCC can have positive p63, P40, and CK5/6, therefore making the diagnosis based on IHC alone difficult (Zhang et al., 2022). In HCCC, histopathologic analysis reveals round to ovoid cells with clear to

eosinophilic cytoplasm and inconspicuous nuclei. The cells are arranged in cords, nests, trabecular and hyalinizing patterns (Wang et al., 2021). Nuclear features of high-grade malignancy are typically absent. The cytoplasm to nuclear ratio is lower in clear cells compared to eosinophilic cells. In contrast, SCC demonstrates a higher degree of nuclear pleomorphism and features suggestive of aggressive malignancy. Molecular studies for *EWSR1* gene rearrangements and *EWSR1-ATF1* gene fusion are diagnostic for HCCC (Takamatsu et al., 2018). Clinically, HCCC appears to have an indolent course, with the majority of reported cases having no evidence of metastatic disease. The HCCC arises from the submucosal minor salivary glands in the airways and, therefore, is commonly endobronchial. Surgical resection could be curative (Shah et al., 2015).

Conclusion

All subtypes of NSCLC can have a clear cell morphology. However, clear cell morphology is extremely rare in patients with squamous cell cancer. Other neoplasms with similar morphologic appearance, such as metastatic ovarian and renal cell cancer, adenocarcinoma of the lung, HCCC, mucoepidermoid carcinoma, and PEComa need to be excluded by immunohistochemistry and molecular testing before reaching the definitive diagnosis.

References

Centers for Disease Control and Prevention (2022) *An update on cancer deaths in the United States*.

Duma, N., Santana-Davila, R., Molina, J. R. (2019) Non-small cell lung cancer: Epidemiology, screening, diagnosis, and treatment. *Mayo Clin. Proc*. **94(8)**, 1623–1640.

Howlader, N., Forjaz, G., Mooradian, M. J., Meza, R., Kong, C. Y., Cronin, K. A., Mariotto, A. B., Lowy, D. R., Feuer, E. J. (2020) The effect of advances in lung-cancer treatment on population mortality. *N. Engl. J. Med*. **383(7)**, 640–649.

Macarenco, R. S., Uphoff, T. S., Gilmer, H. F., Jenkins, R. B., Thibodeau, S. N., Lewis, J. E., Molina, J. R., Yang, P., Aubry, M.-C. (2008) Salivary gland-type lung carcinomas: An EGFR immunohistochemical, molecular genetic, and mutational analysis study. *Mod. Pathol*. **21(9)**, 1168–1175.

Nicholson, A. G., Tsao, M. S., Beasley, M. B., Borczuk, A. C., Brambilla, E., Cooper, W. A., Dacic, S., Jain, D., Kerr, K. M., Lantuejoul, S., Noguchi, M., Papotti, M., Rekhtman, N., Scagliotti, G., van Schil, P., Sholl, L., Yatabe, Y., Yoshida, A., Travis, W. D. (2022) The 2021 WHO Classification of Lung Tumors: Impact of advances since 2015. *J. Thorac. Oncol*. **17(3)**, 362–387.

Shah, A. A., Mehrad, M., Kelting, S. M., Lewis, J. S., Stelow, E. B. (2015) An uncommon primary lung tumour: Hyalinizing clear cell carcinoma, salivary gland-type. *Histopathology* **67(2)**, 274–276.

Shen, C., Che, G. (2014) Clinicopathological analysis of pulmonary mucoepidermoid carcinoma. *World J. Surg. Oncol*. **12(1)**, 33.

Takamatsu, M., Sato, Y., Muto, M., Nagano, H., Ninomiya, H., Sakakibara, R., Baba, S., Sakata, S., Takeuchi, K., Okumura, S., Ishikawa, Y. (2018) Hyalinizing clear cell carcinoma of the bronchial glands: Presentation of

three cases and pathological comparisons with salivary gland counterparts and bronchial mucoepidermoid carcinomas. *Mod. Pathol*. **31(6)**, 923–933.

Travis, W. D., Brambilla, E., Noguchi, M., Nicholson, A. G., Geisinger, K. R., Yatabe, Y., Beer, D. G., Powell, C. A., Riely, G. J., Van Schil, P. E., Garg, K., Austin, J. H. M., Asamura, H., Rusch, V. W., Hirsch, F. R., Scagliotti, G., Mitsudomi, T., Huber, R. M., Ishikawa, Y., Jett, J., Sanchez-Cespedes, M., Sculier, J. P., Takahashi, T., Tsuboi, M., Vansteenkiste, J., Wistuba, I., Yang, P. C., Aberle, D., Brambilla, C., Flieder, D., Franklin, W., Gazdar, A., Gould, M., Hasleton, P., Henderson, D., Johnson, B., Johnson, D., Kerr, K., Kuriyama, K., Lee, J. S., Miller, V. A., Petersen, I., Roggli, V., Rosell, R., Saijo, N., Thunnissen, E., Tsao, M., Yankelewitz, D. (2011) International Association for the Study of Lung Cancer/American Thoracic Society/European Respiratory Society international multidisciplinary classification of lung adenocarcinoma. *J. Thorac. Oncol*. **6(2)**, 244–285.

Wang, M., Gilani, S., Xu, H., Cai, G. (2021) Salivary gland-type tumors of the lung: A distinct group of uncommon lung tumors. *Arch. Pathol. Lab. Med*. **145(11)**, 1379–1386.

Zarbis, N., Barth, T. F. E., Blumstein, N. M., Schelzig, H. (2007) Pecoma of the lung: A benign tumor with extensive 18F-2-deoxy-D-glucose uptake. *Interact. CardioVasc. Thorac. Surg*. **6(5)**, 676–678.

Zhang, Y., Han, W., Zhou, J., Yong, X. (2022) Primary lung hyalinizing clear cell carcinoma: A diagnostic challenge in biopsy. *Diagn. Pathol*. **17(1)**, 35.

 Prague Medical Report / Vol. 125 (2024) No. 2, p. 146–150

Unveiling a Silent Obstructor: Phytobezoar in the Third Duodenal Segment

Ana Fernanda Muñoz Durán[1], Juan Alberto Llanos Visbal[2], Leidy Vanessa Aguirre Carvajal[3], Juan Daniel Ayala Torres[4], Nicolás Álvarez Gärtner[5], Julián Andrés Muñoz Durán[6]

[1] Faculty of Medicine, Fundación Universitaria San Martin, Sabaneta, Antioquia, Colombia;
[2] Department of Surgery, Universidad de Cartagena, Clínica Panamericana, Apartadó, Antioquia, Colombia;
[3] Department of Emergencies, Universidad de Antioquia, Clínica Panamericana, Apartadó, Antioquia, Colombia;
[4] Department of Radiology, Universidad de Antioquia, Antioquia, Colombia;
[5] Department of Emergencies, Fundación Universitaria San Martin, Sabaneta, Clínica Soma, Antioquia, Colombia;
[6] Department of Radiology, Universidad CES, Clínica Panamericana, Apartadó, Antioquia, Colombia

Received January 9, 2024; Accepted May 7, 2024.

Key words: Bezoars – Intestinal obstruction – Abdomen – Acute – Tomography

Abstract: We present a case of obstruction in the third portion of the duodenum secondary to a phytobezoar in an adult patient with no surgical history and without a vegan diet. High intestinal obstruction due to a phytobezoar is rarely described in the literature, posing a diagnostic challenge when evaluating potential differentials in the emergency setting. Subsequently, we conduct a review focusing on tomographic findings and the surgical specimen, highlighting key points to consider when addressing such pathologies.

Mailing Address: Ana Fernanda Muñoz Durán, Faculty of Medicine, Fundación Universitaria San Martin, Calle 75 sur No. 34-50 vía la Doctora, Sabaneta, Antioquia, 055450, Colombia; e-mail: anamunozd@hotmail.com

https://doi.org/10.14712/23362936.2024.13

Introduction

Small bowel obstruction is a common condition, primarily attributed to intestinal adhesions and hernias; etiology secondary to bezoars is unusual, accounting for only 2–4% of reported cases (Aydin et al., 2022). Bezoars act as foreign bodies in the gastrointestinal tract, arising after the ingestion of undigested organic material, leading to intraluminal mechanical intestinal obstruction. Here, we present the case of a patient with no prior surgical history who experienced an episode of acute abdomen. Subsequently, an intestinal obstruction caused by a phytobezoar was identified at a tertiary care institution in Antioquia, Colombia. The presentation of this case is unusual compared to the current medical literature.

Case report

A 45-year-old male patient of mixed ethnicity, residing in an urban area, presented to the emergency department with chronic abdominal pain that escalated to acute over the preceding two weeks. The pain was localized in the epigastric region and was accompanied by vomiting of food content and oral intolerance. Physical examination revealed no remarkable findings. Laboratory studies revealed mild hypokalemia. Due to persistent symptoms and limited clinical improvement, a contrast-enhanced

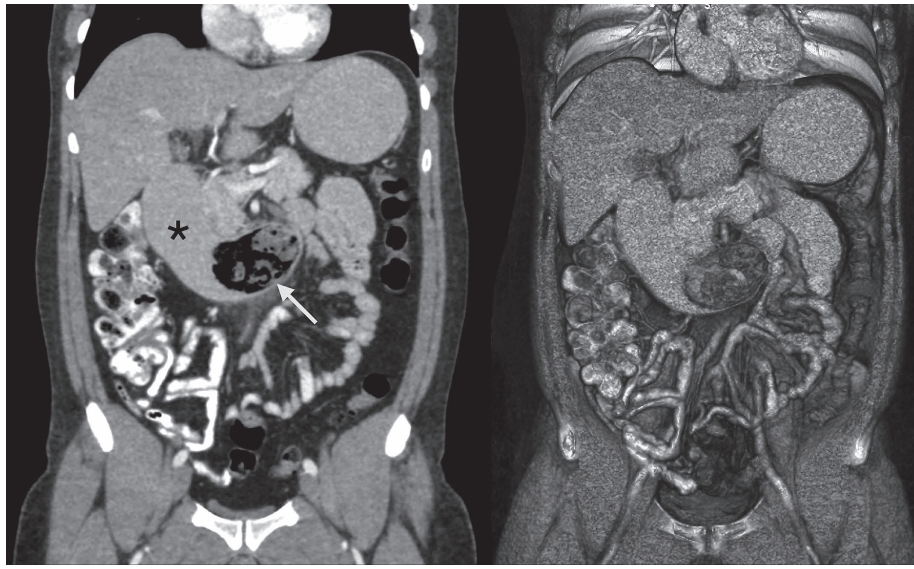

Figure 1 – Phytobezoar in the third portion of the duodenum. Coronal reconstruction of contrast-enhanced tomography and 3D rendered image, demonstrating a rounded foreign body with a density of –87 HU (Hounsfield units) consistent with a phytobezoar in the third portion of the duodenum (arrow). Note the proximal duodenal dilation (*) due to compressive effects.

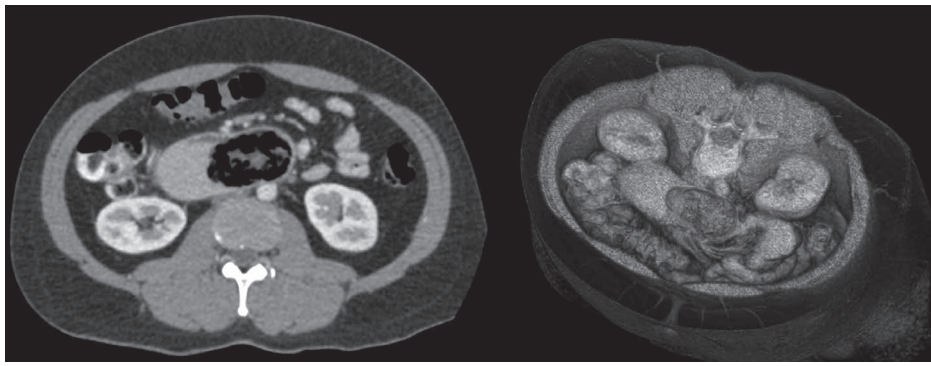

Figure 2 – Phytobezoar in the third portion of the duodenum. Axial section of contrast-enhanced tomography and 3D rendered image, illustrating the third portion of the duodenum and its anatomical relationships with the surrounding structures.

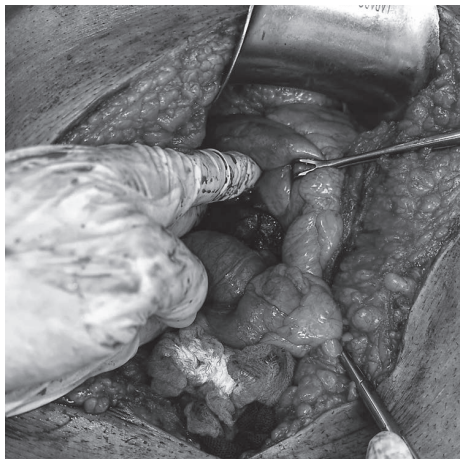

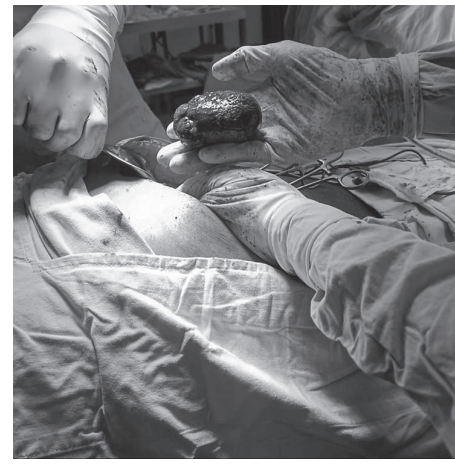

Figure 3 – Surgical specimen of duodenal phytobezoar.

abdominal tomography was performed, revealing the presence of an intraluminal foreign body in the third portion of the duodenum associated with proximal dilation (Figures 1 and 2).

Due to the persistence of symptoms and clinical deterioration despite instituted treatment, the patient underwent surgery. A gastrotomy and antrotomy were performed, successfully extracting the foreign body and confirming the diagnosis as indicated in imaging studies (Figure 3).

Discussion

Phytobezoar refers to the formation of a mass in the gastrointestinal tract due to the consumption of non-digestible substances such as fiber (Aydin et al., 2022). Foods with high cellulose, lignin, and tannin content, when exposed to the acidic stomach environment, polymerize and clump together, promoting the formation of a sticky substance to which other materials adhere, gradually hindering its transport through the digestive system. Rarely do they surpass the pyloric sphincter, settling in the gastric chamber (Manatakis et al., 2019). The seed bezoar is a subtype of phytobezoar, characterized by the accumulation of fruit or vegetable seeds in the intestinal lumen. Seeds in the intestinal lumen can navigate through narrow areas like the pylorus and ileocecal valve, slowly accumulating in a segment of the intestine and eventually causing obstruction (Manatakis et al., 2019). Clinically, the diagnosis is challenging due to presenting with generic symptoms such as abdominal pain, nausea, or vomiting, similar to other cases of intestinal obstruction. The preoperative diagnosis of intestinal obstruction due to phytobezoar is rarely established in the clinical context (Ko et al., 1997).

The formation of phytobezoars is commonly predisposed by various factors, such as gastric surgery, diabetes mellitus, mixed connective tissue disease, hypothyroidism, and end-stage renal disease with dialysis (Pergel et al., 2012; Yang et al., 2013). These conditions predispose to their formation (Ko et al., 1997), altering gastric emptying, which, combined with poor chewing technique and excess consumption of high-fiber foods, increases individuals' susceptibility to bezoar formation (Ko et al., 1997).

Phytobezoars located in the duodenum are extremely rare (Fan et al., 2016), with a reported incidence of less than 0.4% in the general population (Fan et al., 2016), and even rarer in the third portion of the duodenum (Yamagata et al., 2017).

In the absence of gastric surgery, phytobezoars in the small intestine are caused by massive intake of high-fiber foods (Verstandig et al., 1989). Imaging studies play a crucial role, especially computed tomography (CT), where the appearance of a phytobezoar is described as an intraluminal mass with bubbles around it, causing an abrupt change in the caliber of the intestine from dilation to collapsed lumen (normally, the small intestine has no luminal content). A focal, well-defined ovoid intraluminal mass with a speckled gas pattern inside, similar to the "faecal sign"

(Mayo-Smith et al., 1995), is observed, which is seen in high-grade small intestinal obstructions or in cystic fibrosis (Ko et al., 1997). Other findings include dilatation of the proximal digestive tract to the obstruction and collapse of the distal loops, signs not different from other types of intestinal obstruction. Specific findings suggestive of a phytobezoar include the identification of a high-grade obstruction in the absence of fat stranding and intraperitoneal fluid, a debris length of < 9.5 cm, and an average attenuation of < –11.75 Hounsfield units (HU) (Chen et al., 2015), which may or may not be accompanied by inflammatory changes in fat and intraperitoneal fluid.

Conclusion

Obstruction of the third portion of the duodenum secondary to a phytobezoar is a rare entity with limited documentation in the literature (Yamagata et al., 2017). Our case is noteworthy due to the site of obstruction and the absence of surgical history or exclusively vegetarian dietary patterns. Early identification of radiological signs guiding towards the diagnosis and the timely implementation of treatment, with a clear understanding of the etiology of the condition, are crucial to prevent delays in interventions and mitigate potential adverse outcomes.

References

Aydin, I., Sengul, I., Sengul, D. (2022) Phytobezoar: An unusual condition leading to small bowel obstruction. *Cureus* **14(4)**, e23885.

Chen, Y. C., Liu, C. H., Hsu, H. H., Yu, C. Y., Wang, H. H., Fan, H. L., Chen, R. C., Chang, W. C. (2015) Imaging differentiation of phytobezoar and small-bowel faeces: CT characteristics with quantitative analysis in patients with small-bowel obstruction. *Eur. Radiol.* **25(4)**, 922–931.

Fan, S., Wang, J., Li, Y. (2016) An unusual cause of duodenal obstruction: Persimmon phytobezoar. *Indian J. Surg.* **78(6)**, 502–504.

Ko, S., Lee, T., Ng, S. (1997) Small bowel obstruction due to phytobezoar: CT diagnosis. *Abdom. Imaging* **22(5)**, 471–473.

Manatakis, D. K., Acheimastos, V., Antonopoulou, M. I., Balalis, D., Korkolis, D. P. (2019) Gastrointestinal seed bezoars: A systematic review of case reports and case series. *Cureus* **11(5)**, e4686.

Mayo-Smith, W. W., Wittenberg, J., Bennett, G. L., Gervais, D. A., Gazelle, G. S., Mueller, P. R. (1995) The CT small bowel faeces sign: Description and clinical significance. *Clin. Radiol*. **50(11)**, 765–767.

Pergel, A., Yucel, A. F., Aydin, I., Sahin, D. A. (2012) Laparoscopic treatment of a phytobezoar in the duodenal diverticulum – Report of a case. *Int. J. Surg. Case Rep*. **3(8)**, 392–394.

Verstandig, A. G., Klin, B., Bloom, R. A., Hadas, I., Libson, E. (1989) Small bowel phytobezoars: Detection with radiography. *Radiology* **172(3)**, 705–707.

Yamagata, Y., Saito, K., Hirano, K., Kubota, Y., Yoshioka, R., Okuyama, T., Takeshita, E., Tagaya, N., Sameshima, S., Noie, T., Oya, M. (2017) Obstruction in the third portion of the duodenum due to a diospyrobezoar: A case report. *BMC Surg.* **17(1)**, 117.

Yang, J. E., Ahn, J. Y., Kim, G. A., Kim, G. H., Yoon, D. L., Jeon, S. J., Jung, H. Y., Kim, J. H. (2013) A large-sized phytobezoar located on the rare site of the gastrointestinal tract. *Clin. Endosc.* **46(4)**, 399–402.

Central Pleomorphic Adenoma of Mandible Mimicking Ameloblastoma – A Rare Case Report

Ravindra Manerikar[1], Amit Mani[2], Manas Bajpai[3], Shyam Reddy Karakalla[4]

[1] Department of Orthodontics and Dentofacial Orthopaedics, Rural Dental College, Pravara Institute of Medical Sciences, Loni (Maharashtra), India;
[2] Department of Periodontology, Rural Dental College, Pravara Institute of Medical Sciences, Loni (Maharashtra), India;
[3] Department of Oral Pathology and Microbiology, Rural Dental College, Pravara Institute of Medical Sciences, Loni (Maharashtra), India;
[4] Kamineni Hospital, Vijayawada (Andhra Pradesh), India

Received November 20, 2023; Accepted May 7, 2024.

Key words: Pleomorphic adenoma – Salivary gland neoplasm – Mandible – Jaw neoplasms

Abstract: Salivary gland neoplasms account for 3% of all head and neck tumours. Pleomorphic adenoma (PA) is the most common salivary gland tumour that mainly occurs in the parotid gland, followed by minor salivary glands of the oral cavity, however, the occurrence of PA inside the jaw bones is exceedingly rare and very few cases have been reported in the literature. Inside jaw bones these lesions tend to imitate large osteolytic lesions encompass a diagnostic challenge. An exhaustive review of the literature revealed only 10 cases of central pleomorphic adenoma. We present a rare case of primary PA that occurred inside the mandible and was provisionally diagnosed as ameloblastoma.

Mailing Address: Dr. Manas Bajpai, Department of Oral Pathology and Microbiology, Rural Dental College, Pravara Institute of Medical Sciences, Loni 413736 (Maharashtra), India; e-mail: dr.manasbajpai@gmail.com

https://doi.org/10.14712/23362936.2024.14

Introduction

Salivary gland tumours account for 3% of all head and neck tumours (Brookstone et al., 1992). Pleomorphic adenoma (PA) is the commonest salivary gland tumour, mainly occurring in the parotid gland and followed by minor salivary glands, although rare salivary gland tumours also occur in the jaw bones (Ojha et al., 2007).

Within the jaw bones mucoepidermoid carcinoma is found to be the most common tumour followed by adenoid cystic carcinoma and acinic cell carcinoma (Ojha et al., 2007; Bajpai et al., 2018; Manola et al., 2019). Occurrence of PA as primary central salivary gland tumour is rare and very few cases have been reported in the literature (Aghaghazvini and Aghaghazvini, 2015). We report a case of a large multilocular, osteodestructive lesion that was provisionally diagnosed as ameloblastoma and finally diagnosed as central PA after microscopic evaluation. We also describe the treatment modality performed in the present case.

Case report

An otherwise healthy 34-years-old man presented to a private dental clinic with the chief complaint of swelling and pain on the left, lower front region of his jaw for 8 months. The swelling was initially small and unnoticeable but gradually it started increasing and reached the current size. In the previous few days patient was suffering with dull pain in the same region. The personal history, family history,

Figure 1 – Extra-oral examination reveals asymmetry on the left side of face (black arrow denoting the swelling area).

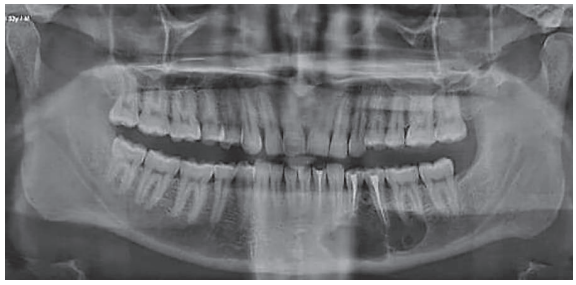

Figure 2 – Panoramic radiograph shows a large multilocular lesion of the left mandible.

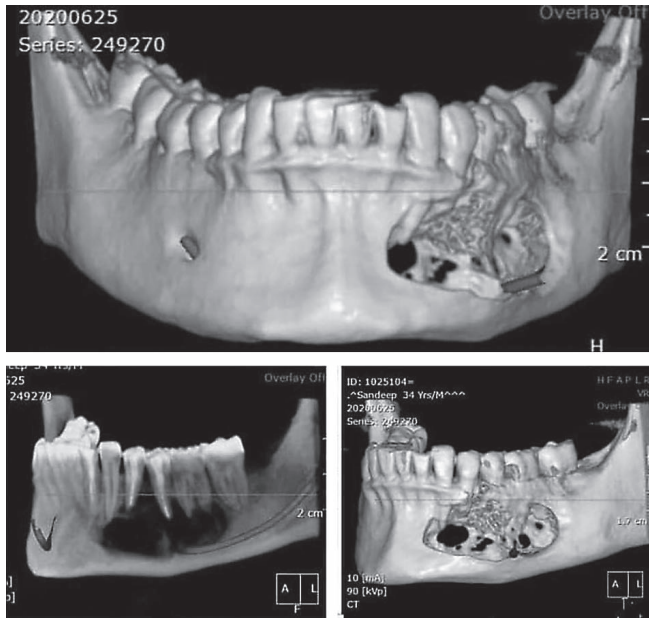

Figure 3 – 3D cone beam computed tomographic image exhibits perforations of buccal and lingual cortical plates.

and past medical history of the patient were found to be non-contributory to the presenting symptoms. Extra-oral examination revealed asymmetry on the left side of the face (Figure 1) on palpation the swelling was found to be hard and non-fluctuant, the overlying skin of the swelling had the same colour as that of the adjacent skin.

Intra-orally it revealed a solitary swelling extending from #33 to #36, on palpation it was found to be firm and tender. No paresthesia was noted in the initial examination. The colour of the mucosa was similar to the adjacent mucosa without any sign of ulceration. A panoramic radiograph revealed a large multilocular radiolucent lesion extending from #32 to #36, the roots of #34 and #35 and the mesial root of #36 were entrapped within the lesion (Figure 2). #32, #34 and #35 were root canal treated. A 3D reconstruction of the cone beam computed tomographic (CBCT) image revealed multiple buccal and lingual perforations (Figure 3).

After the correlation of clinical and radiographic features, a provisional diagnosis of ameloblastoma was given with the differential diagnosis of odontogenic keratocyst. An incisional biopsy was performed under local anesthesia and the specimen was sent for histopathological evaluation.

Hematoxylin and eosin-stained soft tissue sections revealed typical ductal and myoepithelial cells arranged in sheet patterns with multiple duct-like structures filled with eosinophilic coagulum (Figure 4). The nests of ductal and myoepithelial cells are interspersed with areas of hyalinization (Figure 5). Areas of extensive squamous metaplasia were also noted (Figure 6).

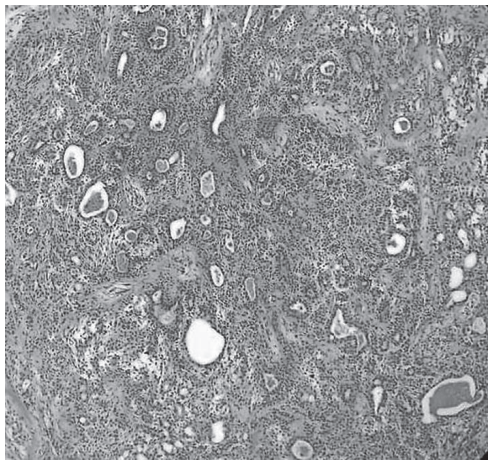

Figure 4 – Ductal and myoepithelial cells arranged in sheet patterns with multiple duct like structures filled with eosinophilic coagulum (hematoxilin and eosin stain 20×).

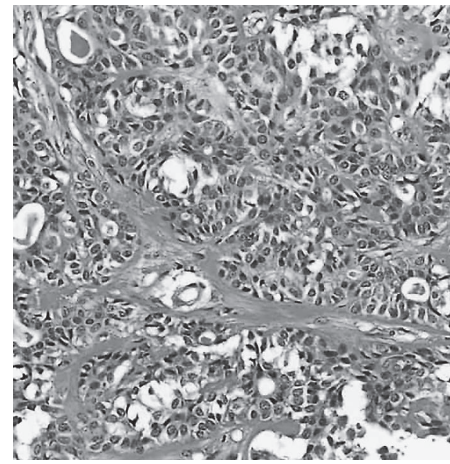

Figure 5 – Nests of ductal and myoepithelial cells are interspersed with areas of hyalinization (hematoxilin and eosin stain 40×).

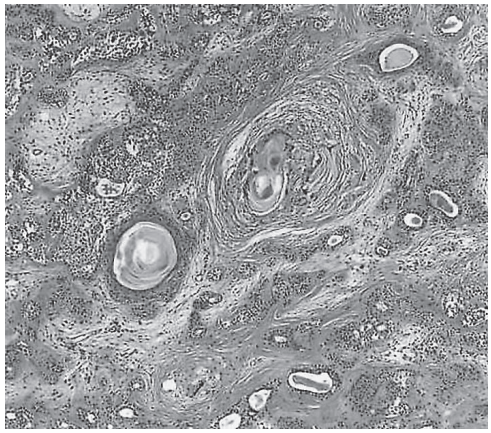

Figure 6 – Areas of extensive squamous metaplasia in the form of keratin pearls (hematoxilin and eosin stain 40×).

A final diagnosis of PA was given. A conservative treatment approach was opted for considering the age of the patient (young). Teeth #35 #36 and #37 were extracted and enucleation of the tumour was performed under general anesthesia, extra-oral approach was opted (Figure 7) because, with the extraction of three teeth and multiple perforations in the buccal and lingual plate, mandible would be susceptible to fracture due to the opposite pull suprahyoid and pterygomassetric sling, so it was decided to place the recon plate to strengthen the mandible, which would have been difficult to place intraorally (Figure 8). The patient was recalled every six months and the follow-up of the patient was uneventful and showed no recurrence to date (Figure 9).

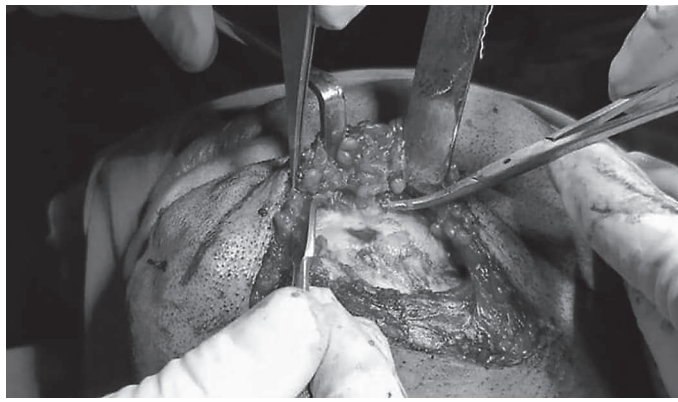

Figure 7 – Removal of the tumour via extra oral approach.

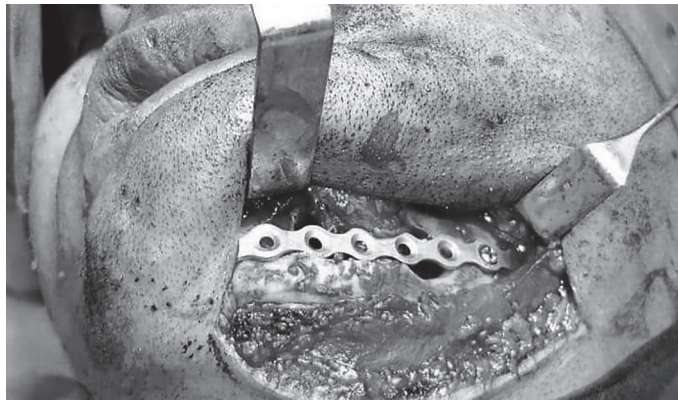

Figure 8 – Insertion of reconstructive plates.

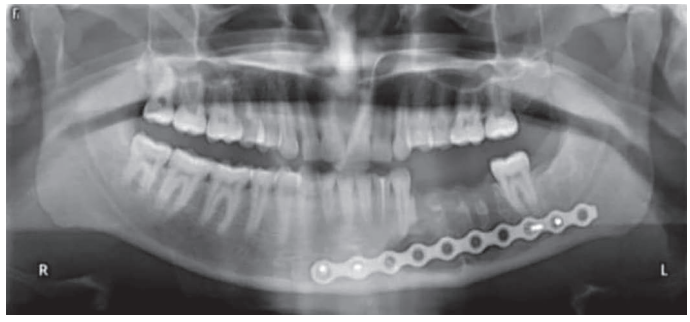

Figure 9 – Follow-up panoramic view reveals no sign of recurrence.

Discussion

The occurrence of salivary gland tumours as an intra-osseous/central tumour is a rare phenomenon. Mucoepidermoid carcinoma is the most common salivary gland tumour that has been reported to occur centrally, followed by adenoid cystic carcinoma (Alshagroud et al., 2017). PAs are the most common salivary gland

tumours that can occur in major and minor salivary glands. Intra-osseous PAs are extremely rare only 10 cases have been reported so to the best of our knowledge (Aver-De-Araujo et al., 2002). Several theories have been proposed to explain the intra-osseous origin of salivary gland tumours. The first theory explains the neoplastic changes in the ectopic glandular tissue inside the bone may give rise to intra-osseous salivary gland tumours, and the second theory explains that such tumours may arise due to the metaplastic changes in a pre-existing odontogenic cystic lining (Bouquot et al., 2000). The present case favours the first theory since it did not show any association with an odontogenic cyst. The mean age of occurrence for central PA is 58.8 (Arcuri et al., 2011). A rare case of central PA occurring in an eleven-year-old boy has also been reported (Bajpai, 2018). Radiologically central PA can predispose a diagnostic challenge to clinicians owing to their diverse radiographic features ranging from a unilocular cystic pattern to a multilocular destructive pattern (Arcuri et al., 2011). The present case showed a multilocular radiolucent pattern similar to ameloblastoma. Histopathologically, central PA shows features quite similar to the conventional PA of major and minor salivary glands (Aver-De-Araujo et al., 2002; Alshagroud et al., 2017). PA with extensive keratinization has also been reported in the literature (Bajpai and Pardhe, 2018), present case also showed squamous metaplasia at a few places. Wide local excision with the removal of the involved periosteum is considered as the treatment of choice though the present case was treated by the thorough enucleation of the mass (Vicente et al., 2008). Regarding why the present case was treated with enucleation rather than resection because we felt that the patient was young and could not be left without a reconstruction, where free fibula was an obvious choice, but that itself could have its possible complications, the patient chose to go conservative with organ preservation, moreover, the peripheral osteotomy was performed to reduce the chance of recurrence.

Recurrence rate of 2–44% has been reported in the parotid gland PA (Kowalik, 1966). There is a paucity of information regarding the recurrence rate of intra-osseous PA.

Conclusion

Central Pleomorphic adenoma is the rarest diagnostic possibility that comes to the mind of a clinician when comes a patient with an osteodestructive central lesion. Such lesions can impose a diagnostic difficulty due to their rarity in jaws and overlapping clinical and radiological features. Centrally located Pleomorphic adenoma should be followed up for a long time because their recurrence rate and malignant transformation have not been sufficiently described yet.

References

Aghaghazvini, L., Aghaghazvini, S. (2015) Intraosseous pleomorphic adenoma of the mandible. *Iran. J. Radiol.* **12(1)**, e6921.

Alshagroud, R., Kamoh, A., Popat, S. R., Brandwein-Weber, M., Aguirre, A. (2017) Metastasizing pleomorphic adenoma case report and review of the literature. *Head Neck Pathol.* **11(4)**, 487–493.

Arcuri, F., Grivetto, F., Poglio, G., Brucoli, M., Benech, A. (2011) Simultaneous palatal pleomorphic adenoma and mandibular keratocystic odontogenic tumor in a pediatric patient. *J. Craniofac. Surg.* **22(6)**, 2347–2350.

Aver-De-Araujo, L. M., Chaves-Tarquinio, S. B., Neuzling-Gomes, A. P., Etges, A. (2002) Intraosseous pleomorphic adenoma: Case report and review of the literature. *Med. Oral* **7(3)**, 164–170. (in English, Spanish)

Bajpai, M. (2018) Central pleomorphic adenoma of mandible – Report of the first case in a pediatric patient. *National Journal of Health Sciences* **3**, 63–65.

Bajpai, M., Pardhe, N. (2018) Pleomorphic adenoma of submandibular gland with extensive cystic keratinization. *J. Coll. Physicians Surg. Pak.* **28(1)**, 84.

Bajpai, M., Pardhe, N., Chandolia, B., Arora, M. (2018) Central acinic cell carcinoma of the mandible simulating as benign odontogenic lesion: A case report. *Iran. J. Med. Sci.* **43(2)**, 223–226.

Bouquot, J. E., Gnepp, D. R., Dardick, I., Hietanem, J. (2000) Intraosseous salivary tissue: Jawbone examples of choristomas, hamartomas, embryonic rests and inflammatory entrapment. *Oral Surg. Oral Med. Oral Pathol. Oral Radiol. Endod.* **90**, 205–217.

Brookstone, M. S., Huvos, A. G. (1992) Central salivary gland tumors of the maxilla and mandible: A clinicopathologic study of 11 cases with an analysis of the literature. *J. Oral Maxillofac. Surg.* **50(3)**, 229–236.

Kowalik, S. (1966) Mixed tumor starting from the jaw bone. *Otolaryngol. Pol.* **20**, 563–564. (in Polish)

Manola, M., Moscillo, L., De Luca, E., Lalinga, A. V., Possidente, L. (2019) Intraosseous pleomorphic adenoma of the maxilla: A case report and literature review. *J. Otolaryngol. Rhinol.* **5**, 064.

Ojha, J., Bhattacharyya, I., Islam, M. N., Manhart, S., Cohen, D. M. (2007) Intraosseous pleomorphic adenoma of the mandible: Report of a case and review of the literature. *Oral Surg. Oral Med. Oral Pathol. Oral Radiol. Endod.* **104(2)**, e21–e26.

Vicente, O. P., Marques, N. A., Aytes, L. B., Escoda, C. G. (2008) Minor salivary gland tumors: A clinicopathological study of 18 cases. *Med. Oral Patol. Oral Cir. Bucal* **13**, 582–588.

 Prague Medical Report / Vol. 125 (2024) No. 2, p. 158–162

Coracoclavicular Joint Arthrosis – An Uncommon Cause of Shoulder Pain

Natã Nascimento de Jesus Graça[1], Márcio Luís Duarte[2]

[1] Department of Internal Medicine, Universidade do Oeste Paulista – Campus Guarujá, Guarujá (SP), Brazil;
[2] Universidade de Ribeirão Preto – Campus Guarujá, Guarujá (SP), Brazil

Received March 25, 2023; Accepted May 7, 2024.

Key words: Tomography – X-ray computed – Shoulder joint – Pain – Radiography

Abstract: The coracoclavicular joint is a diarthrodial synovial joint that is eventually located between the upper surface of the horizontal part of the coracoid process and the conoid tubercle of the clavicle, and is considered an unusual anatomical alteration. The coracoclavicular joint has a low prevalence and can be diagnosed by imaging tests – radiography and computed tomography. Treatment can be performed both conservatively and surgically. We report a case of an 81-year-old female patient presenting of pain in her left shoulder due to coracoclavicular joint arthrosis. A radiograph of the left shoulder was performed, which detected a deformity in the lower portion of the middle third of the clavicle and the upper portion of the coracoid process, corresponding to the coracoclavicular joint, a finding confirmed by computed tomography. The patient was treated conservatively with analgesics (Dipyrone) and anti-inflammatories (Ibuprofen) with improvement in symptoms.

Mailing Address: Dr. Márcio Luís Duarte, Department of Radiology, Universidade de Ribeirão Preto (UNAERP) – Campus Guarujá, Av. D. Pedro I, 3.300, Enseada, Guarujá (SP), 11440-003, Brazil; Phone: 005 513 339 810 00; e-mail: marcioluisduarte@gmail.com

https://doi.org/10.14712/23362936.2024.15

Introduction

The coracoclavicular joint is a diarthrodial synovial joint that eventually lies between the superior surface of the horizontal part of the coracoid process and the conoid tubercle of the clavicle. It was first described by Gruber in the late 19th century. The coracoclavicular joint is considered an uncommon anatomical alteration (Singh et al., 2009).

It is essential to emphasize the higher incidence in Asians than in Europeans or Africans (Paraskevas et al., 2009). The mean age at which shoulder pain related to the coracoclavicular joint presents is 42 years old, with a ratio between men and women of 1.1:4 (Willekens et al., 2013).

Although coracoclavicular diarthrosis is considered a neglected structure, its presence is clinically relevant to determine the origin of shoulder pain and the decision to treat it in some cases (Paraskevas et al., 2009). The presence of such a joint can cause, in some cases, shoulder pain radiating to the arm (Singh et al., 2011).

Herein, we report the case of an 81-year-old female patient presenting pain in her left shoulder for three months.

Case report

An 81-year-old female patient presenting pain in her left shoulder for three months. She informs that the pain radiates to the arm, limiting daily activities, having difficulty lifting weights, and hang clothes on the clothesline. She denies a history of trauma and previous surgeries.

On physical examination, she doesn't show edema and hematoma, but has a positive Hawkins-Kennedy impingement test. Refers pain with elevation of the left upper limb and in Jobe's test.

The radiography of the left shoulder was performed, which detected a deformity in the lower portion of the middle third of the clavicle and the upper portion of the coracoid process, corresponding to the coracoclavicular joint arthrosis (Figure 1), later confirmed by computed tomography (CT) scan (Figure 2).

The patient was treated conservatively with analgesics (Dipyrone) and anti-inflammatories (Ibuprofen) with improvement in symptoms in one week.

Discussion

Some authors report few symptomatic cases. Singh et al. (2011) analysed 21 symptomatic cases of the coracoclavicular joint and detected that the predominant characteristic was pain in the shoulder followed by movement limitation. In addition, other associated complaints can be exemplified, such as

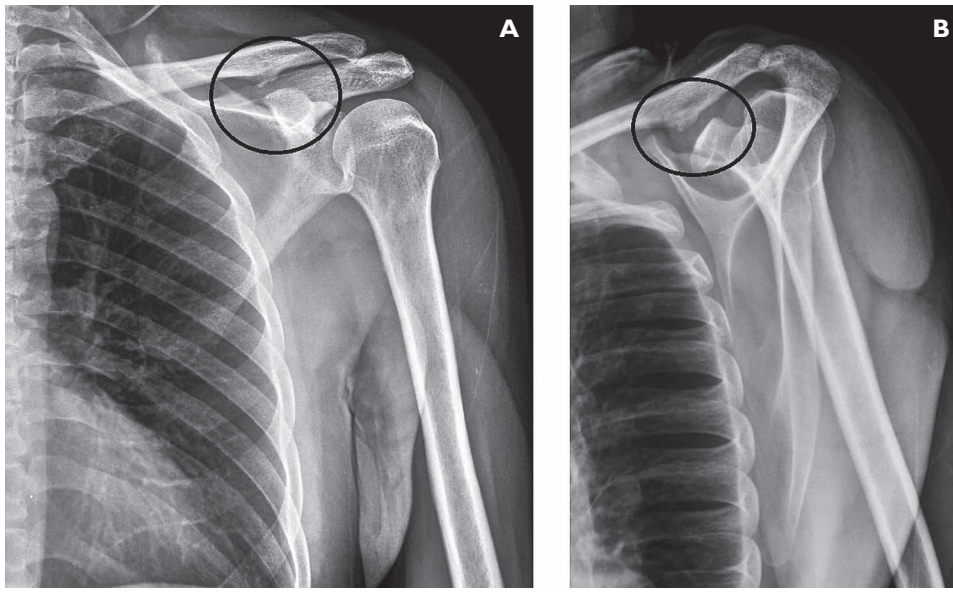

Figure 1 – Radiography of the left shoulder in the posteroanterior view (A), and in the lateral scapular view (B), demonstrating arthrosis of the coracoclavicular joint (black circle).

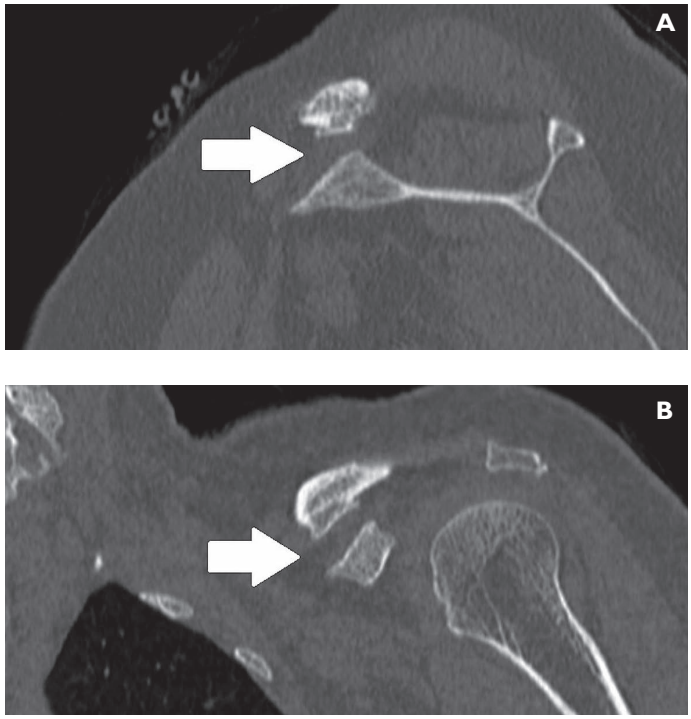

Figure 2 – Computed tomography scan bone window of the left shoulder in the sagittal section (A), and in the coronal section (B), demonstrating arthrosis of the coracoclavicular joint (white arrow).

upper limb paresthesia, brachialgia, and pain with ipsilateral irradiation. Patients had localized swelling and tenderness at the site of the anomalous joint and hand weakness (Schuh et al., 2018).

The coracoclavicular joint has been associated with cervicobrachial syndrome, decreased shoulder movement, and degenerative changes in adjacent joints (Willekens et al., 2013). The origin of the pain is attributed to impairment of the brachial plexus, where microscopic nerves are compressed and are relieved after joint removal (Paraskevas et al., 2009). Another cause described in the literature is the set of degenerative alterations of the joint and its proximity to the brachial plexus (Paraskevas et al., 2009). Compression of the brachial plexus can be seen on magnetic resonance imaging (MRI) in extreme shoulder abduction (Nehme et al., 2004).

Aging is an important factor in the development of this joint. In an osteological study, five coracoclavicular joints were observed. Among them, joint facets were found in adults over 25-years-old, being found bilaterally in two individuals; in an individual unilaterally to the left; in two unilaterally to the right. The analysis of 1,000 adult individuals aged between 18 and 95 years to analyse the incidence of the coracoclavicular joint resulted in: an incidence of 10.1% in men, 5.7% bilateral, and 4.4% unilateral, while the incidence in women was 8.3%, 3.6% bilateral and 4.8% unilateral (Nehme et al., 2004).

Some authors claim that the formation of the coracoclavicular joint is conditioned by genetics. Likewise, some cadaveric studies have not found a coracoclavicular joint in neonates and young children. Another study evaluated paired clavicles of 50 neonates and 35 fetuses in northwest India but concluded that the facet joints were absent, leading to the reasoning that the coracoclavicular joint has a non-congenital cause (Kaur and Jit, 1991; Nehme et al., 2004).

Local anesthesia with the aid of imaging tests helps to understand the location of the origin of the pain. If there is partial symptomatic remission after targeted injectable analgesia, the coracoclavicular joint should be considered as the pathological site. This joint can be seen by radiography and confirmed by CT scan, presenting it with degenerative alterations (Willekens et al., 2013), as in the case reported. However, dynamic MRI can be used if the symptoms are secondary to neurovascular impact – the result of the mechanical alteration of the shoulder – because conservative treatment will not be effective. MRI visualizes the anatomy of soft tissues, and bones, and also evidence of traction or impingement of neurovascular structures in various regions of the arm (Singh et al., 2011).

The treatment can be surgical or conservative. Conservative treatment is the first line of treatment and has low efficacy, consisting of the use of anti-inflammatories, physiotherapy, lifestyle modification, or local injection of corticosteroids under fluoroscopy. It is indicated for a specific group of patients, being elderly people with low functional demand, patients who do not want to be admitted to surgery, and patients with a high American Society of Anesthesiologists (ASA) score for high

respiratory risk. Due to the failure of conservative treatment, there is justification for surgical excision of the joint, which has a success rate of 100% (Singh et al., 2011).

It is possible to observe that in the clinical presentation of the exposed case, the image pattern in the diagnostic methods used and the conduct performed – conservative therapy – as the first-choice treatment followed the recommended literature, with no need for surgical intervention. However, even though conservative therapy has a low success rate, it is undeniable that the symptomatic treatment was effective for the patient in this case.

Conclusion

In this case, we report the presence of a coracoclavicular joint, which has a low prevalence, in an elderly patient, whose diagnosis was confirmed with imaging tests – radiography and CT scan. Treatment can be performed both conservatively and surgically. However, it has been reported that the invasive process (surgical excision of the joint) is 100% effective and has a curative effect, promoting immediate pain relief.

References

Kaur, H., Jit, I. (1991) Brief communication: Coracoclavicular joint in Northwest Indians. *Am. J. Phys. Anthropol.* **85(4)**, 457–460.

Nehme, A., Tricoire, J. L., Giordano, G., Rouge, D., Chiron, P., Puget, J. (2004) Coracoclavicular joints. Reflections upon incidence, pathophysiology, and etiology of the different forms. *Surg. Radiol. Anat.* **26(1)**, 33–38.

Paraskevas, G., Stavrakas, M. E., Stoltidou, A. (2009) Coracoclavicular joint, an osteological study with clinical implications: A case report. *Cases J.* **2**, 8715.

Schuh, A., Seehaus, F., Onyemaechi, N. O., Hönle, W. (2018) Osteoarthritis in a symptomatic coracoclavicular joint. *Glob. Med. Ther.* **3(1)**, 10.15761/gmt.1000106.

Singh, V. K., Singh, P. K., Balakrishnan, S. K. (2009) Bilateral coracoclavicular joints as a rare cause of bilateral thoracic outlet syndrome and shoulder pain were treated successfully by conservative means. *Singapore Med. J.* **50(6)**, e214–e217.

Singh, V. K., Singh, P. K., Trehan, R., Thompson, S., Pandit, R., Patel, V. (2011) Symptomatic coracoclavicular joint: Incidence, clinical significance, and available management options. *Int. Orthop.* **35(12)**, 1821–1826.

Willekens, I., Maeseneer, M. D., Boulet, C., Verhelle, F., de Mey, J. (2013) Coracoclavicular joint with shoulder pain. *JBR-BTR* **96(1)**, 44.

Accessory Flexor Carpi Ulnaris Muscle in Humans: A Rare Anatomical Case with Clinical Considerations

Dibakar Borthakur, Arthi Ganapathy, Mohammed Ahmed Ansari, Ritu Sehgal

Department of Anatomy, All India Institute of Medical Sciences, New Delhi, India

Received November 28, 2023; Accepted May 7, 2024.

Key words: Accessory flexor carpi ulnaris muscle – Human anatomical variation – Forearm flexors

Abstract: Anatomical variations of the forearm flexor muscles are occasionally encountered. Though usually observed incidentally during autopsies or imaging studies, they may at times cause concern due to associated clinical symptoms. This report presents a case of unilateral accessory flexor carpi ulnaris (AFCU) muscle observed in a human male cadaver aged 78 years. During routine cadaveric dissection, an anomalous AFCU muscle was observed in the left forearm of a human male cadaver aged 78 years. Standard institutional guidelines pertaining to the use of human cadaver for teaching and research were followed. A thorough literature review about the flexor carpi ulnaris (FCU) through the PubMed, Embase and Google scholar databases was undertaken, using the keywords – accessory flexor carpi ulnaris muscle, aberrant flexor carpi ulnaris muscle and anatomical variation of flexor carpi ulnaris muscle. Relevant gross anatomical findings were recorded and photographed. AFCU was identified on the medial aspect of the distal third of the left forearm. The AFCU was found originating from the ante-brachial fascia and the fascia covering the FCU on the left forearm, forming a small separate belly deep to the main muscle. It terminated as a thin tendon running alongside the hypothenar muscles and attached distally to the base of the proximal phalanx of the little finger. The AFCU was found to be innervated by a branch of the ulnar nerve. Awareness about the rare AFCU muscle is clinically important as a possible cause of ulnar nerve compression but also as a possible graft in reconstruction surgeries.

Mailing Address: Dr. Ritu Sehgal, Department of Anatomy, Preclinical Block, All India Institute of Medical Sciences, Ansari Nagar, New Delhi 110029, India; e-mail: ritusehgal.aiims@gmail.com

https://doi.org/10.14712/23362936.2024.16

Introduction

The flexor carpi ulnaris (FCU), the most medial of the superficial forearm flexors, arises from two heads, humeral and ulnar, connected by a tendinous arch called the arcuate ligament of Osborne (Tubbs et al., 2016). The smaller *humeral head* originates from the medial epicondyle through the common flexor origin together with other superficial forearm flexors. The *ulnar head* has an extensive origin from the medial aspect of the olecranon process, an aponeurotic origin from the proximal two-thirds of the posterior border of ulna, and a minor origin from the intermuscular septum separating it from the flexor digitorum superficialis. The thick tendon forming along its anterolateral border in its distal half, descends on the medial aspect of the forearm to insert initially to the pisiform bone. From the pisiform, it is prolonged to the hook of the hamate and the fifth metacarpal bone by pisohamate and pisometacarpal ligaments (Sookur et al., 2008; Watts, 2021). The ulnar nerve innervates the two heads separately (Sookur et al., 2008).

The FCU functions as a palmar flexor of the wrist, and as an ulnar deviator in combination with extensor carpi ulnaris. Additionally, the FCU also supports the medial collateral ligament of the elbow joint. The FCU may be used as a free vascularised flap, if its unique surgical anatomy is taken under consideration. The muscle is also commonly utilized for tendon transfer to extensors of the wrist, particularly in cases of radial nerve palsy (Niumsawatt et al., 2013).

Aberrant and accessory muscles, often detected as incidental findings during surgeries and imaging studies, may confuse clinicians and surgeons (Sookur et al., 2008). Sometimes they become clinically important owing to their potential for

Table 1 – A brief literature review to summarize observations about the accessory flexor carpi ulnaris (AFCU) and other related variations of the flexor carpi ulnaris (FCU) muscle

Authors	Population and study type	Cohort size (number of probands)	Notable findings
López Milena et al. (2001)	Spanish, clinical case	single case	Symptomatic unilateral AFCU (side not mentioned in the report) in a 25-year-old fisherman, causing ulnar nerve compression, treated by partial resection of the muscle.
Campos et al. (2010)	Brazilian, cadaveric case	single case	Incidental AFCU on the left forearm, observed in a 59-year-old male cadaver.
Ang et al. (2010)	Australasian, clinical case	single case	Incidental AFCU at the left wrist, observed in a 29-year-old man during ulnar nerve repair.

Authors	Population and study type	Cohort size (number of probands)	Notable findings
Çıftçıoğlu et al. (2011)	Turkish, cadaveric case	single case	Incidental AFCU in the left forearm in a 65-year-old male cadaver.
Alvin et al. (2011)	American, cadaveric case	single case	Incidental AFCU in the left forearm in a 87-year-old male cadaver.
Niumsawatt et al. (2013)	–	review	Proposed an improved system of classification of the AFCU variants, different from the existing system earlier described by Testut and Latarjet.
Sakthivel and Verma (2017)	Indian, cadaveric case	single case	AFCU observed in the left forearm of a 61-year-old male cadaver, along with an absent palmaris longus muscle.
Wang and Ng (2021)	Malaysian, clinical cases	two cases	Distal ulnar nerve compression due to AFCU reported: one in the left wrist of a 29-year-old female and the other in the right wrist of a 58-year-old male patient.
Sawant (2013)	Indian, cadaveric case	single case	Additional slips of FCU (not convincing enough to be classified as AFCU) passing over the ulnar artery and ulnar nerve in the right wrist.
Vollala and Kumar (2006)	Indian, cadaveric study	100 cases	1% incidence of the AFCU on the left forearm among 100 dissected upper limbs was reported.
Bhardwaj et al. (2013)	Indian, clinical case	single case	Two heads of FCU observed (one regarded as AFCU) in a 31-year-old male patient, tendons of which were utilized for reconstruction procedures following Volkmann's ischemic contracture deficits. This case highlighted the clinical utility of the AFCU for the first time.
Iliev et al. (2016)	Bulgarian, cadaveric case	single case	Bilateral crescent-shaped fibro-muscular-tendinous structure arising from FCU muscle in a 69-year-old female cadaver.
Yonguç et al. (2018)	Turkish, cadaveric case	single case	Split AFCU on the left side in a male cadaver.
Kunc et al. (2019)	European, cadaveric case	single case	Incidental AFCU inserting on the flexor retinaculum in the right forearm of a 74-year-old male cadaver.
Pressney et al. (2020)	British, clinical case	single case	AFCU presenting as a symptomatic pseudo-tumour on the right wrist of a 13-year-old girl.

causing neurovascular compression or limb deformity (López Milena et al., 2001; Niumsawatt et al., 2013). The accessory flexor carpi ulnaris (AFCU) is a very rare anatomical variation of FCU, with only a very few cases described in literature which are summarized in Table 1. In fact, as of today there are less than 20 reported cases of AFCU, with an approximate incidence ranging between 0.02–2.0% (Vollala and Kumar, 2006; Ang et al., 2010; Kunc et al., 2019). Table 1 summarizes observations about FCU variations reported earlier. The AFCUs exhibit great variation in origin, insertion, arrangement in relation to the main FCU, and in their innervation patterns.

An accidentally observed cadaveric case of AFCU on the left forearm is presented in this case report, together with an updated literature review.

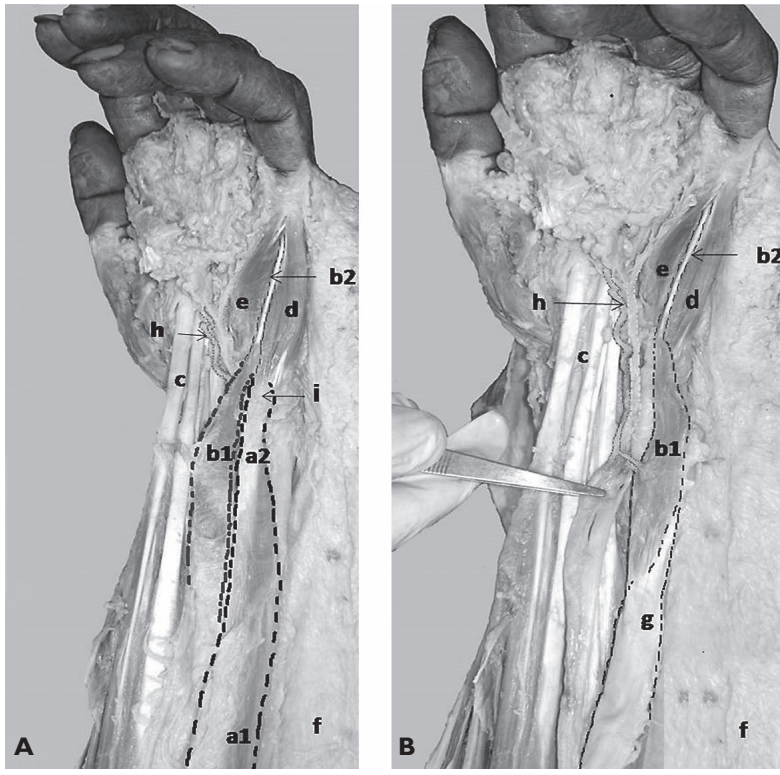

Figure 1 – Left forearm, medial view (A), anterior view (B). A) Dissected accessory flexor carpi ulnaris muscle observed between the flexor digitorum superficialis and the flexor carpi ulnaris muscle tendons in the forearm. B) Accessory flexor carpi ulnaris muscle reflected medially showing the ulnar nerves and vessels (the flexor carpi ulnaris muscle is placed posterior to the accessory flexor carpi ulnaris muscle and not seen in this image). The structures labelled in the images are: a1 – flexor carpi ulnaris muscle belly; a2 – flexor carpi ulnaris tendon; b1 – accessory flexor carpi ulnaris muscle belly; b2 – accessory flexor carpi ulnaris tendon; c – flexor digitorum superficialis tendons; d – abductor digiti minimi muscle belly; e – flexor digiti minimi muscle belly; f – superficial fascia of the forearm; g – deep fascia of the forearm; h – ulnar vessels and nerves outlined in broken lines; i – pisiform bone.

Case report

Both upper limbs of a 78-year-old male cadaver were dissected following standard steps of dissection, and the findings recorded and photographed (Figure 1). The various dimensions of the FCU and AFCU (if present) muscles such as length, breadth and thickness of the muscle belly, length and breadth of the tendinous portion, were measured using a non-stretchable measuring tape and Vernier callipers.

On the left side, the entire FCU was found to measure 25.3 cm in total length, of which the muscle belly measured 22.5 cm and its tendon measured 2.8 cm. The lower third of the left forearm was found to exhibit an additional muscle which was identified as the AFCU. The AFCU was located between the FCU and the flexor digitorum superficialis (FDS) in the left forearm, and found to originate from the deep fascia of the forearm and from the fascia covering the FCU muscle.

The muscle belly of the AFCU was seen as fusiform in shape, measuring 7.3 cm in length, 2.1 cm in breadth and 0.4 cm in thickness. The tendon of the AFCU measured 5.4 cm in length, 0.3 cm in breadth and coursed lateral to the tendon of the FCU, passing superficial to the flexor retinaculum and giving a few tendinous slips to the pisiform bone. More distally, the tendon was seen to merge with tendons of the flexor digiti minimi and abductor digiti minimi muscles, eventually terminating at the ventrolateral aspect of the base of the proximal phalanx of the little finger (Figure 1B). The left AFCU muscle belly was observed to be much smaller than the left FCU muscle, transitioning into a slender tendon just proximal to the wrist joint, and passing distally superficial to the flexor retinaculum (Figure 1A). The ulnar nerve and artery were found to run between the AFCU and the FDS in the lower part of the forearm. The neurovascular supply of the AFCU muscle was seen to be derived from the ulnar nerve and vessels. The right forearm was not found to exhibit any accessory or aberrant muscle.

Discussion

The upper limb bud is formed as an outgrowth of the somatic mesoderm on the ventrolateral aspect of the embryo at approximately 4 weeks of intrauterine life, under the master regulation of sonic hedgehog (SHH) gene expressed by the notochord. The mesodermal outgrowth is visible as an apical ectodermal ridge (AER). The embryological upper limb bud forms four zones; the *stylopod* or the future arm, the *zeugopod* or the future forearm, the *mesopod* or the future wrist and the *autopod* or the future hand (Al-Qattan and Kozin, 2013). Zeugopod cells express HOXA11 and HOXD9 during the period of establishment of these zones.

The central group of cells initially forms a blastema in the developing upper limb bud. Development of muscles starts with segmentation of the paraxial mesoderm

into somites. Each somite has two parts: the *sclerotome* and the *dermo-myotome*. At about 5 weeks of gestation, the myoblasts originating from the myotomes migrate to specific sites in the upper limb bud to develop into the musculature of the upper limb. Myoblast cells aggregate into two muscle masses – the ventral and the dorsal muscle masses, which give rise to the flexor and the extensor group of muscles respectively (Pires et al., 2019). The skeletal muscle fibres may be identified in an embryo by approximately 7 weeks of intrauterine life. Proximal and superficial groups of muscles differentiate earlier than the distal and deeper groups of muscles with simultaneous nerve ingrowths. There are different proteins and transcription factors which regulate the spatial organization of the developing upper limb. Engrailed-1 (EN-1) expressed by the ventral ectoderm and WNT7 expressed by dorsal ectoderm mediate the dorsoventral axis. The proximo-distal axis is regulated by the FGF8, FGF4, FGF2 and WNT3A secreted by the AER (Al-Qattan and Kozin, 2013). Overall, signals from the neural tube, ectoderm and the lateral mesoderm provide signals for medio-lateral patterning so that the myogenic cells effectively migrate to form limb muscles.

The definite postnatal morphology of individual muscles is attained through complex interactions of several growth stimulators and apoptotic factors that influence the optimal differentiation of the myogenic cells during intrauterine life. The definitive form of a limb muscle is attained very early during embryonic development. It has been suggested that it is not the myogenic cells themselves, but the associated connective tissue which guides the myogenic precursor cells to differentiate into a specific muscle type and attain their final form. The myogenic precursor cells are morphogenetically neutral in behaviour (Carlson, 2014). Accessory muscles are formed in response to an imbalance in cell growth stimulating factors and factors controlling apoptosis (Buckingham et al., 2003). According to another theory, anomalies of the flexor muscles of the forearm have been attributed to a faulty separation of the flexor blastema (Bhardwaj et al., 2013).

A rough estimate of incidence of anatomical variations in the forearm flexors varies between 5–25%, but the incidence of AFCU is approximately 0.16% (Ang et al., 2010). The approximate incidence of AFCU from existing reports ranges between 0.02–0.2% (Niumsawatt et al., 2013; Tubbs et al., 2016). A study on 100 upper limbs of cadavers of South Indian origin reported an incidence of 1% for the AFCU, which seems to be an overestimate (Vollala and Kumar, 2006).

Very few cases of the AFCU have been reported by different authors in the erstwhile literature, and there is inconsistent nomenclature for the variations. Different authors named the FCU variations differently: supernumerary belly of FCU, aberrant FCU, accessory FCU, digastric FCU, flexor carpi ulnaris palmaris muscle etc. (Arnold and Zech, 1977; Ang et al., 2010; Alvin et al., 2011). In their seminal multi-volume anatomical tome entitled “Traité d’anatomie humaine”, Testut and Latarjet described a classification system for FCU anomalies as early as 1928. More recently, Bhardwaj and co-workers (2013) suggested a new system of

classification and nomenclature, mentioning the various subtypes of the variant FCU. They classified the FCU anomalies into three distinct groups: type I – single muscle belly with split or bifurcate tendons; type II – digastric or two muscle bellies with an intermediate tendon; type III – accessory FCU characterized by the presence of an additional muscle belly adjacent to the main muscle belly. The additional muscle belly and tendon may not have similar attachments as the main muscle or may share attachments with any of the other forearm flexor muscles in the vicinity.

The type III insertion of the AFCU on the pisiform bone has been reported (López Milena et al., 2001). A few reports described this AFCU attachment to pisiform further getting prolonged to merge with the hypothenar muscles, similar to that which has been observed in the present case (Mori, 1964). Such a prolonged distal tendinous slip may compress the ulnar neurovascular bundle and give rise to diverse clinical symptoms (O'Hara and Stone, 1988). There are reported cases of ulnar nerve compression in the Guyon's canal due to the AFCU or accessory abductor digiti minimi tendon (Kwak et al., 2011; Yasen, 2012; Paget et al., 2013). As the AFCU is very rare, it may be often overlooked as a possible cause of ulnar nerve entrapment. Furthermore, presence of such an accessory muscle may also be confused with a mass in the distal forearm. Newer imaging techniques can be effectively utilized to confirm the presence of a suspected AFCU muscle when presenting as a mass or causing neurovascular compression (López Milena et al., 2001). Presence of the AFCU seems to be easily diagnosable using magnetic resonance imaging (MRI) scans (Rau et al., 2014), and this modality may be a convenient means for elucidating further details about the morphology of this muscle.

The muscle presented here resembles a rare small muscle known as the ulno-carpeus brevis observed in 1.9% of cases (Tubbs et al., 2016), with a proximal attachment on the ulnar medial or anterior surface and a distal attachment variably on the pisiform bone, the hook of hamate, the proximal end of the fifth metacarpal bone or the abductor digiti minimi (Mori, 1964; Tubbs et al., 2016). A unilateral flexor carpi ulnaris brevis was recently described in a 19-year-old boy during repair surgery of forearm flexor tendons in the right wrist following an accidental cut injury. The presence of the additional muscle was later confirmed by an MRI study (Chong et al., 2009). We observed the small AFCU muscle belly in relation to the distal part of the left FCU which became tendinous distally and blended with the tendons of the hypothenar muscles. Thus the present case may be identified as of the type III variety, according to the classification system proposed by Bhardwaj and co-workers in 2013. Only a very few AFCU cases reported are of type III variety, though their precise incidence has not yet been estimated. Considering the extremely few reported cases, the proper identification and reporting of every single case is warranted. Table 1 presents a comprehensive summary of the AFCU anomalies reported so far. Although it is improper to comment on the predilection of AFCU variations for a particular side (left/right) considering the few reported cases, it may be observed from this table that these variations are more common on the left side.

Conclusion

Although very rare in occurrence, the accessory flexor carpi ulnaris should be considered and ruled out in all cases of ulnar nerve entrapment. Awareness about this forearm variation is essential for hand surgeons to avoid misinterpretation of the muscle as a mass and to avoid iatrogenic injuries. Additionally, the AFCU may be used as a free vascularised muscle flap and utilized in tendon transfer surgeries.

References

Alvin, M., Alan, N., Leone, J., Fredieu, J. R. (2011) A unilateral accessory flexor carpi ulnaris muscle observed during cadaveric dissection. *Clin. Anat*. **24(8)**, 971–973.

Al-Qattan, M. M., Kozin, S. H. (2013) Update on embryology of the upper limb. *J. Hand Surg. Am*. **38(9)**, 1835–1844.

Ang, G. G., Rozen, W. M., Vally, F., Eizenberg, N., Grinsell, D. (2010) Anomalies of the flexor carpi ulnaris: Clinical case report and cadaveric study. *Clin. Anat*. **23(4)**, 427–430.

Arnold, G., Zech, M. (1977) An accessory muscle and additional variants of the forearm. *Handchirurgie* **9(3)**, 135–136.

Bhardwaj, P., Bhandari, L., Sabapathy, S. R. (2013) Supernumerary flexor carpi ulnaris – Case report and review. *Hand Surg*. **18(03)**, 393–397.

Buckingham, M., Bajard, L., Chang, T., Daubas, P., Hadchouel, J., Meilhac, S., Montarras, D., Rocancourt, D., Relaix, F. (2003) The formation of skeletal muscle: From somite to limb. *J. Anat*. **202(1)**, 59–68.

Campos, D., Nazer, M. B., Bartholdy, L. M., Souza, P. L. (2010) Accessory flexor carpi ulnaris muscle: A case report of a rare variation in human. *J. Morphol. Sci*. **27(1)**, 30–31.

Carlson, B. M. (2014) *Human Embryology and Developmental Biology*, 5th Edition. Elsevier/Saunders, Philadelphia.

Chong, S. J., Al-Ani, S., Pinto, C., Peat, B. (2009) Bilateral flexor carpi radialis brevis and unilateral flexor carpi ulnaris brevis muscle: Case report. *J. Hand Surg. Am*. **34(10)**, 1868–1871.

Çıftçıoğlu, E., Kopuz, C., Çorumlu, U., Demır, M. T. (2011) Accessory muscle in the forearm: A clinical and embryological approach. *Anat. Cell Biol*. **44(2)**, 160–163.

Iliev, A., Georgiev, G. P., Landzhov, B. (2016) A rare case of bilateral flexor carpi ulnaris variation: Anatomical and clinical considerations and literature review. *Rev. Arg. Anat. Clin*. **8(2)**, 98–103.

Kunc, V., Stulpa, M., Feigl, G., Kachlik, D. (2019) Accessory flexor carpi ulnaris muscle with associated anterior interosseous artery variation: Case report with the definition of a new type and review of concomitant variants. *Surg. Radiol. Anat*. **41**, 1315–1318.

Kwak, K. W., Kim, M. S., Chang, C. H., Kim, S. H. (2011) Ulnar nerve compression in Guyon's canal by ganglion cyst. *J. Korean Neurosurg. Soc*. **49(2)**, 139.

López Milena, G., Ruiz Santiago, F., Chamorro Santos, C., Cañadillas Barea, L. (2001) Forearm soft tissue mass caused by an accessory muscle. *Eur. Radiol*. **11**, 1487–1489.

Mori, M. (1964) Statistics on the musculature of the Japanese. *Okajimas Folia Anat. Jpn*. **40(3)**, 195–300.

Niumsawatt, V., Soliman, B. A., Rozen, W. M. (2013) The aberrant flexor carpi ulnaris and its clinical implications. *J. Plast. Reconstr. Aesthet. Surg*. **66(6)**, e172–e174.

O'Hara, J. J., Stone, J. H. (1988) Ulnar neuropathy at the wrist associated with aberrant flexor carpi ulnaris insertion. *J. Hand Surg. Am*. **13(3)**, 370–372.

Paget, J., Patel, N., Manushakian, J. (2013) Ulnar nerve compression in Guyon's canal: MRI does not always have the answer. *J. Surg. Case Rep*. **2013(1)**, rjs043.

Pires, L. A., Machado, G. D., Fernandes, R. M., Manaia, J. H., Champs, J. F., Babinski, M. A. (2019) Notes on the accessory flexor carpi ulnaris muscle: A rare supernumerary variation. *J. Morphol. Sci*. **36(02)**, 138–140.

Pressney, I., Upadhyay, B., Dewlett, S., Khoo, M., Fotiadou, A., Saifuddin, A. (2020) Accessory flexor carpi ulnaris: Case report and review of the literature. *BJR Case Rep*. **6(3)**, 20200010.

Rau, C. L., Yen, T. H., Wu, L. C., Huang, Y. Y., Jaw, F. S., Liou, T. H. (2014) Neglected ruptured flexor carpi ulnaris tendon mimics a soft tissue tumor in the wrist. *Am. J. Phys. Med. Rehabil*. **93(4)**, 355–358.

Sakthivel, S., Verma, S. (2017) Accessory flexor carpi ulnaris and bilaterally variant vascular anatomy of upper limb: An unusual presentation. *Int. J. Appl. Basic Med. Res*. **7(2)**, 143–145.

Sawant, S. P. (2013) A case report on an additional muscle slip of flexor carpi ulnaris with variant ulnar artery and ulnar nerve in the forearm. *World Res. J. Cardiol*. **1(1)**, 7–9.

Sookur, P. A., Naraghi, A. M., Bleakney, R. R., Jalan, R., Chan, O., White, L. M. (2008) Accessory muscles: Anatomy, symptoms, and radiologic evaluation. *Radiographics* **28(2)**, 481–499.

Tubbs, R. S., Shoja, M. M., Loukas, M. (2016) *Bergman's Comprehensive Encyclopedia of Human Anatomic Variation*. John Wiley and Sons Inc., Hoboken.

Vollala, V., Kumar, P. (2006) Additional belly of flexor carpi ulnaris muscle found in a South Indian male cadaver. *Internet J. Orthop. Surg*. **5(1)**, 5–8.

Wang, C. K., Ng, C. Y. (2021) Accessory flexor carpi ulnaris: A rare cause of distal ulnar nerve compression. *J. Hand Surg. Eur. Vol*. **46(2)**, 197–199.

Watts, A. C. (2021) Elbow and forearm. In: *Gray's Anatomy: The Anatomical Basis of Clinical Practice*, 42nd Edition. Standring, S., Elsevier, Amsterdam.

Yasen, S. (2012) Acute calcific tendinitis of the flexor carpi ulnaris causing acute compressive neuropathy of the ulnar nerve: A case report. *J. Orthop. Surg. (Hong Kong)* **20(3)**, 414–416.

Yonguç, G. N., Cirpan, S., Sayhan, S., Eyüboğlu, C., Güvençer, M. (2018) A variation of flexor carpi ulnaris muscle: A case report. *J. Basic Clin. Health Sci*. **2**, 57–59.

Weight-bearing Ultrasound to Diagnose Talar Dislocation Causing Tarsal Tunnel Syndrome

Márcio Luís Duarte[1], Mayara Oliveira da Silva[2], Ocacir de Souza Reis Soares[3], Norma Sueli Albino Moreira[4], Eduardo Kenzo Arie[5]

[1] Universidade de Ribeirão Preto – Campus Guarujá, Guarujá (SP), Brazil;
[2] Universidade Federal de São Paulo, Santos (SP), Brazil;
[3] Clínica Radiológica Ocacir Soares, Presidente Prudente, São Paulo, Brazil;
[4] Hospital Brasil, Santo André (SP), Brazil;
[5] Irmandade da Santa Casa de Misericórdia de Santos, Santos (SP), Brazil

Received May 16, 2023; Accepted May 7, 2024.

Key words: Nerve compression syndromes – Tarsal tunnel syndrome – Tibial nerve – Ultrasonography – Diagnosis

Abstract: The neuropathic compression of the tibial nerve and/or its branches on the medial side of the ankle is called tarsal tunnel syndrome (TTS). Patients with TTS presents pain, paresthesia, hypoesthesia, hyperesthesia, muscle cramps or numbness which affects the sole of the foot, the heel, or both. The clinical diagnosis is challenging because of the fairly non-specific and several symptomatology. We demonstrate a case of TTS caused by medial dislocation of the talar bone on the calcaneus bone impacting the tibial nerve diagnosed only by ultrasound with the patient in the standing position.

Mailing Address: Dr. Márcio Luís Duarte, Department of Radiology, Universidade de Ribeirão Preto (UNAERP) – Campus Guarujá, Av. D. Pedro I, 3.300, Enseada, Guarujá (SP), 11440-003, Brazil; Phone: 005 513 339 810 00; e-mail: marcioluisduarte@gmail.com

https://doi.org/10.14712/23362936.2024.17

Introduction

The tibial nerve goes by via the medial flank of the ankle and branches into the branches: medial plantar nerve, lateral plantar nerve, and medial calcaneal branch. This location is named the tarsal tunnel and is formed of the posterior tibial tendon, long flexor tendon of the fingers, neurovascular bundle, and flexor hallucis longus tendon (medial to lateral). Thus, little modifications in this area can easily result in neuropathy (de Souza Reis Soares et al., 2022).

The neuropathic compression of the tibial nerve and/or its branches on the medial side of the ankle is called tarsal tunnel syndrome (TTS). It has several etiologies, and the nature of the squeeze is detected in around 60–80% of the patients (Fantino et al., 2011). It is a difficult diagnosis that comprises manifestations originating from injury to the posterior tibial nerve or its branches as they move via the tarsal tunnel below the flexor retinaculum in the medial ankle. Although it is considered rare, TTS is easily overlooked and underdiagnosed (Tawfik et al., 2016). The prevalence of TTS established on electrophysiological investigations is registered as 0.4–0.5% (Khodatars et al., 2022).

Patients with TTS presents pain, paresthesia, hypoesthesia, hyperesthesia, muscle cramps or numbness which affects the sole of the foot, the heel, or both; the symptoms can appear during walking or exercise (Fantino, 2014). TTS can mimic plantar fasciitis (Khodatars et al., 2022). When the patient in at rest the symptoms can appear at night. The dorsiflexion and eversion of the foot can provoke the symptoms. Physical examination may show a potential deformation of the foot – varus or valgus deformity (Fantino, 2014). The clinical diagnosis is challenging because of the fairly non-specific and several symptomatology. Electrophysiological investigations can be non-specific and can be normal in 30% of the cases (Khodatars et al., 2022).

We demonstrate a case of TTS caused by medial dislocation of the talar bone on the calcaneus bone impacting the tibial nerve diagnosed by ultrasound with the patient in the standing position.

Case report

A 30-year-old man reported pain and numbness in the medial region of both ankles for five years. He refers worsening when walking or standing for a long time limiting him from walking distances greater than 100 meters. With this limitation, he stopped to play sports. On physical examination, he presents bilateral flatfoot (Figure 1) and normal movements of the ankles, but has a bilateral positive Tinel's sign in the tibial nerve region. He denies previous surgeries and traumas.

The patient has an electromyography diagnosing TTS and a normal magnetic resonance imaging (MRI). Bilateral ankle ultrasound without load does detect tibial

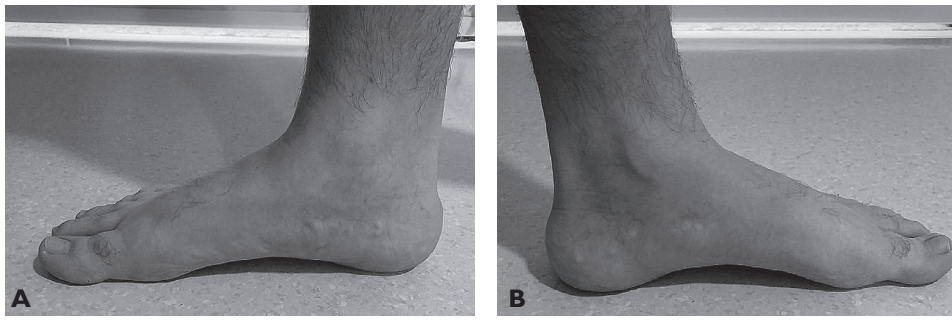

Figure 1 – A) Right flatfoot foot. B) Left flatfoot foot.

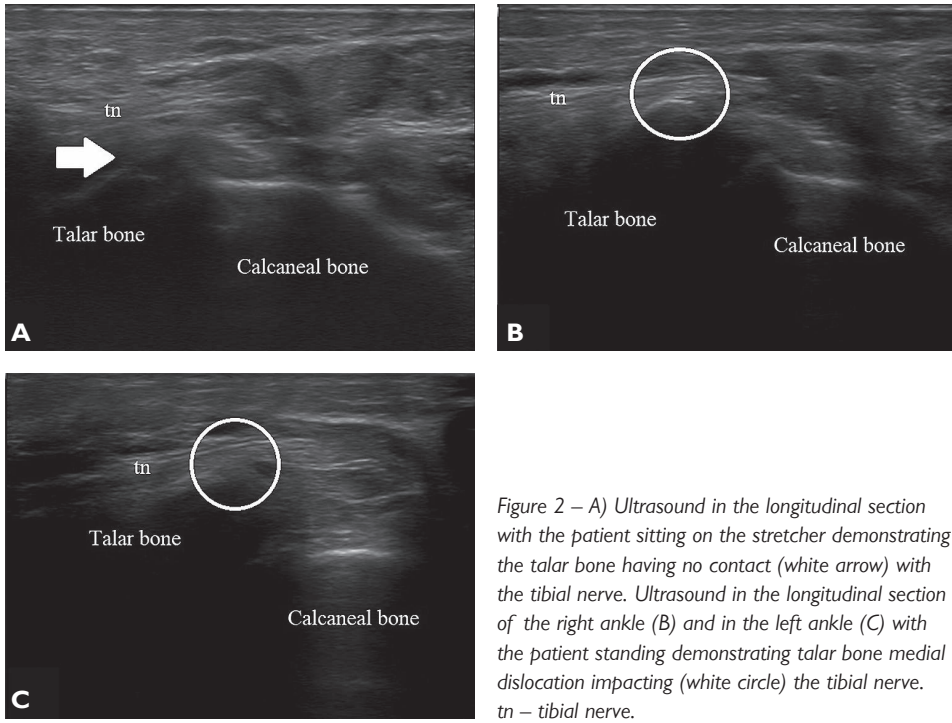

Figure 2 – A) Ultrasound in the longitudinal section with the patient sitting on the stretcher demonstrating the talar bone having no contact (white arrow) with the tibial nerve. Ultrasound in the longitudinal section of the right ankle (B) and in the left ankle (C) with the patient standing demonstrating talar bone medial dislocation impacting (white circle) the tibial nerve. tn – tibial nerve.

nerve enlargement – cross-sectional area of the right tibial nerve was 0.22 cm^2 and the left tibial nerve was 0.20 cm^2. In the ultrasound study with the patient standing, 0.5 cm of medial dislocation of the talar bone on the calcaneus bone is observed impacting the tibial nerve in both ankles, characterizing TTS caused by medial talar dislocation (Figure 2).

With the diagnosis, a bone arthrodesis with a screw between the talar and calcaneal bones was performed (Figure 3). Following surgery, the patient performed

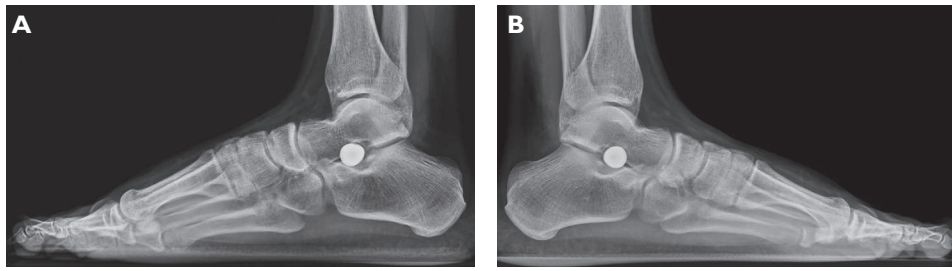

Figure 3 – Lateral X-ray of the right foot (A) and left foot (B), showing arthrodesis with a screw between the talar and calcaneal bones.

physiotherapy for six months and, after this period, the ultrasound with the patient standing was normal. The patient refers no symptoms and affirms he even played soccer for the first time since symptoms emerged reporting improvement of your quality of life.

Discussion

Changing the foot posture can affect the alignment of the tibia, talus, or calcaneus. Hindfoot valgus, tibia valgus, talus valgus, calcaneal valgus, flatfoot deformity, talocalcaneal coalition, or supination are possible bone causes of TTS. Radiography and computed tomography (CT) scan permit for examination of tarsal tunnel bone anatomy and pathology which have been implicated in patients with suspected TTS (Khodatars et al., 2022). A bone can touch or impact the tibial nerve or its branch (de Souza Reis Soares et al., 2022).

Longitudinal images with ultrasound enable the evaluation of bone alignment. When the ultrasound is performed with the patient in the standing position the sensitivity of TTS grows. The medial process of the talus touch or even compresses the distal portions of the tibial and plantar nerves (de Souza Reis Soares et al., 2022). Weight-bearing radiographs and/or CT scans (weight-bearing or conventional) are the tests of preference for recognizing hindfoot valgus, talus dislocation or varus deformity. Imaging of both ankles should be executed to compare them (Khodatars et al., 2022). Ultrasound, as demonstrated is this case, can diagnose both: talus dislocation and nerve compression.

Tinel's test can be executed with ultrasound by touching the nerve to induce symptoms. If positive, TTS is the leading diagnostic hypothesis, notably when symptoms are associated to potential causes of compression (Fantino, 2014). Due to superficial location of tibial nerve, ultrasound can reveal morphological peripheral nerve lesions that can be related to neuritis/neuropathy like hypoechogenicity, partial or complete loss of echogenic fat, and fascicular morphology with a definition

better than MRI (Samarawickrama et al., 2016). This is one of the reasons that ultrasonography should be performed routinely when the syndrome of the tarsal tunnel is suspected (Fantino, 2014).

Ultrasonography offers the advantage of detecting small injuries that may not always be identifiable on MRI scans. Furthermore, the ultrasound dynamic method enables the evaluation of nerve compressibility due to vascular causes, such as varicosities and arterial tortuosity. Ultrasound has a crucial role in pre-operative appraisal and description and can aid for minimally invasive procedure in some cases, like ganglia's comprising the tibial nerve that can be aspirated (Khodatars et al., 2022).

Although MRI is considered the imaging gold standard test for the diagnosis TTS, the role of ultrasound is increasing thanks to several advantages in relation to MRI, such as (Fantino, 2014; Tawfik et al., 2016):

- Better spatial resolution compared to MRI
- Quicker examination performing axial scans (elevator technique)
- Dynamic analysis and the possibility to perform the test with the patient in the standing position
- Positive ultrasound Tinel sign can be detected
- Doppler ultrasound analysis
- Is cheaper and has a widespread availability compared to MRI

Ultrasonography can be performed with the patient in the standing position – position in which CT scan and MRI cannot be performed routinely nowadays – detecting precisely the talar dislocation touching or even compressing the tibial nerve, as illustrated in this case, or its branches – medial plantar nerve or lateral plantar nerve. To avoid false-positive or false-negative errors, the sonographer must be aware that cause of TTS is one that compresses, displaces or touches the tibial nerve or its branches. The most common differential diagnosis is plantar fasciitis which is easily evaluated with ultrasound (de Souza Reis Soares et al., 2022).

Ultrasound imaging has some limitations. Ultrasound is operator dependent, and to diagnose TTS, the sonographer must know the anatomy of the tarsal tunnel and the possible causes of the syndrome. In some cases, video files enhance the quality of data supplied and improve understanding. Ultrasound delivers details on the morphology, but not on the harshness of the neuropathy and the effect on the nerve. Also, this test does not assess the function of the nerve. Ultrasound does not distinguish muscle edema provoked by denervation like MRI (Fantino et al., 2011). Obesity can also limit the utility of ultrasound (de Souza Reis Soares et al., 2022).

Conclusion

Although TTS has several possible causes, some of them are better evaluated with ultrasound, mainly when the analysis in the standing position is necessary. Ultrasound

has a better resolution of the tibial nerve and its branches when compared to MRI, but is an operator-dependent technique, requiring the knowledge of the different sorts of causes of TTS and their imaging appearances to permit an accurate diagnosis.

References

de Souza Reis Soares, O., Duarte, M. L., Brasseur, J. L. (2022) Tarsal tunnel syndrome: An ultrasound pictorial review. *J. Ultrasound Med.* **41(5)**, 1247–1272.

Fantino, O. (2014) Role of ultrasound in posteromedial tarsal tunnel syndrome: 81 cases. *J. Ultrasound* **17(2)**, 99–112.

Fantino, O., Coillard, J. Y., Borne, J., Bordet, B. (2011) Ultrasound of the tarsal tunnel: Normal and pathological imaging features. *J. Radiol.* **92(12)**, 1072–1080. (in French)

Khodatars, D., Gupta, A., Welck, M., Saifuddin, A. (2022) An update on imaging of tarsal tunnel syndrome. *Skeletal Radiol.* **51(11)**, 2075–2095.

Samarawickrama, D., Therimadasamy, A. K., Chan, Y. C., Vijayan, J., Wilder-Smith, E. P. (2016) Nerve ultrasound in electrophysiologically verified tarsal tunnel syndrome. *Muscle Nerve* **53(6)**, 906–912.

Tawfik, E. A., El Zohiery, A. K., Abouelela, A. A. K. (2016) Proposed sonographic criteria for the diagnosis of idiopathic tarsal tunnel syndrome. *Arch. Phys. Med. Rehabil.* **97(7)**, 1093–1099.

 Prague Medical Report / Vol. 125 (2024) No. 2, p. 178–181

Instructions to Authors

Prague Medical Report is an English multidisciplinary biomedical journal published quarterly by the First Faculty of Medicine of the Charles University. Prague Medical Report (Prague Med Rep) is indexed and abstracted by Index-medicus, MEDLINE, PubMed, EuroPub, CNKI, DOAJ, EBSCO, and Scopus.

Articles issued in the journal

a) Primary scientific studies on the medical topics (not exceeding 30 pages in standardized A4 format – i.e. 30 lines and 60–65 characters per line – including tables, graphs or illustrations)
b) Short communications
c) Case reports
d) Reviews
e) Lectures or discourses of great interest
f) Information about activities of the First Faculty of Medicine and other associated medical or biological organizations

Layout of the manuscript

a) Title of the study (brief and concise, without abbreviations)
b) Information about the author(s) in the following form:
   - first name and surname of the author(s) (without scientific titles)
   - institution(s) represented by the author(s)
   - full corresponding (mailing) author's reference address (including first name, surname and scientific titles, postal code, phone/fax number and e-mail)
c) Abstract (maximum 250 words)
d) Key words (4–6 terms)
e) Running title (reduced title of the article that will appear at the footer (page break), not more than 50 typewritten characters including spaces)
f) Introduction
   - The use of abbreviations should be restricted to SI symbols and those recommended by the IUPAC-IUB. Abbreviations should be defined in brackets on first appearance in the text. Standard units of measurements and chemical symbols of elements may be used without definition.

g) Material and Methods
h) Results
i) Discussion
j) Conclusion
k) References
   - All the sources of relevant information for the study should be cited in the text (citations such as "personal communication" or "confidential data" are not accepted).
   - It is not permitted to cite any abstract in the References list.
   - References should be listed alphabetically at the end of the paper and typed double-spaced on separate pages. First and last page numbers must be given. Journal names should be abbreviated according to the Chemical Abstract Service Source Index. All co-authors should be listed in each reference (et al. cannot be used).
   - Examples of the style to be used are:
     Yokoyama, K., Gachelin, G. (1991) An Abnormal signal transduction pathway in CD4–CD8– double-negative lymph node cells of MRL *lpr/lpr* mice. *Eur. J. Immunol.* **21**, 2987–2992.
     Loyd, D., Poole, R. K., Edwards, S. W. (1992) *The Cell Division Cycle. Temporal Organization and Control of Cellular Growth and Reproduction.* Academic Press, London.
     Teich, N. (1984) Taxonomy of retroviruses. In: *RNA Tumor Viruses,* eds. Weiss, R., Teich, N., Varmus, H., Coffin, J., pp. 25–207, Cold Spring Harbor Laboratory, Cold Spring Harbor, New York.
     References in the text should be cited as follows: two authors, Smith and Brown (1984) or (Smith and Brown, 1984); three or more authors, Smith et al. (1984) or (Smith et al., 1984). Reference to papers by the same author(s) in the same year should be distinguished in the text and in the reference list by lower-case letters, e.g. 1980a, or 1980a, b.
l) tables, figures, illustrations, graphs, diagrams, photographs, etc. (incl. legends)

Technical instructions

a) Manuscripts (in UK English only) must be delivered in the electronic form via Online Manuscript Submission and Tracking system (http://www.praguemedicalreport.org/). In case of problems, contact the Prague Medical Report Office (medical.report@lf1.cuni.cz). The online submission has to include the complete version of the article in PDF format, separately the manuscript as a MS Word file and a cover letter. The detailed version of the Instructions to Authors can be found at: http://www.praguemedicalreport.org/download/instructions_to_authors.pdf.

b) Text should be written in MS WORD only. We accept only documents that have been spell-checked with UK English as a default language.
c) Please, write your text in Times New Roman script, size 12, and line spacing 1.5.
d) Text should be justified to the left, with no paragraph indent (use Enter key only); do not centre any headings or subheadings.
e) Document must be paginated-numbered beginning with the title page.
f) Tables and graphs should represent extra files, and must be paginated too.
g) Edit tables in the following way: Make a plain text, indent by Tab (arrow key) all the data belonging to a line and finish the line by Enter key. For all the notes in table, use letter x, not *.
h) Make your graphs only in black-and-white. Deliver them in electronic form in TIFF or JPG format only.
i) Deliver illustrations and pictures (in black-and-white) in TIFF or JPG format only. The coloured print is possible and paid after agreement with the Prague Medical Report Office.
j) Mark all the pictures with numbers; corresponding legend(s) should be delivered in an extra file. Mark the position of every picture (photo) in the manuscript by the corresponding number, keep the order 1, 2, 3...

Authors' Declaration

The corresponding (or first author) of the manuscript must print, fill and sign by his/her own hand the Authors Declaration and fax it (or send by post) to the Prague Medical Report Office. Manuscript without this Declaration cannot be published. The Authors' Declaration can be found by visiting our web pages: http://pmr.lf1.cuni.cz or web pages of Prague Medical Report Online Manuscript Submission and Tracking system: http://www.praguemedicalreport.org/.

Editorial procedure

Each manuscript is evaluated by the editorial board and by a standard referee (at least two expert reviews are required). After the assessment the author is informed about the result. In the case the referee requires major revision of the manuscript, it will be sent back to the author to make the changes. The final version of the manuscript undergoes language revision and together with other manuscripts, it is processed for printing.
Concurrently, proofs are electronically sent (in PDF format) to the corresponding (mailing) author. Author is to make the proofs in PDF paper copy and deliver it back to the editorial office by fax or as a scanned file by e-mail. Everything should be done in the required time. Only corrections of serious errors, grammatical mistakes and

misprints can be accepted. More extensive changes of the manuscript, inscriptions or overwriting cannot be accepted and will be disregarded. Proofs that are not delivered back in time cannot be accepted.

Article processing charge

Authors do not pay any article processing charge.

Open Access Statement

Copyright Statement

Editorial Office
Prague Medical Report
Kateřinská 32, 121 08 Prague 2, Czech Republic
e-mail: medical.report@lf1.cuni.cz
Phone: +420 224 964 570. Fax: +420 224 964 574

Prague Medical REPORT

(Sborník lékařský)

Published by the First Faculty of Medicine, Charles University, Karolinum Press,
Ovocný trh 560/5, 116 36 Praha 1 – Staré Město, Czech Republic, www.karolinum.cz

Editorial Office: Prague Medical Report, Kateřinská 32, 121 08 Prague 2, Czech Republic,
Phone: +420 224 964 570, Fax: +420 224 964 574,
e-mail: medical.report@lf1.cuni.cz
Editor in Chief: Kateřina Jandová, MD., PhD.
Foreign Language Editor: Prof. Jaroslav Pokorný, MD., DSc.
Executive Editor: Mgr. Lucie Šulcová
Editorial Board: Prof. Jan Betka, MD., DSc.; Zdeněk Kostrouch, MD., PhD.;
Prof. Emanuel Nečas, MD., DSc.; Prof. Karel Smetana, MD., DSc.;
Prof. Karel Šonka, MD., DSc.; Assoc. Prof. Jan Tošovský, MD., PhD.;
Prof. Jiří Zeman, MD., DSc.

Published as quarterly journal. Typeset and printed by Karolinum Press.
Annual subscription (4 issues) EUR 60,–. Single copy EUR 20,–.
Distribution: Karolinum Press, Ovocný trh 560/5,
116 36 Praha 1, Czech Republic, e-mail: journals@karolinum.cz

ISSN 1214-6994 (Print)
ISSN 2336-2936 (Online)

Reg. No. MK ČR E 796